RECOMBINATION, IONIZATION, AND NONEQUILIBRIUM ELECTRICAL CONDUCTIVITY IN SEEDED PLASMAS

Thesis by

Terrill Alan Cool

In Partial Fulfillment of the Requirements

For the Degree of

Doctor of Philosophy

California Institute of Technology

Pasadena, California

1965

(Submitted May 27, 1965)

ACKNOWLEDGMENTS

The author wishes to express his deep gratitude and appreciation to Professor Edward E. Zukoski for his most excellent guidance, advice, and enthusiastic encouragement during the course of this investigation and throughout the author's graduate study.

Special acknowledgment is given here to Professor Jack L. Kerrebrock of the Massachusetts Institute of Technology for the motivation that his original studies in this field, conducted at the California Institute of Technology, has given to this work.

Appreciation is also expressed to Dr. Alfred C. Pinchak for his contributions in making the plasma-arc facility the useful apparatus that it now is.

My sincerest thanks to Mr. Frank T. Linton for his talented work both in the fabrication of the test equipment for this study and in the drawing of the figures for this thesis. The author also wishes to thank Mrs. Robert Duffy for her work in preparing the typed manuscript.

Financial assistance to the author in the form of National Science Foundation Fellowships, a Clinedinst Foundation Scholarship, and a California Institute of Technology Graduate Teaching Assistantship have made graduate study possible and have been greatly appreciated.

ABSTRACT

This study is concerned with the theoretical and experimental description of the behavior of dense seeded plasmas under the influence of applied electric fields under steady-state conditions as well as during electronic ionizational and recombinational relaxations. Extensive experimental measurements of nonequilibrium electrical conductivities, electron temperatures, recombination rates, and ionization rates have been performed in dense potassium-seeded plasmas. Measurements have been made under conditions of practical importance for proposed MHD energy converters in argon-potassium and helium-potassium plasmas. Translational gas temperatures ranged from 1250 to 2000^{o}K; seed concentrations were varied between .1 and 1 mole percent; and the total gas pressure was 1 atmosphere.

Extensive steady-state measurements of nonequilibrium electrical conductivity, and the influence upon it of variations in gas temperatures, seed concentrations, atomic cross sections, current densities, electric field strengths, and energy loss processes have been made. This detailed experimental work has led to important modifications of existing theory which have enabled an accurate description of the plasma in terms of a simple physical model. Electron temperature measurements provide a conclusive and quantitative verification of the validity of this physical model. The essential theoretical modifications made here are the inclusion of both inelastic and elastic electronic collisional energy loss mechanisms in a manner which

accurately reflects the essential physical differences between these two processes in terms of fundamental atomic properties, and employs no adjustable parameters. Additionally, consideration of the detailed energy dependence of the atomic cross sections and the inclusion of both electron-ion and electron-atom interactions has been essential in accurately describing the experimental results.

Experimental measurements of recombination rates, ionization rates, and electronic collisional relaxation characteristics of potassium seeded plasmas have been performed. Measured recombination and ionization rates for potassium show good agreement with theoretical calculations based upon a formulation employing the Gryzinski classical inelastic collision cross sections and a simple physical model of the relaxing plasma.

TABLE OF CONTENTS

LIST OF FIGURES

I. INTRODUCTION

In recent years, many scientists and engineers have directed considerable efforts toward the achievement of the direct conversion of heat into electrical energy on a large scale by means of various types of magnetohydrodynamic (MHD) devices. One approach to this problem of energy conversion has been the utilization of a closed-cycle MHD system which employs a working fluid composed of a monatomic gas seeded with a small amount of an alkali vapor to enhance the electrical conductivity of the gas at a given gas temperature. In such a device, one would also hope to take advantage of the potentially large enhancement of ionization caused by electronic collisional processes in a two-temperature, dense plasma system. This two-temperature plasma results from the fact that the electron temperature can be substantially elevated above the translational temperature of the heavy species due to acceleration of the electrons by electromagnetic forces.

The motivation for the work of this thesis has been two-fold. First, an effort has been made to obtain useful engineering data and calculation methods for the determination of the electrical conductivity and ionizational relaxation characteristics of seeded plasmas of engineering interest with regard to MHD energy-conversion systems. Secondly, and more fundamentally, this study is concerned with the theoretical description of these plasmas in terms of a physical model of the plasma, and the experimental verification of the validity of key assumptions in this theoretical formulation.

In order to gain a basic insight into energy transfer processes in the plasma and to retain an unambiguous interpretation of experimental results without undue experimental complexity, it was felt necessary to restrict the scope of this study to plasma behavior under the influence of electric fields only. The results of this study are fundamental to an understanding of plasma behavior in practical systems with combined electric and magnetic fields, and this understanding is the justification of this study as well as an incentive to the continued study of more complicated systems which more nearly approximate proposed MHD configurations.

More specifically, the behavior of dense argon-potassium and helium-potassium plasmas were examined when the plasma was subjected to either a constant electric field or to pulsed increases and decreases in electric field strength. The basic experimental determinations include measurements of plasma electrical conductivity, as well as various excited state populations of the seed atom. These measurements additionally provide the determination of ionization and recombination rates, electron densities, and electron temperatures. These experimentally determined quantities are compared with theoretical calculations based upon a two-temperature plasma model which adequately explains the observed plasma phenomena over an extensive range of variation of experimental parameters.

These calculations include some important features which were found to be essential in understanding energy transfer processes in these seeded plasmas. The energy balance used here treats both elastic and inelastic collision energy losses from the free electrons

in an independent manner which reflects the essential physical differences of the two loss mechanisms. The inclusion of electron-ion encounters as well as electron-atom encounters was necessary to fully define the electronic elastic collision losses. The theoretical calculations involve integrals over the electron energy distribution function in terms of the fundamental atomic cross sections; no adjustable parameters appear in the formulation.

The excellent agreement between the experimental measurements of electrical conductivity and the theoretical calculations show that the calculation mechods used here are quite accurate for the determination of plasma characteristics in practical engineering systems.

In addition, the calculated values of electron density and electron temperature are shown to be accurate by the direct experimental measurement of excited state populations and recombination rate coefficients. These experimental measurements provide direct experimental justification of the key assumption of the two-temperature model: that electronic collisional processes provide mutual electronic collisional (Saha) equilibrium between the free electrons and the electronically excited states of the seed atom.

Measurements of ionization and recombination rates were made by observations of transient plasma behavior in response to step increases and decreases in electric field strength. A simplified plasma model for these relaxation processes provides a theoretical development leading to theoretical calculations of ionization and recombination rates in terms of the recently developed Gryzinski

classical electron-atom inelastic collision cross sections. These calculations show that measured and theoretical values of ionization and recombination rates agree well with values calculated with the simple plasma model. The relaxation data and the theoretical development describing these relaxation processes show that ionization and recombination occur by multi-step electronic collisional processes.

Finally, the measured ionization and recombination rates provide essential data for the design of MHD energy converters, and show that inlet ionizational relaxation processes will not be a limiting factor in practical MHD generator performance. Further, the theoretical description discussed here provides a useful means for the calculation of relaxation characteristics in large scale MHD devices.

No effort has been made in this brief introduction to give an account of the historical development of this field of research. Rather, the contributions of individual authors will be cited at the points where their technical contributions enter naturally into the logical development of this work.

II. QUALITATIVE PLASMA BEHAVIOR FOLLOWING AN ABRUPT APPLICATION OF AN ELECTRIC FIELD

In order to begin this study, it is useful to present qualitatively a description of plasma phenomena occurring immediately following a step function application of an essentially constant electric field to a plasma. This examination will focus on the energy transfer processes which occur as the plasma electrons are accelerated by the applied electric field. The discussion will be limited to the plasmas of interest here which possess monatomic heavy species with translational temperatures of about 2000°K, electron densities above about 10^{13} cm^{-3}, total heavy species number densities of about 10^{18} cm^{-3}, and potassium atom densities near 10^{16} cm^{-3}. This qualitative examination is useful at this point in explaining the principal phenomena to be presented here, and the quantitative accuracy of these simple interpretations will be examined in detail in following sections of this study.

The rate at which the free electrons gain energy immediately following the application of an electric field is given by the difference between the rate of energy input from the applied field and the rates of energy loss due to elastic and inelastic collisions with the various heavy species, both neutral and ionized, of the plasma. The electron temperature increases rapidly in response to the initial energy input from the field. For plasmas in which the electron density is a sufficiently large fraction of the total plasma particle density, it is meaningful to characterize the electrons with a temperature given by

a quasi-steady electronic energy balance at some relatively short interval of time after the application of the electric field. In this quasi-steady condition, the energy input and energy loss terms of the free electrons approximately balance, and the rate of change of the free electron energy is no longer rapid. For the conditions of the plasmas studied, the time scale for the establishment of this quasi-steady electron temperature is typically less than 3 microseconds (as determined in Section V-B). The electron temperature may increase from its initial value, near the translational temperature of the heavy species, to relatively high values during this short time interval.

Following this initial electron temperature elevation, an ionizational relaxation period occurs during which the populations of the various excited states and the density of the free electrons increase in response to this increased electron temperature as a result of excitations and ionizations by electronic collisions*. During this period the electron temperature, given by the quasi-steady energy balance, may increase somewhat further in value as the energy input to the electrons increases due to the increasing electrical conductivity. This ionizational relaxation period is terminated when the populations of free and bound states increase to values such that de-excitations and recombinations are sufficient to balance the forward excitation and ionization rates. At this "steady state" condition, the predominant electron-energy loss mechanism is elastic collisions with the

* Under some conditions, the initial temperature relaxation and the ionizational process occur simultaneously in a more closely coupled fashion; see discussion in Section V-B.

various heavy species for the typical electron densities of these experiments ($N_e \gtrsim 10^{14}$). Thus, this condition is characterized by a translational temperature difference between the free electrons and the heavy species of the plasma. The energy input to the free electrons by the field is transferred primarily into the translational energy of the heavy species,and the whole plasma heats up relatively slowly, provided that the total number density of the heavy species greatly exceeds the number density of free electrons.

This "steady-state" condition, hereafter to be referred to as "the steady state," at the end of the ionizational transient can be of practical importance for MHD energy conversion in high density plasmas. This condition is interesting, provided that this state of enhanced ionization resulting from the elevation of electron temperature and the attendant electronic collisional processes can be achieved without a substantial increase in the translational temperature of the heavy species of the plasma.

In practical terms, then, two important questions must be answered. In the first place, the coupling between the free electrons and the heavy species by elastic collisions at the steady state must be "weak" enough that a substantial temperature difference exists between the free electrons and the heavy species. Secondly, this "steady state" condition must be achieved in times which are short compared to the times necessary for the occurrence of appreciable increases in the heavy-species translational temperature during this ionizational transient.

The experimental measurements and the theoretical discus-

sion which will be presented in this study will show that the seeded plasmas investigated here do exhibit a large enhancement in the level of ionization for moderate applied field strengths, and that this enhanced ionization may be achieved rapidly enough to achieve the steady-state condition without a substantial increase in gas temperature.

This qualitative introduction illustrates the two separate phenomenological regions of interest that will be discussed in this study. The experimental results will be separated into these two groups; the first dealing with a discussion of the steady state, and the second dealing with the ionization and recombination relaxation processes. Before presenting the experimental results, it will be necessary to develop the theoretical arguments somewhat. The following section will treat this theoretical formulation in terms of a physical model of the plasma. Following this discussion, the experimental apparatus, techniques, and results will be discussed.

III. THEORETICAL DESCRIPTION OF PLASMA BEHAVIOR IN RESPONSE TO AN APPLIED ELECTRIC FIELD

This section deals with the theoretical plasma model used to describe the characteristics of the dense monatomic seeded plasmas of interest here. A description of plasma properties would include a detailed knowledge of the populations of all bound electronic states, a knowledge of the translational energies of the free electrons and the various monatomic atomic species, and a determination of the free electron density. This description would need to be determined as a function of time during the ionizational relaxation transients, and would require a knowledge of the interactions between the various plasma species. In the general case, this specification would require the simultaneous solution of the infinite set of differential equations determining the time variation of energy level populations, along with energy equations relating the instantaneous translational energies of the various species to the instantaneous energy level populations.

This formulation involves the solution of the Boltzmann equation for each plasma species in terms of the various collisional interactions to specify the distribution functions of these various species. This complex problem can be simplified when certain key assumptions can be made. The most essential simplification arises from treating only small deviations from equilibrium. That is, the velocity distribution functions of the various atomic species, as well as that of the free electrons, are assumed to be Maxwellian to the first approximation. The establishment of the validity of this as-

sumption requires an investigation of the influence of the various interactions between the plasma species and the effects of the applied field upon the distribution functions of the various species. An investigation of these effects indicates that the atomic species, neutral and ionized, interact sufficiently to ensure that they possess a common Maxwellian distribution of velocities, and thus a common translational temperature. Further, at sufficiently high electron densities, mutual electronic interactions are sufficient to ensure that the electronic distribution is also Maxwellian to the first approximation. The validity of these assumptions has been investigated by several authors[1 - 3], and Appendix C includes a discussion pertaining to the experimental plasma conditions encountered here.

Also, when the electron density is high enough, then electronic collisional processes dominate over atomic collisional processes in the population rate equations. Under these conditions, the populations of the various excited states, as well as that of the free electrons, are determined principally by electronic collisional processes and the various radiative processes which occur. The collisional rate coefficients can then be determined in terms of the electron temperature and inelastic electron-atom cross section expressions.

An additional simplification results from the fact that the ionization potentials and excitation energies of the inert carrier gas are sufficiently large compared to those of the potassium seed that excitation and ionization of the carrier gas can be neglected at the electron temperatures considered here. The carrier gas thus acts only as a sink for the transfer of translational energy from the free electrons,

as well as a barrier for diffusion of electrons and potassium ions. It should also be mentioned that gas temperatures and carrier gas densities are assumed large enough to ensure that the potassium vapor is essentially monatomic and that the dimer form of potassium does not exist in appreciable quantities.

Thus these assumptions simplify the description of the plasma to a specification of the electron temperature, the atomic species' translational temperature, the populations of the excited states for the potassium atoms, and the number density of the free electrons.

The plasma energy-transfer mechanisms which must be examined are the energy gain to the free electrons from the field, elastic and inelastic transfer of energy between the electrons and the various heavy plasma species, as well as free-free, free-bound, and bound-bound radiative transfer. The following sections will deal briefly with these energy transfer mechanisms as well as simplified plasma descriptions for both steady and transient plasma conditions.

A. Electron Temperature

Utilizing the foregoing simplifications, the electron temperature can be determined by considering the equation for the conservation of energy of the free electron gas when the electronic energy distribution can be regarded as Maxwellian. We consider a stationary monatomic plasma system in which energy from the free electrons is transferred into either translational energy of the atomic species or into excitational energy of the bound states of the seed atom by either elastic or inelastic collisions, respectively. In

general, the populations of the various energy levels will be determined by radiative processes as well as electronic collisional processes.

We can write the local energy balance for the free electrons under the application of an electric field E as

$$\frac{d}{dt}\left[N_e(\epsilon_e+V_o)\right] = \sigma E^2 - \mathring{\Omega} - \sum_i V_i \frac{dN_i}{dt} - \mathring{R}_{b-b} - \mathring{R}_{f-b} - \mathring{R}_{f-f} \quad . \tag{1}$$

The rate of change per unit volume of the energy of the free electrons as measured relative to the ground electronic state of the seed atom is written on the left hand side of eqn. (1), where the ionization potential of the potassium atom is given by V_o and is 4.34 ev. This must equal the net rate of energy input per unit volume to the free electrons given by the terms on the right hand side of eqn. (1). The rate of energy input per unit volume to the free electrons by acceleration in the electric field is given by σE^2. Electrons lose energy by elastic collisions at a rate per unit volume given by $\mathring{\Omega}$. Electrons transfer their kinetic energy into the creation of excited states in the seed atom at the net rate $\Sigma V_i(dN_i/dt)$ per unit volume, provided there are no radiative losses from the system. Here, V_i is the energy, as measured from the ground state, of the i^{th} energy level with population N_i. For all systems of finite size, net radiative losses do occur, and so some of the energy transferred from the free electrons due to inelastic collisions which would otherwise appear as an increase in the density of excited and ionized states is instead lost from the system as radiation. This radiative loss can be either that due to free-bound transitions, $\mathring{R}_{f-b}$, i.e., the local

rate of energy loss per unit volume where the energy of direct radiative recombination is transferred from the volume element, or that due to bound-bound transitions, $\mathring{R}_{b-b}$, which is the local rate of energy loss per unit volume when the energy of radiative transitions between bound states escapes the volume element. For very dense, hot plasmas, energy may also be lost from the free electrons by free-free transitions (Bremsstrahlung), resulting in the escape of photons from the plasma volume. The rate of energy loss per unit volume by this means is designated $\mathring{R}_{f-f}$ and is quite unimportant for plasma systems considered here (see Appendix B), and will be neglected in this analysis.

Equation (1) can be re-written to obtain a perhaps clearer interpretation of the terms as

$$N_e \frac{d\varepsilon_e}{dt} = \left\{ \left[- (\varepsilon_e + V_o) \frac{dN_e}{dt} - \sum_i V_i \frac{dN_i}{dt} \right] - \mathring{R} \right\} + \sigma E^2 - \mathring{\Omega} \quad . \tag{2}$$

The quantity inside the curly brackets represents the instantaneous net rate that energy is transferred either to or from the free electrons per unit volume due to inelastic collisional processes. Note that when d/dt is positive, as during the ionizational process, the quantity confined to the square brackets represents the net rate of energy loss per unit volume from the free electrons due to collisional excitations and ionizations if there were no radiative losses from the system. During recombination the quantity in square brackets is positive, designating the rate of energy input to the free electrons by collisional recombination and de-excitation, when radiative losses can be neglected.

When radiative losses are important, we must thus subtract the net local rate of radiative energy loss per unit volume to obtain the net rate of energy loss or gain by the free electrons as a result of inelastic electronic collisional processes (given in the curly brackets). For the conditions of these experiments, free-bound transitions are also negligible compared to the bound-bound transitions, as is justified in Appendix B , and thus $\mathring{R}$ will be taken to represent the total rate per unit volume at which energy leaves the system due to bound-bound transitions only unless otherwise stated. If the electron energy can be regarded as quasi-steady, then $N_e(d\varepsilon_e/dt)$ is a small term compared to the others; also, under some conditions (see Section V), the populations of most of the excited states can be regarded as quasi-steady and then the corresponding $V_i(dN_i/dt)$ terms are also negligible.

Another quasi-steady state occurs when all the d/dt terms are zero, and then the temperature of the whole system increases relatively slowly as the energy is transferred to the heavy species (see Section V-B). For this "steady-state" case, we have

$$\sigma E^2 = J^2/\sigma = \mathring{\Omega} + \mathring{R}_s \quad . \tag{3}$$

The remainder of this section will be devoted to the discussion of the terms in equation (3), which gives the local electron energy balance of a two-temperature plasma under the influence of a steady electric field after the initial ionization relaxation transients have vanished.

Note that the quantities such as electron density, electrical conductivity, etc., which occur in the energy balance equations can

also be interpreted as volume-averaged quantities to describe the behavior of the experimentally measurable volume-averaged plasma properties, provided that non-uniformities near plasma boundaries are not so large that the characterization of the plasma in terms of equations dealing with average quantities has no meaning. Further discussion of this is given in Section III-D.

B. Electron Density

The plasmas of interest throughout this study can be considered to possess electron densities and excited state populations which are determined primarily by electronic collisional processes as well as spontaneous radiative transitions. The validity of this statement is discussed in Appendix C , and evidence of an exception to this is given in Section VII-A. The complete specification of the populations of the various excited states, as well as the density of free electrons under these conditions, is given for a plasma with an instantaneous electron temperature, T_e, by the solution of an infinite set of rate equations of the form[4]:

$$\frac{dN_n}{dt} = \sum_{m\neq n}^{\infty} N_m A_{mn} - N_n \sum_{m\neq n}^{\infty} A_{nm} + N_e \sum_{m\neq n}^{\infty} (N_m C_{mn} - N_n C_{nm}) \tag{4}$$

where dN_n/dt is the net local rate of change per unit volume of the number of atoms in an arbitrary state, n , with $n = 1$ describing the ground state and $1 \leq n \leq \infty$. N_e is the density of free electrons. The rate coefficients C_{nm} and C_{mn} for electronic collision processes are those for the processes

$$K_n + e^- \rightleftharpoons K_m + e^-$$

in the forward and reverse directions, respectively. We can include transitions between the continuous energy states of the free electrons to or from the bound states by electronic collision with the processes

$$K_n + e^- \rightleftharpoons K^+ + e^- + e^-$$

with forward rate coefficient $C_{n,c}$.

Radiative processes included in (4) are

$$K_m \rightleftharpoons K_n + h\nu_{mn}$$

where the rate constant in the forward direction is the Einstein coefficient, A_{mn}, for spontaneous emission of radiation in amount $h\nu_{mn}$ for a transition from state m to state n. For resonance lines, in particular, the reverse reaction is not small, as the probability of re-absorption of radiation in the plasma can be large in the dense plasmas considered here. These reabsorption effects are included in a formal way in eqn. (4), by considering the summation in the first term of the right hand side to include values of m for $m < n$ and in the second term to include values of $m > n$ and thus $N_n A_{nm}$ is the local rate of transitions (reabsorptions) inverse to the local forward rate of emissions, $N_m A_{mn}$. When the effect of reabsorption is large, then forward and backward radiative rates approximately balance, and then the populations of the various states are governed by electronic collisional processes only.

Implicit in this set of equations is the assumption that the free electron energy distribution is Maxwellian. The conditions under which this approximation is valid are considered briefly in Appendix C.

In general, one should also include the radiative processes

$$K^+ \rightleftharpoons K_n + h\nu_{cn} ,$$

But these processes are relatively unimportant for the plasmas discussed here, as is explained in Section V-A, and Appendix B.

We have included only volume effects in eqn. (4). This is valid when the rates of diffusion of the various excited and ionized atoms to the plasma boundaries can be neglected compared to volume de-excitation and recombination rates. It is shown in Appendix C. that diffusion losses probably have no important effect on the dense plasmas considered here except possibly very near the walls. See also Section III-F.

It is assumed, as discussed in Appendix C , that electron densities will generally be high enough to permit the neglect of atom-atom processes of the forms

$$X + K_m \rightleftharpoons K_n + X$$

and

$$X + K_m \rightleftharpoons K^+ + e^- + X \ .$$

Further, the concentrations of the dimer form of potassium can be considered so small at the gas temperatures of interest here that one can neglect processes involving the dimer form such as the dissociative reaction

$$K + K \rightleftharpoons K_2^+ + e^- ,$$

see Section V-A and Appendix C.

For the steady-state case, the equations (4) reduce to an infinite set of algebraic equations which can be solved in principle

when the rate coefficients and effective local radiative transition probabilities are known. This infinite set can in general be reduced to a finite set, since for sufficiently high electron densities the populations of the higher states will be determined essentially by electronic collisional processes as discussed in Appendix C . For these states, the population of a given state, n , is given in terms of the electron density and electron temperature by the condition of collisional equilibrium at the electron temperature. The condition is expressed by Saha equations of the form

$$N_n = \frac{g_n}{g_e g_{ion}} \left(\frac{h^2}{2\pi m_e k T_e} \right)^{3/2} e^{+E_n/kT_e} N_e^2 , \qquad (5)$$

where E_n is the binding energy of the state n with degeneracy g_n . g_e and g_{ion} are the degeneracies of the free electrons and the ions, respectively.

The question of whether or not this condition extends down to a given low-lying state depends critically on the electron density as well as on the re-absorption of radiation within the plasma. This question has been considered in some detail by several authors[1, 4-7] and is complicated somewhat due to a lack of information regarding the magnitudes of the various rate coefficients. However, one can make reasonable estimates of the critical electron density above which a given plasma can be regarded as possessing state populations given essentially by the condition of electronic collisional equilibrium. As is shown in Appendix C , for the plasmas considered here, collisional equilibrium between all electronic energy levels probably exists for electron densities above $10^{14}/cm^3$.

If we now consider the case where electronic collisional equilibrium extends down to the ground state, we can calculate electron densities in terms of electron temperatures. For the plasmas considered here, only potassium is appreciably ionized and is thus the only contributing species. For potassium, for the electron temperature range considered here*, we can write

$$N_e^2 = \left(\frac{2\pi m_e kT_e}{h^2}\right)^{3/2} (2)(\tfrac{1}{2})(N_k)\, e^{-4.34/kT_e} \quad . \qquad (6)$$

Here, N_k is the number density of neutral potassium existing at the electron temperature T_e; that is, $N_k = N_{ko} - N_e$, where N_{ko} is the total number density of potassium atoms, both neutral and ionized. When T_e is less than $3000^\circ K$, then $N_k \cong N_{ko}$.

In summary, this brief discussion of the determination of excited state populations and free electron densities in transient and steady plasmas illustrates some of the difficulties that occur under arbitrary plasma conditions when combined collisional and radiative effects determine the instantaneous values of given population levels. The determination of these populations requires a detailed description of radiative transition probabilities, spectral absorption characteristics, the various collisional rate coefficients, etc., even to begin to solve the infinite set of simultaneous rate equations. Further, the electron temperature is not independent, but depends on the electron

---

* Equation (6) will not be valid for quite high electron temperatures ($kT_e \gtrsim 0.4$ ev) since higher order terms in the electronic partition functions for K and K^+ have been omitted, assuming their ratio of partition functions to be the ratio of their ground state degeneracies.

density through the detailed local energy balance. If these difficulties were not enough, often,for laboratory plasmas, the effects of diffusion to the walls of the plasma container and radiative losses from the plasma boundaries can be so large that one cannot characterize the plasma accurately by uniform properties,and the local formulation of the rate equation and energy balance becomes extremely difficult.

Fortunately,for the high density plasmas considered here, the problem can be drastically simplified and yet give meaningful results. Several authors[1, 7, 11] have considered the description of plasmas similar to those considered here in terms of simplified physical plasma models. The work of BenDaniel and Tamor[1] showed that the use of grossly simplified energy level structures enabled the qualitative discussion of essential features regarding the density of free electrons in nonequilibrium plasmas with substantial radiative losses. The development of the classical inelastic cross section expressions of Gryzinski[8] enabled a complete quantitative theoretical formulation of the problem valid over a wide range of conditions in plasmas of hydrogenic species by Bates, et al.[4, 9] Careful experiments have established the validity of these calculations and demonstrated the usefulness of various simplifications in treating the problem of non-hydrogenic plasmas[6, 7, 10, 12].

The next section will give a brief description of the electrical conductivity expressions used in this study, and then plasma energy-transfer processes will be discussed. This will enable an approximate theoretical description of the steady state and transient plasmas considered here.

C. Electrical Conductivity

The method used to calculate values of the scalar electrical conductivity for comparison with the experimental results is discussed in this section. Theoretical description of the transport processes occurring in a slightly ionized gas is complex, and only a brief outline can be given here. Calculations of electrical conductivity in an ionized gas reduce to calculations of effects resulting from perturbations of the electronic velocity distribution function under the influence of externally-applied electric fields.

Two expansion techniques have been used to determine the electrical conductivity in terms of the electron distribution function and the effects of binary collisions. The first, based on the Enskog procedure, was applied by Chapman and Cowling[13]. The second, a somewhat more rapidly converging procedure based on the expansion of the distribution function in spherical harmonics, was discussed by Allis[14]. This latter technique leads quite directly to integral relations which easily allow the inclusion of cross sections with arbitrary energy dependences. This result is particularly important for the atomic species considered here because of the pronounced dependence of the cross sections on quantum effects.

The desired scalar conductivity expression is obtained with minor manipulation from eqn. (31.9) of Allis[14]. The result for elastic collisions between electrons and neutral atoms is

$$\sigma_c = \left(-\frac{4\pi}{3}\right)\frac{e^2}{m_e}\int_0^\infty \frac{df_o}{dc}\left[\frac{c^2}{\sum_n n_n Q_n}\right]dc \quad . \tag{7}$$

It has been assumed that the heavy species of the plasma have an isotropic distribution. Also, the Lorentz gas approximation is used, i.e., the mass of the electron is assumed negligible compared to that of the heavy particles, and also the influences of electron-electron interactions upon the electron distribution function are neglected. Here, f_o is the first approximation to the electronic distribution function, which is not necessarily the Maxwell distribution function. However, as explained in Appendix C , the conditions for the attainment of a Maxwellian distribution are probably satisfied for the present experiments, and for this case,

$$\sigma_c = \frac{(8/\pi)^{\frac{1}{2}} e^2 N_e}{3(kT_e m_e)^{\frac{1}{2}}} \frac{1}{\overline{\sum_n n_n Q_n}} = \frac{0.532\, e^2 N_e}{(kT_e m_e)^{\frac{1}{2}} \overline{\sum_n n_n Q_n}} \tag{8}$$

when the definition

$$\frac{1}{\overline{\sum_n n_n Q_n}} \equiv \int_0^\infty \frac{\xi e^{-\xi} d\xi}{\sum_n n_n Q_n(\xi)} \tag{9}$$

is used, and $\xi = \frac{1}{2} m_e c^2 / kT_e$. Note that the averaged value of the reciprocal sum of the momentum-transfer cross sections appearing here is not the simple average over the velocity distribution used by several other authors[15]. From the point of view of the present analysis, the latter average is incorrect, and, for gases such as potassium or argon, the averaged cross-sectional values change appreciably with the average used.

We can consider equation (8) for the case of collision cross sections which are independent of electron speed and compare the resulting conductivity expression with the equivalent result of Chap-

man and Cowling. Utilizing the Chapman-Enskog procedure with use of a second approximation to the electronic distribution function and also using the Lorentz gas approximation, they derive an expression[16] identical to the result given here, for this case.

Spitzer[17] and Chapman and Cowling[18] have shown that the effects of electron-electron interactions cannot be neglected as the plasma approaches the fully ionized state. To illustrate this, we can obtain a first approximation to the conductivity of a fully ionized gas by using the Coulomb cross section given by[19]

$$Q_c \cong 2\pi \left(\frac{e^2}{m_e c^2}\right)^2 \ell n \left[\frac{9(kT_e)^3}{8\pi N_e e^6}\right] \tag{10}$$

in the electrical conductivity expression for a Lorentz gas of eqn. (8). Spitzer has shown that the resulting expression must be reduced by a factor $\gamma_E = .582$ to account for the effects of electron-electron interactions on the distribution function. The resulting conductivity is

$$\sigma_s = \frac{8(2)^{1/2}(kT_e)^{3/2}\gamma_E}{\pi^{3/2} m_e^{1/2} e^2 \ell n \Lambda^2} \quad \text{where } \Lambda^2 = \frac{9(kT_e)^3}{8\pi N_e e^6} . \tag{11}$$

Difficulties arise in the calculation of electrical conductivity in a plasma where both close encounters and distant encounters interact simultaneously to determine the resultant conductivity. In principle, the distribution function expansion techniques can give the desired conductivity when the interaction cross sections are known and when the effects of electron-electron interactions are included. In practice, this has been difficult, and only restricted formulations

valid for certain cross-sectional energy dependences have been considered[20]. To this author's knowledge, no completely satisfactory formulation has been established which allows the calculation of electrical conductivities for arbitrary cross-sectional energy dependences and which consistently retains the proper effect of electron-electron interactions.

Faced with this difficulty, it was found useful to make the conventional approximation that,in this combined region of both close and distant encounters, the resultant conductivity may be expressed as[15]

$$1/\sigma = 1/\sigma_c + 1/\sigma_s \quad . \tag{12}$$

This approximation appears to be fairly good for the range of experimental conditions explored here, as will be demonstrated in Section VII-A.

The remainder of this section will deal with a description of the electron energy losses due to elastic and inelastic collisions with the atomic species. The inelastic losses will be considered for only the steady-state case in this section, and attention will be given to inelastic electronic energy losses in transient plasmas in Section V.

D. Elastic Collision Energy Losses

The rate of energy loss from the free electrons by elastic encounters with atomic species, both neutral and ionized, can be expressed in terms of the momentum transfer cross sections occurring in the conductivity expressions. Petschek and Byron[19] have given a formulation for this rate of energy loss. They consider the conservation of energy and momentum in a single binary classical

collision with a particular scattering angle in the center-of-mass system, and then obtain the total elastic energy loss rate per unit volume by summing over all collisions with the use of the velocity distribution functions for the electrons and the heavy species. They assume that the atomic species have an isotropic distribution and that $m_e/m_a \ll 1$.

If, in addition, we assume that the electron distribution function is Maxwellian to the first approximation, then the rate of energy loss per unit volume from the electron component to the atomic species m is

$$\dot{\Omega}_m = \frac{8}{3}\frac{m_e}{m_m}(\varepsilon_e - \varepsilon_m)N_e\bar{\nu}_m \tag{13}$$

where

$$\bar{\nu}_m = N_m\bar{c}\bar{Q}_m = N_m\bar{c}\int_0^\infty \frac{Q_m\{\xi\}\xi^2 e^{-\xi}d\xi}{2} \quad . \tag{14}$$

Here, $Q_m(\xi)$ is the momentum transfer cross section for elastic electronic collisions with species m. If the species m is an ion, then $Q_m(\xi)$ is the Coulomb cross section given to a good approximation, as in eqn. (10), by

$$Q_c(\xi) \simeq 2\pi\left(\frac{e^2}{2kT_e\xi}\right)^2 \ell n\left[\frac{9(kT_e)^3}{8\pi N_e e^6}\right] \tag{15}$$

when $\xi \equiv \frac{1}{2}\frac{m_e c^2}{kT_e}$.

Summing over all species, we obtain the total rate of elastic energy loss per unit volume:

$$\dot{\Omega} = \Sigma_m \frac{8}{3}\frac{m_e}{m_a}(\varepsilon_e - \varepsilon_a)N_e\bar{\nu}_m \quad . \tag{16}$$

For the argon-potassium plasma, the masses of argon and potassium are nearly equal and are represented by m_a to give

$$\mathring{\Omega} = \frac{8}{3}\frac{m_e}{m_a}(\varepsilon_e-\varepsilon_a)N_e\,\Sigma\bar{\nu}_m \quad , \tag{16a}$$

or, for this case, in terms of the conductivity expressions which were presented in equations (8) and (10) of Section III-C.

$$\mathring{\Omega} = \frac{m_e}{m_a}(\varepsilon_e-\varepsilon_a)N_e\left[\left(\frac{e^2N_e}{m_e}\right)\left(\frac{64}{3\pi}\frac{\gamma_E}{\sigma_s}+\frac{64}{9\pi}\frac{\Sigma_n N_n \bar{Q}_n}{\Sigma_n N_n Q_n}\cdot\frac{1}{\sigma_c}\right)\right] . \tag{17}$$

E. Steady-State Radiation Losses

The net effect of inelastic electronic collisions as an energy loss mechanism from the free electrons can be accounted for at the steady state by calculating the total local radiative energy loss from the plasma due to free-free, free-bound, and bound-bound transitions, as discussed at the beginning of this section. This is valid only when the populations of the excited states and the continuum are determined essentially by radiative and electronic collisional processes. Detailed results, and a discussion and interpretation of the many assumptions made in accounting for these inelastic energy losses, are included in Appendix B ; however, brief mention of the principal assumptions will be made here.

The populations of the excited states of potassium were assumed to be in thermal equilibrium at the electron temperature. All densities and temperatures were assumed uniform throughout the plasma volume. The contributions to the total radiant energy loss due to free-free and free-bound transitions were calculated to be negligible compared to that of the bound-bound transitions. The geometrical shape of the plasma and the use of the mean beam length concept in estimating radiation losses is discussed in Appendix B.

The spectral line widths for the plasmas considered here are primarily fixed by dispersion broadening due to Lorentz and quadratic Stark effects, as well as by Doppler broadening. Broadening due to quadratic Stark effects was originally calculated by the approximate impact theory formula given by Margenau[21], but recently Griem[22] has calculated Stark broadening parameters for potassium in a more exact fashion, and use was therefore made of his calculations. The differences in calculated total radiation from the plasma between the two methods turned out to be negligible. Line widths due to Doppler and Lorentz broadening were computed by conventional formulas. The effective half-widths for dispersion broadening were assumed to be the sums of the Lorentz and Stark half-widths. Transition probabilities were taken from many sources[23]. Experimental data exist for the lines of primary importance and agree quite well with theoretical values found by the method of Bates and Damgaard[24].

The method of calculation of line radiancies utilized the well-known "curves of growth" valid for the case of combined Doppler and dispersion broadening effects, as outlined by Penner[25]. Calculations of total radiancies were carried out for transitions between the lower states of potassium. This included about 75 lines due to s-p, p-d, and d-f transitions, and for $2200 \leq T_e \leq 3500^{\circ}K$ and $0.002 \leq n_K/n_A \leq 0.008$. These calculations were performed at gas temperatures of 1500 and $2000^{\circ}K$, and for helium-potassium and argon-potassium systems. These calculations were extensive enough to demonstrate that the contribution from the omitted higher spectral

transitions is completely negligible for these conditions. It should be pointed out that over this temperature range, roughly 70 per cent of the total radiation could be accounted for by the resonance transitions from the 4p level of potassium. Further, the primary source of line broadening was that due to collisions by neutral argon. The calculation details are presented in Appendix B , along with the calculated results.

F. Nonuniformities in Plasma Properties

The theoretical description used throughout this study has been developed with the assumption that all plasma properties are uniform throughout the plasma volume. In some region very near the plasma boundaries, nonuniformities will be large because of gradients in the translational gas temperature, the diffusion of electrons and ions to the walls, and the radiative transport of energy from the plasma. The validity of a theoretical treatment based upon uniform properties depends on how accurately one can characterize a given plasma property in terms of its volume average or bulk value, which one measures experimentally.

We should note here that the mean free paths for the various interactions between plasma species are all much less than a characteristic plasma dimension and that diffusion losses to the walls are much less than measured volume recombination rates. Further, over the theoretically described experimental region, the populations of the various excited states are determined essentially by electronic collisional processes rather than radiative processes, and that even

in those ranges where radiative depopulation may be important, the effective average mean free path for a substantial fraction of the radiation leaving the plasma is much less than plasma dimensions (see Appendices B, C). Thus it is reasonable to treat the plasma properties as varying in a continuous manner with local properties given in terms of a local energy balance. Appendix C gives estimates of the effects of nonuniformities based upon experimental translational gas temperature measurements and approximate local energy balance calculations. These calculations indicate that the characterization of plasma properties by the bulk value should be valid and that local values of electron and translational atom temperatures are within 10 per cent of the bulk values over nearly all of the cross-sectional area. Thus the approach used throughout this study has been to interpret the quantities, such as electric field, conductivity, electron density, etc., appearing in the equations to be bulk values, not local values. The energy balance expressions can then be interpreted to give volume averaged rates of change.

Some additional comment should be made concerning the influence of nonuniformities upon the radiative loss calculations. These calculations have been intended to apply to plasma conditions where the electronic collisional processes determine the populations of the excited states and where the influence of radiative transitions can be neglected in this regard. Thus the primary sources of nonuniformity will not be radiative depopulation, but instead, gradients in translational temperature, as well as electron and ion diffusion to the walls will determine these nonuniformities. This results in a major

simplification in the radiative transfer calculation; for when radiative depopulation influences can be neglected, one can perform a uniform property calculation of the radiative loss with the same degree of confidence that one has in relating a uniform electron temperature calculation to a bulk electron temperature measurement, for example.

An additional simplification has been employed in the radiative transfer calculation. The energy balance derived in this section applies locally in the plasma, and the radiative loss term $\mathring{R}$ is the local rate of loss of energy per unit volume from the plasma. For the purpose of this analysis, the calculation of the detailed radiation from each local plasma element is not relevant, since we intend to characterize all experimental results by a bulk measurement of a given quantity and relate this experimental value to a theoretically calculated uniform quantity. Thus, it is perfectly consistent to estimate the total radiative loss from the plasma volume assuming uniform properties and then divide by the plasma volume to obtain a volume-averaged value of $\mathring{R}$ to employ in the electron energy balance.

A final comment on the radiative loss term should be made. The general approach used here is applicable to systems where both electronic collisional processes and radiative processes determine excited state populations. That is, the radiative loss calculation would still be useful in estimating net electronic inelastic-collision energy loss rates in steady-state plasmas. However, when electron densities are low enough so that radiative processes become im-

portant in fixing energy level populations, then appreciable radiative depopulation and appreciable radial nonuniformity of excited state populations may result. A specification of the populations of these excited states would require a detailed knowledge of the electronic collisional rate processes which couple with the radiative processes to determine the steady-state populations. An estimation of the local radiative loss term then becomes extremely difficult to make, and the approximations that have been useful in this analysis are no longer valid. Further discussion of the radiation calculation and approximations are given in Appendix B.

IV. STEADY STATE DESCRIPTION OF A PLASMA UNDER THE INFLUENCE OF A CONSTANT ELECTRIC FIELD

A. The Steady-State Two-Temperature Plasma Model

This section will recapitulate the preceding discussion and interpret the findings in terms of a physical plasma model valid for the steady state condition described by eqn. (3), when initial ionization transients have terminated.

Under certain conditions, energy inputs to the free electrons in the plasma can cause the energy of the electrons to significantly exceed the translational energies of the atomic species. The reason for this is that a large portion of the energy input to the free electrons may be lost by elastic collisions with the neutral and ionized atomic species. The rate of energy transfer by elastic collisions with a given atomic species is approximately proportional to the ratio of the electronic mass to that of the given atomic species multiplied by the average difference in energy between the electrons and the heavy species. Thus, for a sufficiently large elastic energy loss rate, the very small values of the mass ratio will mean that an appreciable translational energy difference must exist between the electrons and the atomic species.

Under conditions in which electron-electron interactions are sufficient to ensure the existence of a Maxwellian distribution of electron energies, as discussed in Appendix C, then it is meaningful to speak of an electron temperature as well as an atomic translational temperature. Thus, in this condition, we have a two-temperature plasma with the electrons at a temperature elevated above the trans-

lational temperature of the heavy species. The concept of a two-temperature plasma was applied to electron diffusion through gases some time ago, e.g. ref. 26. However, application of this model to the present problem was brought to the author's attention by the work of Kerrebrock[27], who further assumed that ionizational equilibrium at the electron temperature would exist in these seeded plasmas. Other authors[1, 28-30] have also motivated this study by their work concerning the description of two-temperature plasmas. Kerrebrock[46] first conjectured that radiation losses might be important in the electronic energy balance at low currents.

A two-temperature model describing the properties of a plasma in the steady state after the initial ionizational relaxation following the application of a steady electric field has been employed to interpret the experimental results presented here. This steady-state model assumes electronic collisional processes are sufficient to ensure thermal equilibrium between the free electrons and the bound states of potassium and that the electron temperature defining this condition is given in terms of an electronic energy balance including both elastic and inelastic energy loss mechanisms from the free electrons, as has been stated.

Several details of the model used here should be emphasized, as these factors were found to be essential in properly describing the experimental results. The elastic and inelastic losses are properly treated independently as two distinct physical processes. The inelastic losses can be determined for the steady state by a detailed plasma radiative loss calculation, as described in Section III-E, and this study will show that this calculation does appear to adequately

describe experimental plasma behavior over the range of validity of the calculations. This formulation employs no adjustable parameters; the elastic energy losses are formulated by expressing the various electron - heavy species interactions in terms of integrals over the electronic velocity distribution in terms of the fundamental momentum transfer cross sections of the various atomic species, as discussed in Section III-D. Electron-ion interactions, as well as electron-atom interactions, are treated in this elastic collision energy loss formulation.

Finally, the electrical conductivity entering into this formulation is also described in terms of integral expressions over the electronic velocity distribution function and reciprocal sums of the various cross sections. The resultant conductivity for the case of combined close and distant encounters is not exact, but the conventional reciprocal sum rule is felt to give a reasonable approximation to the conductivity under these conditions.

The remainder of this section will deal with a description of the calculation methods used to calculate the properties of the steady-state plasmas considered here.

B. Steady-State Calculations of Plasma Parameters

If we consider the steady-state condition described by equation (3), we can determine the electron temperature when the composition and temperature of the atomic species is known along with the relation between electron temperature and density given by equation (6), subject, of course, to the assumptions and justifications that have been discussed. In practice, it is more convenient to pick an electron

temperature and solve for N_e from equation (6), σ from equation (12), determine $\mathring{R}_s$ (see Section III-E), and finally solve for J and E from equations (3) and (17). In all calculations of interest here, the quasi-steady state can be assumed to have been established in times short compared with the time in which appreciable changes have occurred in T_a (see Section V-B). Hence, to a very good approximation, T_a is the initial temperature of the atomic species.

The integral expressions for electrical conductivity and elastic collision losses due to close encounters were evaluated numerically using the total scattering cross-section values of Ramsauer and Kollath[31] for argon, and those of Brode[32] for potassium. The cross sections used are shown as a function of energy in Figure 1. Unfortunately, these data give the total scattering cross section, whereas the momentum transfer cross section is required. However, in the range of electron energies of interest here, there is no pronounced forward or backward scattering, and there is probably less than a 10 per cent difference between the two cross sections[33].

The cross sections for helium in the range of interest do not show nearly as pronounced a variation with electron energy as is the case in argon and potassium, and in this case it was possible to use a mean value for the momentum transfer cross section. In making the calculations, a mean value of 5.1×10^{-16} cm^2 of the momentum transfer cross section for helium was used in agreement with the work of Gould and Brown[34] and that of Normand as discussed in ref. 34. Ramsauer and Kollath[35] obtained total cross-section values about 15 per cent higher than the total cross sections of Normand, as

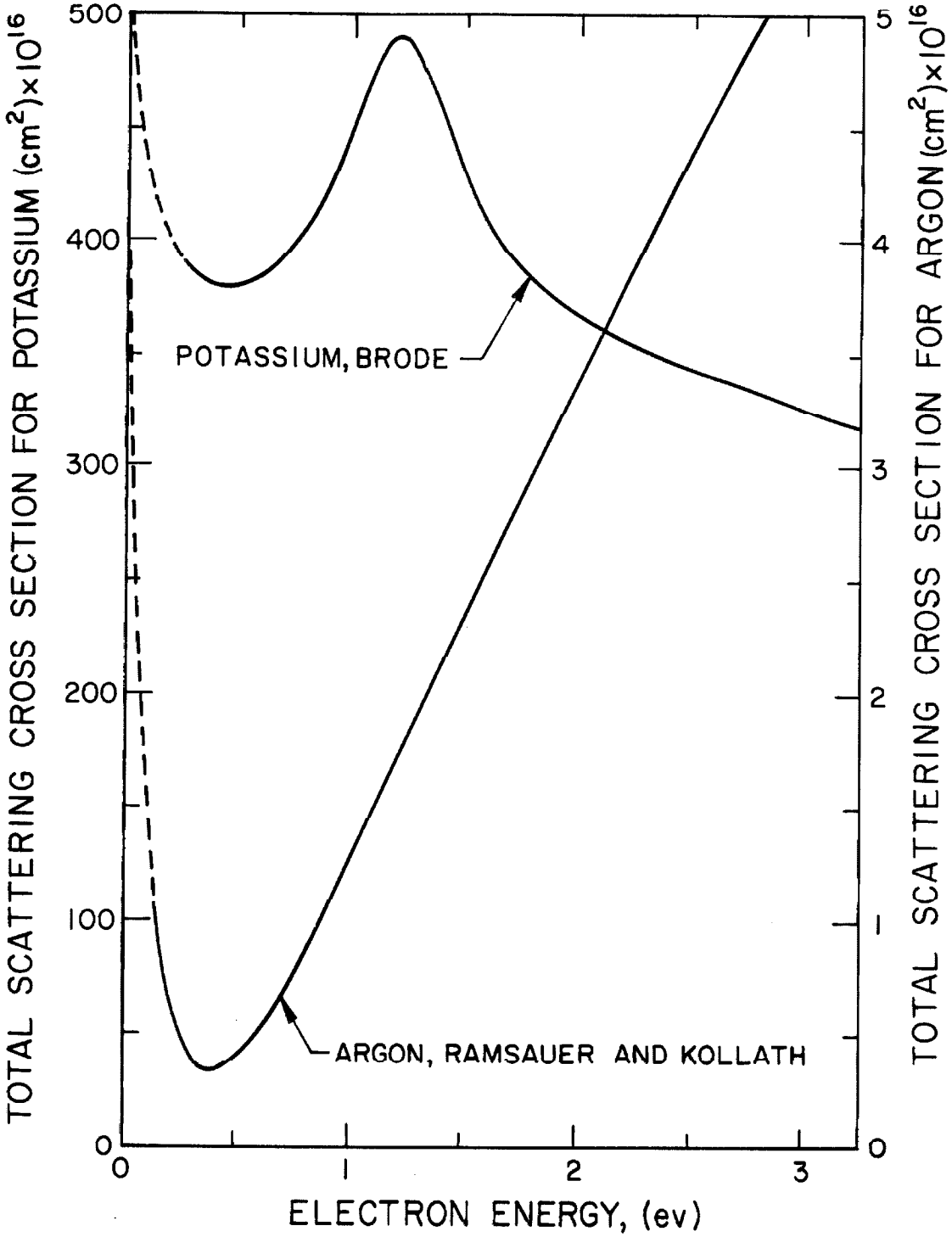

FIG. 1 ELASTIC COLLISION CROSS SECTIONS

shown in ref. 36. These values would give an average momentum transfer cross section of about 6×10^{-16} cm^2, and thus theoretical calculations were also performed with this value.

Values of the electrical conductivity and other parameters entering into its determination are given in Table I for the argon-potassium system for a wide range of electron temperatures, a potassium concentration, $n_K/n_A = .004$, and a translational atomic temperature, $T_a = 2000^oK$. Several results are of interest. First, consider the elastic collision energy loss term $\mathring{\Omega}$. Close encounter interactions dominate at the lower electron temperatures, but for higher electron temperatures, and hence higher degrees of ionization, the distant Coulomb encounters give the largest contribution to the total elastic collision energy loss rate. A similar situation exists with regard to the electrical conductivity, that is, at $T_e \approx 3100^oK$, the contributions to the electrical conductivity due to the close and distant encounters are about equal; but for higher electron temperatures, the Spitzer term dominates the conductivity expression.

Secondly, the radiation loss is small compared to the elastic collision losses when the current density is above 4 amp/cm^2 ($T_e \approx 2800^oK$). For current densities below 1 amp/cm^2, the radiation loss is dominant; and for much smaller currents, the assumptions made in the two-temperature model probably fail (see Section VII-A). Third, for the conditions studied here, the calculated values for close encounter conductivity obtained with the integral expression of equation (9) could be closely reproduced by the use of energy inde-

TABLE I

Argon - Potassium

$T_a = 2000^{\circ}K$, $n_K/n_A = 0.004$, Pressure = 1 atm.

T_e	$^{\circ}K$	2000	2200	2400	2600	2800	3000	3200	3500
N_e	$10^{14}/cm^3$	.060	.205	.57	1.34	2.85	5.35	9.46	19.0
σ_c	mho/cm	.063	.20	.54	1.22	2.5	4.5	7.6	14.5
σ_s	mho/cm	2.4	3.0	3.7	4.4	5.2	6.1	7.0	8.5
σ	mho/cm	.061	.19	.47	.96	1.68	2.58	3.65	5.35
$\mathring{\Omega}$	watts/cm^3	-	.085	.57	2.53	9.25	28.2	78.5	282
$\mathring{R}_s$	watts/cm^3	-	.86	1.6	2.9	5.1	8.6	14	26
J	amp/cm^2	-	.42	1.0	2.3	4.9	9.74	18.4	40.5
E	volts/cm	-	2.22	2.16	2.38	2.92	3.77	5.04	7.55

pendent cross sections of magnitude $Q_a = 0.70 \times 10^{-16}$ cm^2 for argon and $Q_k = 400 \times 10^{-16}$ cm^2 for potassium. However, the averaged cross sections that appear in the elastic energy loss terms of equation (16) had a stronger dependence on electron energy, and mean values could not be considered to give valid approximations to the integrated results.

For reference, theoretical values of electrical conductivity as a function of current density for various seed concentrations in the potassium-argon system are presented in Figures 2 and 3 for the case where inelastic losses are neglected. The influence of inelastic losses on these curves will be shown in Figures 12 to 20, when the experimental results are presented in Section VII-A. Also shown are tabulated values of the equilibrium electrical conductivity (i. e., when $T_e = T_a$).

Referring to the curves of Figures 2 and 3, we observe an interesting result. Note that a reduction in seed concentration, while keeping the current density constant, tends to increase the electron temperature and hence increase the electron density and electrical conductivity. This is of some practical importance, economically speaking, as one would desire MHD operation with minimum concentrations of alkali vapor in the working fluid. This result reflects the fact that,for these nonequilibrium plasmas, changes in the seed concentration at a fixed current density or fixed applied field strength result in significant changes in the electron temperature as required by the electronic energy balance when a large portion of the energy input to the electrons is lost by elastic collisions. Quantitatively, one

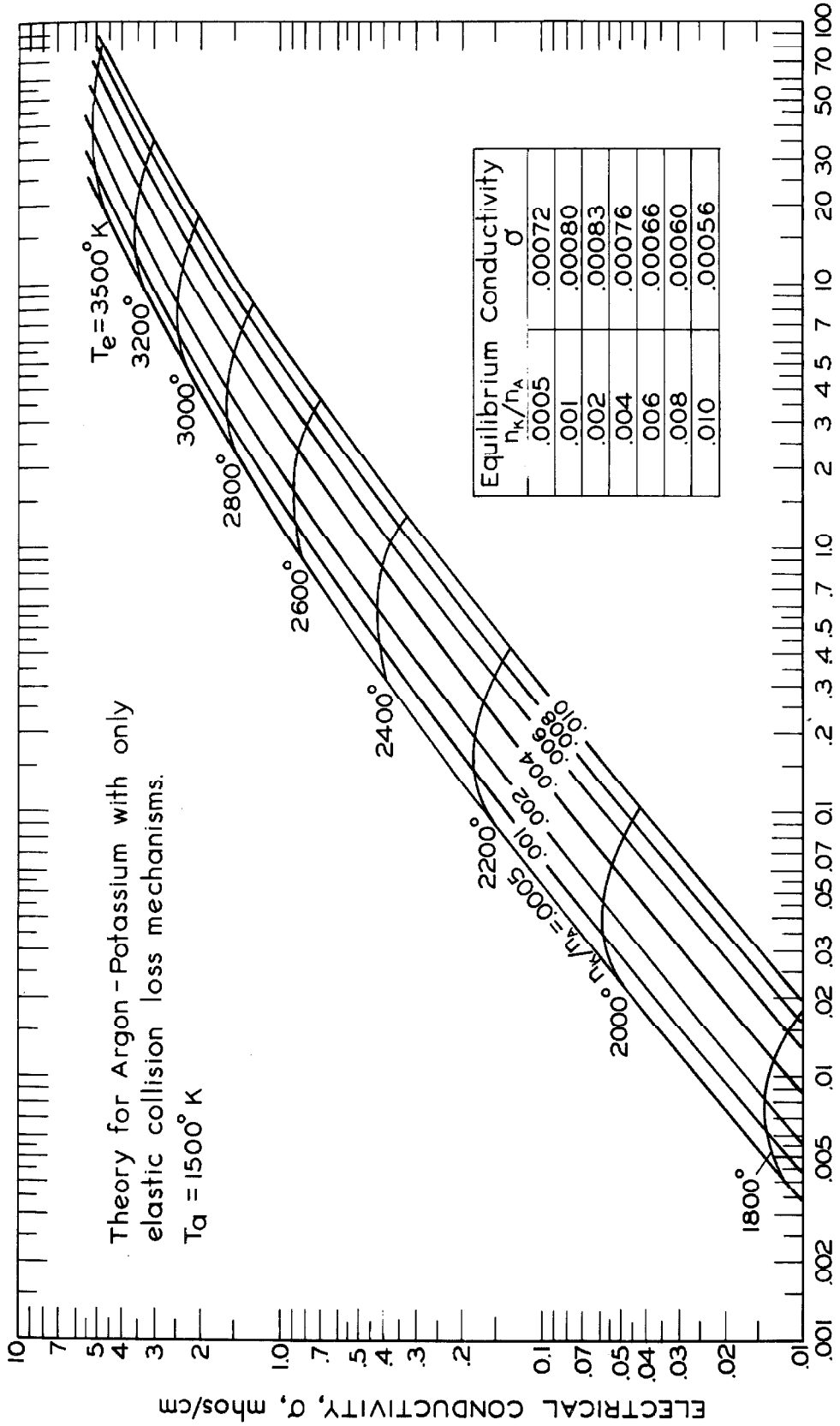

FIG. 2 ELECTRICAL CONDUCTIVITY FROM TWO-TEMPERATURE THEORY WITH ELASTIC ENERGY LOSSES ONLY

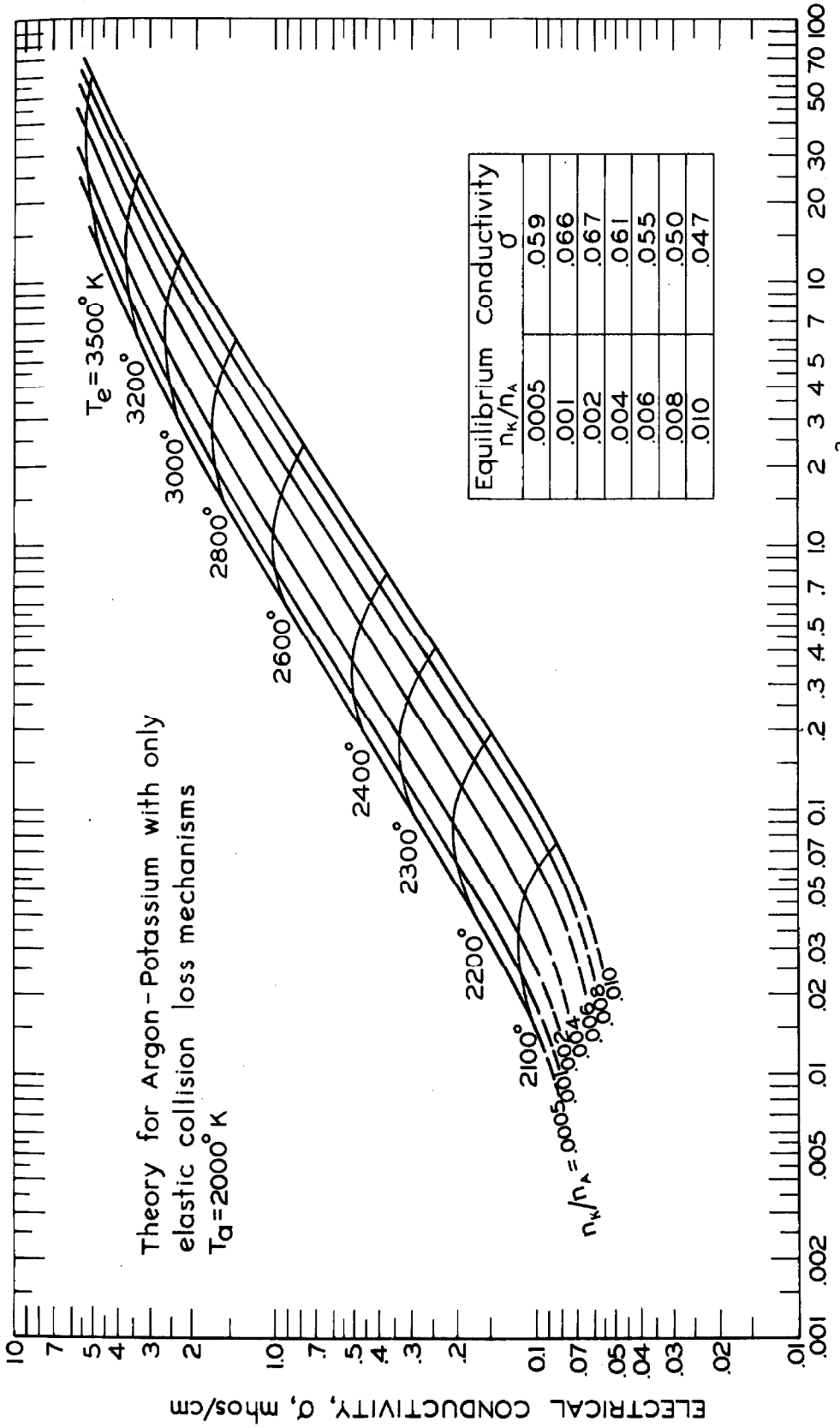

FIG. 3 ELECTRICAL CONDUCTIVITY FROM TWO-TEMPERATURE THEORY WITH ELASTIC ENERGY LOSSES ONLY

can try to determine if a critical value of seed concentration exists such that the conductivity is maximized when either the current density or electric field is kept constant. Calculations (Appendix D) show that as the seed concentration is reduced, for either constant current or constant field, that the electron density steadily increases with the increase in temperature and the seed approaches a fully ionized state. Further lowering of the seed concentration would then tend to reduce the electron density, provided the electron temperature is still not sufficient to produce significant ionization of the carrier gas. The surprising result is that the seed concentration can be reduced to extremely low values in these nonequilibrium plasmas and still obtain an increase in electrical conductivity for a given J or E. This is a completely different result from the results of an optimization of seed concentration assuming that gas and electron temperatures are equal and constant in value, as would occur in an equilibrium plasma, as discussed by Pinchak[37]. For the equilibrium case, an optimum value exists at relatively large values of seed concentration for the argon-potassium plasma. This is not the case for the nonequilibrium plasmas considered here, as stated above.

Practical difficulties may define some other criterion which fixes a minimum value on the seed concentration, however. Sheindlin, et al.[38] report a constricted, arc-like discharge occurring as the seed approaches the fully ionized state due to an unstable condition occurring from ionization of the carrier gas. Relatively large seed concentrations may also be necessary to provide a sufficiently large electron emission from cathode surfaces[39].

More discussion of the theoretical results and their relation to observed experimental behavior will be given with the experimental results presented in Section VII-A.

V. THEORETICAL DESCRIPTION OF PLASMA RELAXATION PROCESSES IN RESPONSE TO STEP CHANGES IN APPLIED ELECTRIC FIELD STRENGTH

The foregoing discussion has been directed primarily towards a plasma description in terms of a two-temperature model at the steady-state conditions existing at the end of the ionization transient following the application of an electric field to the plasma. This section will be devoted to a description of transient plasma behavior in terms of a similar simplified plasma model. The discussion will deal with both the recombination relaxation following an abrupt decrease in electric field as well as ionizational transients following step increases in electric field strength.

In order to analyze the transient behavior of a plasma, one must have a detailed knowledge of the reaction mechanisms and the various rate coefficients involved. Until recently, this knowledge was not extensive enough to allow a theoretical discussion of these transient processes except in a very crude, qualitative manner. Fortunately, with the recent development of the classical cross-section expressions of Gryzinski[8], it has been possible to formulate expressions for the rate coefficients for the electronic collisional processes occurring in high density plasmas similar to the ones studied here. These rate expressions have led to theoretical formulations of recombination and ionization processes in plasmas whose properties are determined by electronic collisional processes as well as radiative processes. Historically, the development has been

directed primarily towards the understanding of the recombination processes for which experimental data have been accumulated. Relatively little attention has been given to the reverse processes of ionization. The discussion here will begin with an analysis of the recombination process, and this formulation will allow consideration of a theory for ionization. These results will be quite useful in discussing the experimental work performed in this study.

A. Recombination

Extensive theoretical recombination formulations have been performed utilizing a model which includes recombination to excited levels by electron-electron-ion collisions, electronic collisionally-induced transitions between excited levels, as well as the radiative transitions between bound states. Careful experimental work has established remarkably good agreement between experimental results and theory for such differing atomic species as hydrogen, helium, and cesium[4, 6, 7, 40]. In addition, detailed theoretical calculations have been performed giving recombinations rates for argon and potassium[11].

There is no need to discuss here the details of the theoretical calculations performed by these several authors and others, but the physical model for the recombination process deserves some comment with regard to the principal assumptions and approximations used in order to relate experiment and theory. A short, informative discussion of these rate processes is given in ref. (41).

As mentioned in Section II , the electron temperature in high density plasmas quickly reaches a quasi-steady value given by an in-

stantaneous energy balance on the free electrons. A similar, and in fact directly coupled, phenomenon exists with regard to the population densities of highly excited states in the recombining plasma. The detailed classical formulation of electronic inelastic collisions indicates that the probability of a collisionally-induced transition between two neighboring atomic levels is inversely proportional to the square of the energy gap separating them. Thus, the number densities of those states most closely spaced adjust rapidly with the changes in electron temperature. In the recombining plasma, this means that the populations of those upper states nearest the continuum tend to come into a mutual quasi-steady collisional equilibrium with the free electrons, and, in addition, closely spaced lower levels reach a mutual quasi-steady equilibrium in times that are small compared to the time scale for changes in the populations of the free electrons and the ground state. This fact has resulted in an enormous simplification in the solution of the coupled rate equations describing the rate of change of the number density of the free electrons as well as the population of the infinite number of excited levels (see Section III-B). The result has been the reduction of an infinite set of coupled differential equations to a finite set of algebraic equations describing the populations of the various states and an equation describing the rate of change of the population of the free electrons and the ground state. Further requirements for this simplification, including that the population of a given level be much less than the free electron density in order for that level to be regarded as having a quasi-steady population, are discussed in detail by Bates, et al. [4].

The important physical result is that the upper levels and the free electrons tend to be in a quasi-steady mutual collisional (Saha) equilibrium, while the quasi-steady populations of the lower levels must in general be described by including the effects of radiative transitions between levels. Bates, et al. have performed detailed calculations for hydrogen and helium using this method, and the resulting rates and population densities have been confirmed experimentally by several authors[6, 7, 12].

Byron, et al.[10, 11] have shown that good results can be obtained with fairly simple calculations by treating the collisional recombination process as a chain of reactions in which the net rate of recombination can be described in terms of the slowest step in the chain. The physical picture consists of a reservoir of upper excited states in quasi-steady collisional equilibrium with the free electrons above a critical energy gap across which recombining atoms must pass to reach the ground state. The critical energy gap will be the one of all possible energy gaps across which the total de-excitation rate is a minimum. A minimum occurs since the probability of de-excitation of a given level will increase with increasing principal quantum number of the level due to more closely spaced gaps, while the populations of the various levels decrease with increasing principal quantum number. In addition, the total probability of radiative decay of a given level decreases with increasing quantum number.

The Byron formulation has the powerful advantage of being easily applied to atoms with arbitrary energy level structures which are not necessarily hydrogenic. This calculation technique has been

used here to obtain recombination rates for potassium in the range of interest of these experiments which occur at slightly higher electron temperatures than the maximum temperatures in the published results of Byron, et al.[11]. As justified in ref. 11, the rate of crossings in the upward direction across an energy gap U located above a level of binding energy E_k and coming from all initial energy levels with binding energies E_i $(E_i \geq E_k)$, to all possible final bound energy states as well as the continuum can be written as

$$\left.\frac{dN}{dt}\right|_u = \sum_i \left.\frac{dN_i}{dt}\right|_u = \sum_i N_i N_e \bar{c}\, \frac{\sigma_o B_i}{(U+E_i-E_k)^2}\left(1+\frac{2kT_e}{U+E_i-E_k}\right)e^{-\frac{U+E_i-E_k}{kT_e}}$$

and writing

$$N_i = \frac{N_k g_i}{g_k}\, e^{(E_i-E_k)/(kT_e)},$$

$$\left.\frac{dN}{dt}\right|_u = N_e\left\{\frac{N_k}{g_k}e^{-U/kT_e}\right\}\bar{c}\,\sigma_o \sum_i \frac{B_i g_i}{(U+E_i-E_k)^2}\left(1+\frac{2kT_e}{U+E_i-E_k}\right) \qquad (18)$$

where $B_i = B_i\{E_i/(E_i-E_k+U)\}$ is the slope of the linear portion of the Gryzinski cross section, as given in Figure 2, ref. (11), $\sigma_o = 6.56\times10^{-14}$ cm^2, and $\bar{c}$ is the mean thermal speed of electrons, $\sqrt{(8kT_e)/\pi m_e}$. N_k and g_k are the number density and degeneracy, respectively, of the energy level with binding energy E_k (the subscript k used here corresponds to the subscript 1 used in reference (11)). N_e and T_e are the free electron density and temperature, respectively.

The summation is to be taken over all energy levels below

the gap ($E_i \geq E_k$) and avoids the necessity of assuming the levels below the gap to be continuous as is done in equation (2), ref. (11).

At equilibrium, the total rate of crossings of the gap in the upward direction must balance the total rate of crossings in the downward direction. Also at equilibrium $N_\ell / N_k = (g_\ell e^{-U/kT_e})/g_k$ where N_ℓ and g_ℓ are the number density and degeneracy, respectively, of the energy level with binding energy $E_k - U$ located immediately above the gap. Thus, at equilibrium

$$\left.\frac{dN}{dt}\right|_d = \frac{(N_{\ell\ \text{equil}})}{g_\ell} N_e \bar{c} \sigma_o \left\{ \sum_i \frac{B_i g_i}{(U+E_i-E_k)^2} \left(1 + \frac{2kT_e}{U+E_i-E_k}\right)\right\} \qquad (19)$$

where $N_{\ell\ \text{equil}}$ is given by

$$N_\ell = \frac{g_\ell}{g_e g_{ion}} \left(\frac{h^2}{2\pi m_e kT_e}\right)^{3/2} e^{+E_\ell/kT_e} N_e^{\ 2},$$

as in eqn. (5).

The minimum value of the total rate of downward crossings, $\left.\frac{dN}{dt}\right|_{d\,min}$, found by calculation from equation (19) for each energy gap can be related to the recombination rate. At this point, some difficulties are encountered. Equation (19) gives the total rate of crossings of the gap in the downward direction at collisional (Saha) equilibrium. However, to find the recombination rate to the ground state, one must subtract from this calculated rate such downward crossings between bound states above and below which are the result of atoms that are de-excited to a lower level, but instead of being eventually further de-excited to the ground state are again re-excited to a level above the gap. An additional complication is the fact that the actual recombination rate may be somewhat less than the total de-excitation

rate calculated at equilibrium, since N_ℓ may not in general be equal to its equilibrium value, $N_{\ell\ \text{equil}}$.

Byron, et al.[10, 11] have investigated these effects and have found that $\frac{dN_e}{dt} = \gamma \left.\frac{dN}{dt}\right|_{d\ min}$ where γ lies between 1/4 and 1. The latter value applies when the minimum is very pronounced, as at very high temperatures, and decreases to 1/4 if the minimum is not well defined, as at lower temperatures. For the temperature range of these experiments, $\gamma \cong 1/3$.

Calculations of $\left.\frac{dN}{dt}\right|_{d\ min}$ were performed for the low-lying levels of potassium to establish that for electron temperatures between 2000°K and 3000°K, the minimum de-excitation rate occurs for the gap lying below the lumped 6s and 4d levels and above the 5p level. Resulting values of the recombination rate coefficient, $\frac{-1}{N_e^3}\frac{dN_e}{dt}$, calculated with $\gamma = 1/3$ for $2000^\circ \leq T_e \leq 3000^\circ$K are shown in Figure 25. The recombination rate coefficient calculated at 2000°K agrees well with the value at 2000°K in ref. 11. Also shown in Figure 25 are the values for cesium as calculated in a more exact fashion with an extensive computer program by Dugan[40]. Note that the calculated rates for cesium and potassium are nearly equal, which would be expected judging from the similarity of their energy level structures.

At no point in the foregoing calculations have the effects of radiative transitions upon the recombination rate appeared explicitly. Such radiative transitions can cause non-equilibrium populations in the levels immediately above the gap. This effect should be considered in addition to the non-equilibrium effects resulting from the fact

that quasi-equilibrium may not have been established because of the relatively long times required for this condition to be established in low-lying states. The factor γ could be interpreted to include all non-equilibrium effects, including radiative depopulation; however, one must still include the possibility of direct radiative recombination when calculating the total rate of recombination. The radiative recombination rate for hydrogenic atoms can be written[42] as $\alpha_r \cong 2.7\times10^{-13}/(kT_e)^{3/4}$ cm^3/sec, and the radiative recombination rate for potassium should not be substantially different. Thus, at $T_e = 2500^oK$, $kT_e \approx 0.215$ ev, and we find $\alpha_r \cong 9\times10^{-13}$ cm^3/sec. Measured values of $\alpha = -\frac{1}{N_e^2}\frac{dN_e}{dt}$ from these experiments are of the order of 10^{-10} cm^3/sec, and hence, direct radiative recombination appears to be negligible.

The effects of diffusion of ions to the walls as well as recombination by the dissociation reaction $K + K \rightleftharpoons K_2^+ + e^-$ are assumed negligible for the densities and temperatures of these experiments. Estimates of the mobility of K^+ in K and K^+ in A, the former based on that for Cs^+ in Cs,[43, 44] indicate diffusion losses to be small compared to measured recombination rates. The very small concentrations of the molecular ions at these temperatures and seed concentrations make dissociative recombination improbable. Harris[45] has reached similar conclusions based on his calculations and measurements in cesium for conditions of temperatures and densities approximating those encountered here. Finally, it should be mentioned that the inert gas plays no appreciable role in the ionization and recombination processes studied here due to its relatively high ioni-

zation potential and the relative inefficiency of atom-atom excitations and ionizations. See Appendix C for further discussion of these approximations.

Energy Balance for Recombination. In order to analyze the recombination data, one must have some means of determining the electron temperature during the relaxation process. The electron temperature and electron density are not independent quantities since an energy balance on the free electrons defines their instantaneous temperature for a given instantaneous electron density, as has been discussed in Section III-A. During the initial steady state before the drop in electric field has been initiated, the electron temperature is defined by a balance between energy input from the electric field and energy loss due to elastic collisions, as well as inelastic collisions, as has been discussed in Section IV-A.

After the abrupt reduction of the electric field, the electron energy loss terms temporarily exceed inputs to the free electrons and cause the electron temperature to decrease. As the electron temperature falls, the rates of recombination and de-excitation exceed those of ionization and excitation. For the electron densities of interest here, the electrons can exchange energy with the heavy species by elastic and inelastic collisions in times much shorter than those associated with changes in the population of the free electrons. This results in the rapid establishment of a quasi-steady condition in which the instantaneous electron temperature is given by an energy balance. The important energy inputs are a result of electronic collisional recombinations and de-excitations and the acceleration of

electrons by the small remaining applied field. The important energy losses are due to electronic excitations and ionizations, and to elastic collisions with the neutral and ionized heavy species.

The quasi-steady energy balance is given in Section III-A as

$$N_e \cancel{\frac{d\epsilon_e}{dt}}^{\approx 0} = \sigma E^2 + \left\{ \left[-(\epsilon_e + V_o) \frac{dN_e}{dt} - \sum_i V_i \cancel{\frac{dN_i}{dt}}^{\approx 0} \right] - \mathring{R} \right\} - \mathring{\Omega} \qquad (20)$$

where the various terms are defined as in equation (2). If the populations of the excited states are also quasi-steady in addition to the electron energy, as has been assumed in the recombination model discussed in the last section, then the $V_i \frac{dN_i}{dt} \approx 0$. This equation neglects the possibility of radiative recombination, as has been justified in the preceding discussion, and $\mathring{R}$ represents the total rate per unit volume at which radiation from bound-bound transitions is lost from the system (see Section III-A).

The above considerations give the electron temperature in terms of measurable experimental quantities. This data reduction procedure is presented below for completeness. It should be noted that currently available experimental techniques for directly measuring electron temperatures in a transient plasma typically do not exhibit the good accuracy desirable for recombination coefficient determinations. This circumstance is a justification for the somewhat indirect calculation procedure that has been employed here in determining the electron temperature during the recombination process.

Data Reduction. The directly measured quantities during the relaxation period immediately following the abrupt reduction in field

strength are the electric field and current density as well as the relative populations of the various transitions in potassium which were observed spectroscopically. From these quantities, we compute the electrical conductivity as a function of time and the number densities in the upper states of the observed transitions. The latter are obtained from the measured relative changes in population and from the measured initial conditions.

In order to determine the electron density and electron temperature, one must solve the equation for the quasi-steady energy balance on the free electrons given in equation (20) simultaneously with the expression for the non-equilibrium electrical conductivity as given in equation (12).

The calculation was carried out numerically using an iterative scheme. The first step was to obtain an initial estimate of the value for the electron density from the measured instantaneous value of the conductivity. In making this calculation, it was found that a good first approximation could be obtained by using the steady state relationship between the non-equilibrium conductivity and the electron density. Given this estimate for the electron density and the measured values of the relative populations of the excited states, it is possible to solve the quasi-steady electron energy balance equation for the electron temperature. This value for the electron temperature is then used to obtain a more accurate value for the electron density from the conductivity expression, and the process is continued until suitable convergence is achieved. Usually, one or two iterations are sufficient for the accuracy desired in these cal-

culations. The various terms in the quasi-steady energy balance equation must be evaluated from the experimental data. The evaluation of these terms is discussed in Section VII-C.

B. Ionization

The analysis of the ionization process following a step increase in electric field strength can be performed with a simplified physical model, as was done for the recombination process treated above.

We again consider the physical plasma model valid after quasi-steady conditions have been established in the relaxing plasma. In this condition, the upper levels above a critical energy gap again tend to be in a quasi-steady, mutual (Saha) equilibrium with the free electrons defined as in equation (5). The various lower levels below the critical gap, however, rapidly reach a quasi-steady condition in which the populations of these various low-lying levels tend to be in mutual electronic collisional equilibrium with the ground state population at the instantaneous electron temperature when radiative depopulation effects can be ignored. This condition is defined by the relation

$$\frac{N_i}{N_1} = \frac{g_i}{g_1} e^{-V_i/kT_e} ,$$

where V_i is the excitation energy of the i^{th} level with respect to the ground state, and N_i and N_1 are the number densities of the i^{th} state and the ground state, respectively. The respective degeneracies of these states are g_i and g_1. Thus we have essentially two quasi-steady "equilibrium" conditions maintained separately due to

their isolation caused by the slow rate of excitation across the critical gap.

The differences between these two population distributions should be emphasized for clarity. Upon abrupt application of the electric field, the electron temperature rises rapidly and the low-lying states are populated relatively rapidly by electronic collisions to establish thermal equilibrium between themselves and the ground state at the instantaneous electron temperature. Simultaneously, the closely-spaced high energy levels located near the continuum tend to be in a mutual collisional equilibrium with the free electrons at the instantaneous electron temperature, as defined in terms of the instantaneous electron density (not necessarily the electron density corresponding to complete thermal equilibrium at the instantaneous electron temperature). Transitions across the critical gap occur on a relatively longer time scale and the total rate of ionization is limited by this critical rate of upward crossings of the critical gap. At the end of the ionizational transient the populations of the excited states and the density of the free electrons tend to be in complete thermal equilibrium at the final electron temperature, provided radiative depopulation effects can be ignored.

Using the calculations of Section V-A, we find from equation (18) that when the population of the energy level immediately below the critical gap is essentially given by the condition of collisional equilibrium with the ground state, then the total rate of crossings in the upward direction across an energy gap U is given in terms of the population of the ground state by

$$\frac{dN}{dt}\Big|_u = N_e \left\{ \frac{N_1}{g_1} e^{-\frac{U+V_o-E_k}{kT_e}} \right\} \bar{c}\sigma_o \sum_i \frac{B_i g_i}{(U+E_i-E_k)^2} \left(1 + \frac{2kT_e}{U+E_i-E_k}\right) \quad (21)$$

where N_1 and g_1 are the number density and degeneracy of the ground state, respectively. From the discussion of the preceding section, the total rate of ionization is given by

$$\frac{1}{N_e}\frac{dN_e}{dt} = \frac{\gamma}{N_e}\frac{dN}{dt}\Big|_{u\,min} \quad (22)$$

where $\frac{dN}{dt}\Big|_{u\,min}$ is the minimum rate of excitation across the critical gap. Here, γ is interpreted to account for non-equilibrium effects and the subtraction of such upward crossings between bound states across the critical gap which are the result of atoms that are excited to a higher level, but instead of being then further excited and finally ionized, are again de-excited to a level below the gap. The factor γ will again be regarded as having the approximate value 1/3 for the conditions of these experiments.

Combined Ionization and Recombination. Near the end of the relaxation transients, both ionization and recombination processes are important, and it is useful to have an expression for the rate of change of electron density for this case. The foregoing expressions for ionization and recombination rates can be combined to give the following result for the net rate of change of electron density.

$$\frac{dN_e}{dt} = \gamma N_e \left\{ \frac{N_1}{g_1} e^{-\frac{U+V_o-E_k}{kT_e}} \right\} \left[1 - \left(\frac{N_e}{N_{eq}}\right)^2\right] \bar{c} \left[\sigma_o \sum_i \frac{B_i g_i}{(U+E_i-E_k)^2} \left(1 + \frac{2kT_e}{U+E_i-E_k}\right)\right]. \quad (23)$$

where the right hand side is evaluated for the critical gap.

Note that the relative importance of recombinational processes relative to ionizational processes is given by the ratio $(N_e/N_{eq})^2$ where N_{eq} is the electron density corresponding to collisional equilibrium conditions at the instantaneous electron temperature. The ionizational transient can be analyzed with consideration of only the forward rate when $(N_e/N_{eq})^2 \ll 1$; the recombinational transient can be analyzed by considering only the recombination rate when $(N_e/N_{eq})^2 \gg 1$. These considerations will be useful in analyzing the data presented in this work. Note that during an ionizational transient that even when the electron density has increased to $(1 - 1/e)$ of its final value, that the net rate of ionization is still 60 per cent of the forward rate.

For completeness, and to illustrate the magnitude of the rates involved, electronic collisional ionization profiles have been calculated for various constant electron temperatures in the range $2200 \leq T_e \leq 3500^{\circ}K$ for a potassium concentration of .004 and $T_a = 2000^{\circ}K$, and are given in Figure 4. Figure 5 gives the ionization rate, $\frac{1}{N_e}\frac{dN_e}{dt}$, as a function of electron temperature (see discussion below eqn. (21)). Calculations of more direct interest for the experiments discussed here are presented in the following section.

Discussion of the Ionization Process. Before presenting the experimental data, a brief discussion of the transient plasma is useful.

The formulation of the ionizational transient as given shows that for the dense, electron-collision dominated plasmas considered here, that ionization occurs by a multi-step process. It is inaccurate to regard ionization as occurring in one step in which an electron

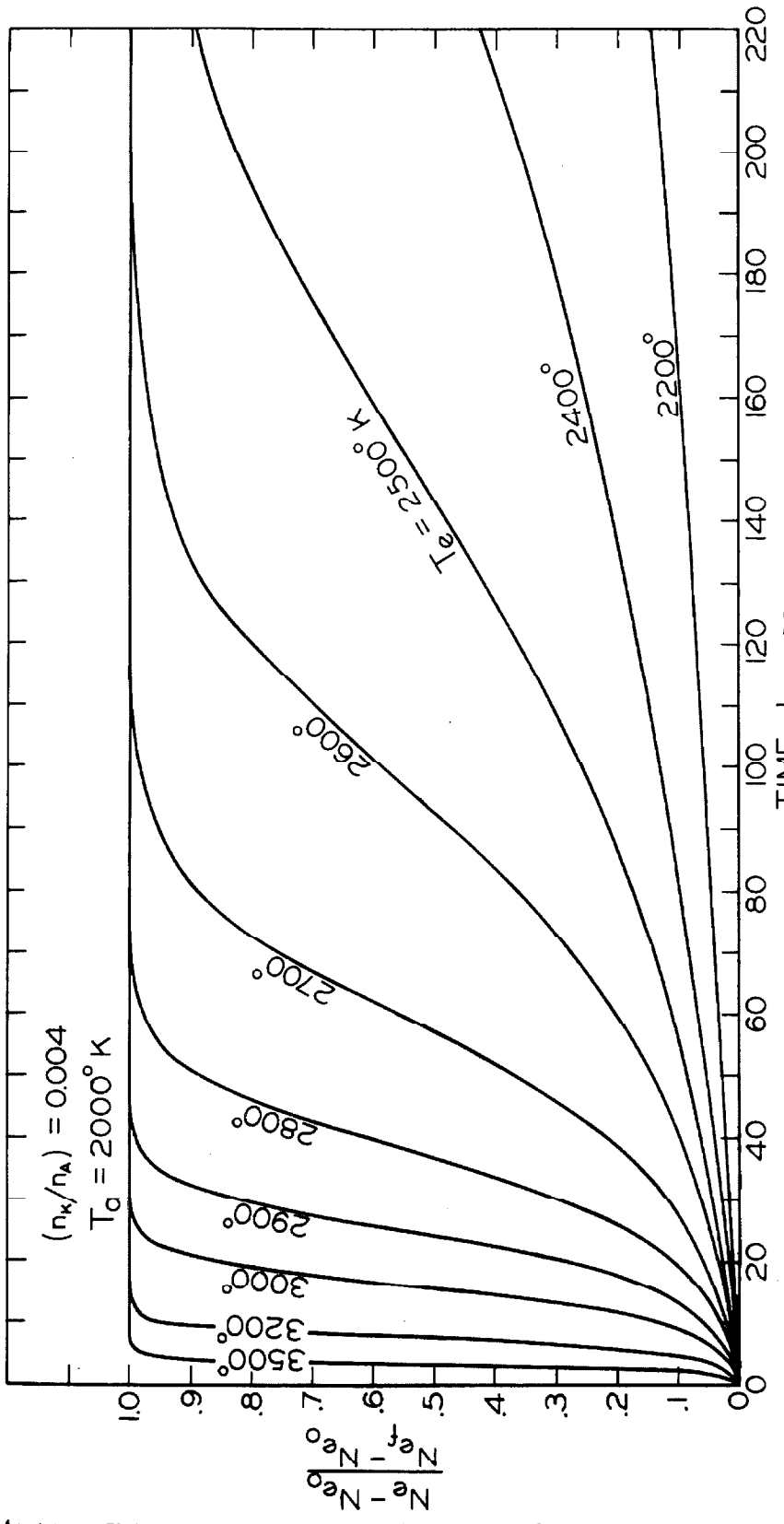

FIG. 4 ELECTRONIC COLLISIONAL IONIZATION PROFILES FOR POTASSIUM

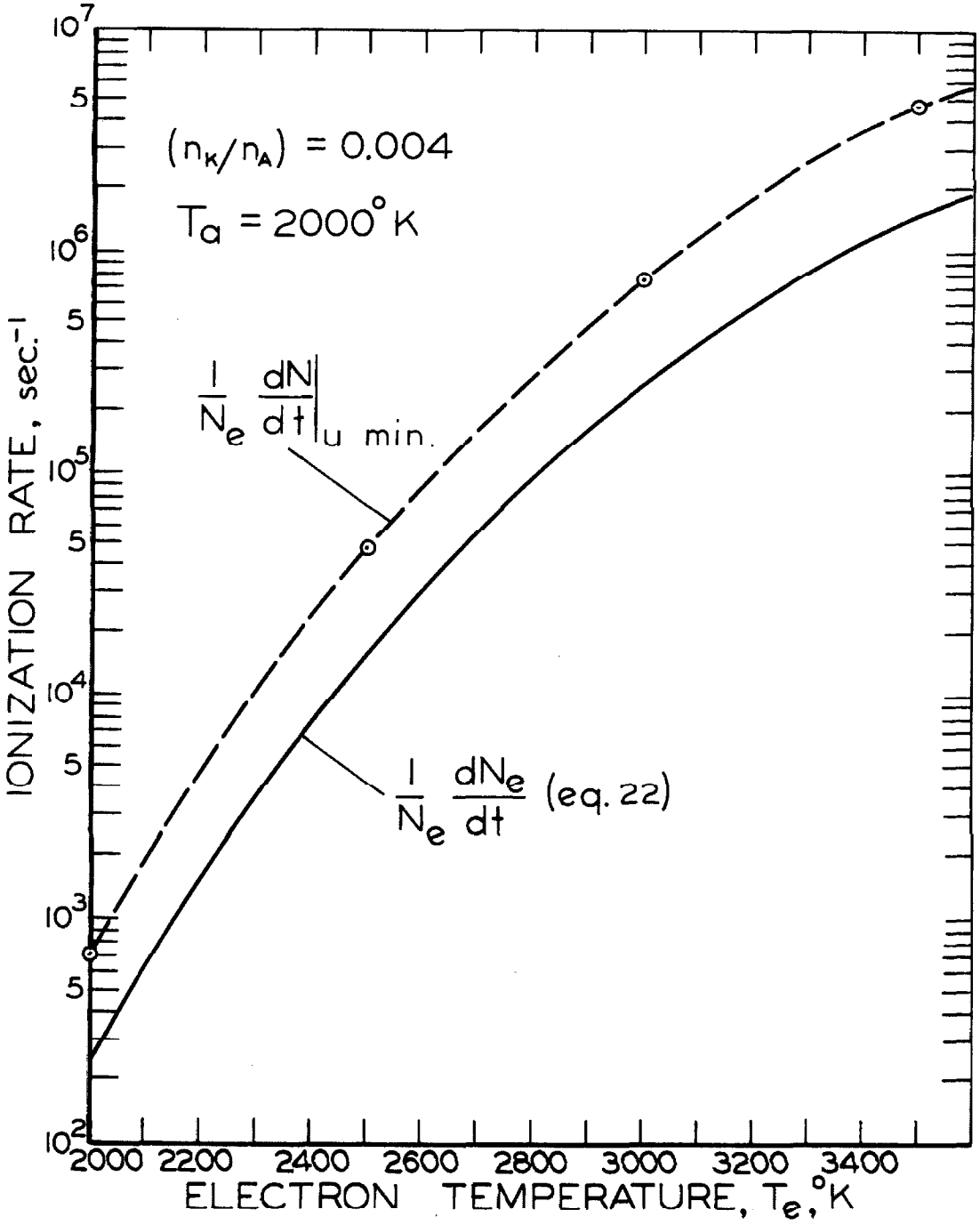

FIG. 5 IONIZATION RATE AS A FUNCTION OF ELECTRON TEMPERATURE FOR POTASSIUM

collides with an atom in its ground state and thereby immediately ionizes the atom. The Gryzinski classical cross-section expressions used here show that the probability of a collisionally-induced transition between two neighboring atomic energy levels is inversely proportional to the square of the energy gap separating them, thus making multi-step collisional processes much more probable than single-step processes. When a well-defined critical gap occurs which limits the overall rate of ionization, the correct activation energy for the ionization process is essentially the energy difference between the energy level immediately above the critical gap and the ground state. Neglect of this consideration can lead to large errors in the calculation of ionization rates.

As an example, for conditions of these experiments, $2000 \leq T_e \leq 3000^{\circ}K$, the energy level lying immediately above the critical gap is .94 ev below the continuum, and thus the effective activation energy is 3.40 ev instead of 4.34 ev. At $T_e = 3000^{\circ}K$, or .258 ev, the multi-step ionization rate, $\frac{1}{N_e}\frac{dN_e}{dt}$, is about 40 times faster than one would calculate using only a single-step process. For higher electron temperatures, the difference can be much larger, and at high enough electron temperatures ($T_e \gtrsim 5000\ ^{\circ}K$), the effective activation energy is reduced to the excitation energy of the first excited state (1.61 ev).

Some further comment should be made about the phenomena occurring during ionization in the plasmas discussed here which have been described in terms of a sequence of events following an abrupt application of electric field to the plasma. First, the electrons are

assumed to heat to some elevated temperature limited by elastic and inelastic collision losses from the electrons. The second phase is one in which transient inelastic rate processes occur and the population levels increase during an ionizational relaxation period. The final phase is established when the ionizational transient is terminated and the net changes in population levels are essentially zero. In this condition, the plasma is in a steady state with most of the energy input to the electrons being transferred into the translational energy of the heavy species.

This picture is verified by an analysis of the various terms in the electronic energy balance when radiative losses and the $\Sigma V_i \frac{dN_i}{dt}$ can be neglected. Equation (2) can be rearranged to give

$$\frac{\sigma}{N_e} E^2 = (V_o + \epsilon_e) \frac{\dot{N}_e}{N_e} + \dot{\epsilon}_e + \frac{8}{3} \frac{m_e}{m_a} (\epsilon_e - \epsilon_a) \sum_m \bar{\nu}_m \quad . \tag{24}$$

We consider the potassium-argon system and analyze this equation to obtain several time constants.

First, assume that all the energy initially goes into heating the electron gas. That is, examine the rate of change of electron energy before its quasi-steady value defined by the balance between electron energy input and energy loss terms has been achieved. Then the first and third terms on the right hand side of equation (24) can be ignored, and the simplified equation shows that the time required to double the electron thermal energy is found to be about 1/10 microsecond for an electric field of 5 volts/cm and is shorter for higher fields.

This initial temperature rise is limited by the elastic and in-

elastic electron energy loss terms which increase rapidly as the electron temperature increases. We now ask how long it takes the electron energy to become established in a quasi-steady fashion assuming that ionization is negligible. Then the first term on the right side of eqn. (24) can be ignored, and the simplified equation can be integrated, assuming that changes of electron energy are not too large ($\Delta\varepsilon_e \sim 0\{\varepsilon_a\}$). The relaxation time for the establishment of the new electron temperature is found to be given by an average value of $1/(\frac{8}{3}\frac{m_e}{m_a}\Sigma\bar{\nu}_m)$, and is less than 3 microseconds for the conditions of these experiments. Now since $\frac{\sigma}{N_e}E^2\Big|_f = \frac{8}{3}\frac{m_e}{m_a}(\Delta\varepsilon_e)\Sigma\bar{\nu}_m\Big|_f$ for this case, then for $\Delta\varepsilon_e \sim 0\{\varepsilon_a\}$, the relaxation time may be roughly stated to be equal to an average value of $\frac{N_e\varepsilon^*}{\sigma E^2}$ where $\varepsilon^* \sim 0\{\varepsilon_e\}$.

Similarly, assume that all the available energy after the step application of the constant E field goes into the ionization process. The second and third terms on the right side of (24) are neglected, and the resulting integration indicates that the relaxation time (now defined as the time required for $\frac{\Delta N_e}{\Delta N_{e_f}}$, instead of $\frac{\Delta\varepsilon_e}{\Delta\varepsilon_{e_f}}$ as above, to reach $1 - \frac{1}{e}$) is proportional to an average value of $(N_e V_o/\sigma E^2)$. For fields of the order of 3 to 10 v/cm, the relaxation time was found to be in the range of 6 to 12 times the initial value of this quantity, given by $N_{eo} V_o/\sigma_o E^2$. For a field strength of 5 v/cm, a relaxation time of about 20 microseconds is obtained.

Note that $\frac{\sigma}{N_e}$ and hence the rate of energy input per electron (i. e., $\frac{\sigma E^2}{N_e V_o}$ if $\varepsilon_e \ll V_o$) does not change markedly except towards the end of the relaxation, when electron-ion interactions may be important.

Finally, consider the case that the electron density is approx-

imately constant and the whole gas is slowly heating up. Then the energy balance for the atomic species leads to the result that for a 10 per cent change in atomic species translational energy, a time of about 300 microseconds is required for a field of 5 v/cm.

These calculations suggest the following picture of the transient process. During the first few microseconds, the electrons absorb an appreciable fraction of the power and reach an elevated temperature. This phase ends when the rate of change of the energy of the free electrons is no longer large compared with other terms in the energy balance. After this initial rise, electron temperatures are determined by a quasi-steady energy balance between the power input to the electrons and the rate of energy loss from the electrons due to both inelastic and elastic collisions. During this phase, the ionizational relaxation occurs and the net rate of ionization depends upon the instantaneous electron temperature and density as related through the quasi-steady energy balance.

The discussion of characteristic times shows that under conditions when $\Delta\varepsilon_e \sim 0\{\varepsilon_a\}$, then the ionizational relaxation process has a characteristic time which is very roughly V_o/ε_e times longer than the characteristic time for the initial electron temperature relaxation*. At the end of the ionizational transient, recombination processes are important, and the net power input into the ionizational process is no longer large as the net rate of change of the electron density (and electron temperature as coupled through the quasi-

* The simplified discussion here is qualitative; energy inputs into the creation of excited state populations, and radiative losses have been ignored.

steady energy balance) becomes small. After this initial transient period, the temperature of the whole system slowly increases.

The above qualitative discussion indicates that the rate of ionization is the limiting factor in determining the length of the ionizational transient period for the electron temperatures of interest here. This discussion can be considered in a more quantitative way by performing approximate calculations of the changes in electron temperature and density during the ionization process by utilization of the rate expression of equation (23), along with a simplified quasi-steady electronic energy balance. If we can neglect radiative losses and the energy inputs into the creation of excited state populations as a first approximation, then the quasi-steady energy balance becomes

$$\frac{\sigma E^2}{N_e} = (V_o + \varepsilon_e) \frac{1}{N_e} \frac{dN_e}{dt} + \frac{\mathring{\Omega}}{N_e} \quad . \tag{25}$$

The omission of the $\Sigma V_i \frac{dN_i}{dt}$ and $\mathring{R}$ terms will not change the results qualitatively and should be valid provided these terms are in fact negligible compared to the loss terms on the right hand side of eqn. (25). The $\Sigma V_i \frac{dN_i}{dt}$ terms should be small after the quasi-steady state has been established (see Section V-A, and discussion in reference 4 of the conditions under which this approximation is valid). The radiative loss term should be negligible for large scale systems, but may be important under some conditions in very small laboratory systems. The effects of radiative loss would be to reduce the electron temperature and ionization rate at a given field strength.

Calculations of the type described have been performed with eqns. (23) and (25) for typical experimental conditions in the argon-

potassium plasma assuming the application of various constant electric field strengths, and the results are given in Figure 6. Note that the electron temperature shown in Figure 6 has a quasi-steady value which is substantially elevated above the gas temperature throughout the entire ionization process. The electron density increases about two orders of magnitude, for average field strengths, while the electron temperature remains nearly constant. After the electron density has increased to about 63 per cent of its final increase, the electron temperature increases about 10 per cent further. During this phase, the electron density more closely approaches equilibrium at the instantaneous electron temperature, and finally, at the end of this phase, the final electron density has the equilibrium value at the final electron temperature. These results show that, according to this analysis, the rate of relaxation is in fact limited by the ionization rate at the instantaneous electron temperature for the conditions discussed here.

This result is contrary to the simple assumptions made by Kerrebrock[46,47] in attempting to calculate ionization relaxation times assuming that forward and backward rates are essentially balanced, and thus that the electron density always corresponds to the equilibrium value for a given instantaneous electron temperature. Under these conditions, the level of ionization would increase as the electron temperature increases, with the rate-limiting process being the rate of increase of the electron temperature in response to the increasing energy input to the electrons.

According to the analysis presented here, however, the assumption of collisional equilibrium during the ionizational relaxation is

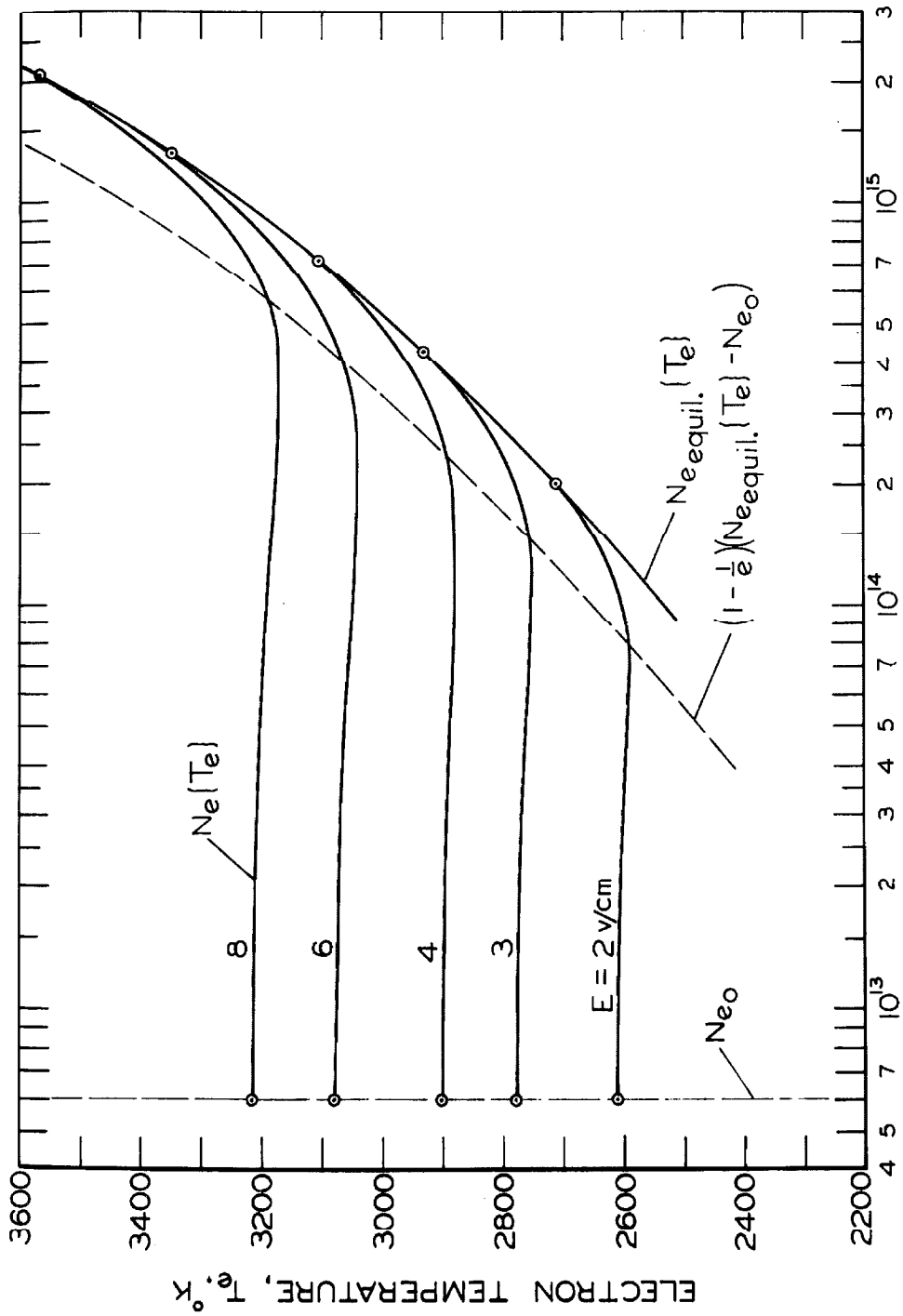

FIG. 6 QUASI-STEADY VARIATION OF ELECTRON TEMPERATURE DURING IONIZATIONAL RELAXATION

clearly invalid. Instead, as discussed here, the electron temperature very rapidly adjusts itself such that eqn. (25) is satisfied instantaneously during the ionizational relaxation. The electron temperature and ionization rate are specified instantaneously (eqns. (23) and (25)), and the rate-limiting process during the relaxation is the rate of ionization at the instantaneous electron temperature and not the rate of increase of electron temperature.

Equation (25) defines what the instantaneous electron temperature and ionization rate must be for a given instantaneous power input to the free electrons. Only in this sense may one state that the rate of ionization is determined by the rate of energy input to the free electrons[48], and this is the basis for the correlation used in Section VII-D, Figure 30. Note that in eqn. (25), for high enough field strengths, $\frac{\dot{\Omega}}{N_e} \ll \frac{V_o+\varepsilon_e}{N_e}\frac{dN_e}{dt}$, and $\frac{1}{N_e}\frac{dN_e}{dt} \simeq \frac{\sigma}{V_o}\frac{E^2}{N_e}$ if $\varepsilon_e \ll V_o$. Thus, for this case, the rates of ionization and energy input per electron are simply related regardless of the details of the ionization mechanism. Hence, the fact that eqn. (13) of ref. (47) agrees with experiment in this limit (as does the analysis given here) does not confirm the validity of the analysis of ref. 46. In fact, for lower field strengths (where $\frac{\dot{\Omega}}{N_e}$ can not be neglected), experimental data will be presented (Figure 30) which show acceptable agreement with the theory given here, whereas eqn. (13) of ref. 47 gives a very poor estimate of actual relaxation times.

Experimental data are given in Section VII-D which show that the electron temperature does increase in the manner explained by the analysis given here over a wide range of experimental conditions, and that observed relaxation times correlate well with the theory given here.

VI. EXPERIMENTAL APPARATUS AND TECHNIQUES

The basic elements of the experimental apparatus are illustrated schematically in Figures 7 to 11 , and a detailed description of apparatus and techniques is given in Appendix A . Figures 7 and 8 depict apparatus used to supply a seeded plasma of uniform properties to a test area. An arc-jet heater is used to heat the larger portion of an argon or helium carrier gas flow. This main flow is then combined with a smaller, secondary flow of argon or helium which has been passed through a potassium boiler with a minimum residence time of 2 sec, and is saturated with potassium vapor. The concentration of potassium in the combined flow is fixed by controlling the boiler temperature and secondary gas flow rate. The combined flow then passes through a mixing chamber with a length-to-diameter radio of 16 in which the flow is equilibrated to a fairly uniform, homogeneous "seeded plasma" before entering the test section. After leaving the test section, the flow is exhausted at one atmosphere into an exhaust duct system.

The power input to the arc jet could be continuously adjusted to give desired gas temperatures at the test section in the range from 1250 to 2250°K. The total pressure in the plasma was always maintained at one atmosphere. Velocities in the test section were typically about 8800 cm/sec, corresponding to a Mach number of about 0.10. Potassium concentrations were varied between 0.1 and 1.0 mole per cent of the total flow. More detailed information about the flow properties is given in Appendix A.

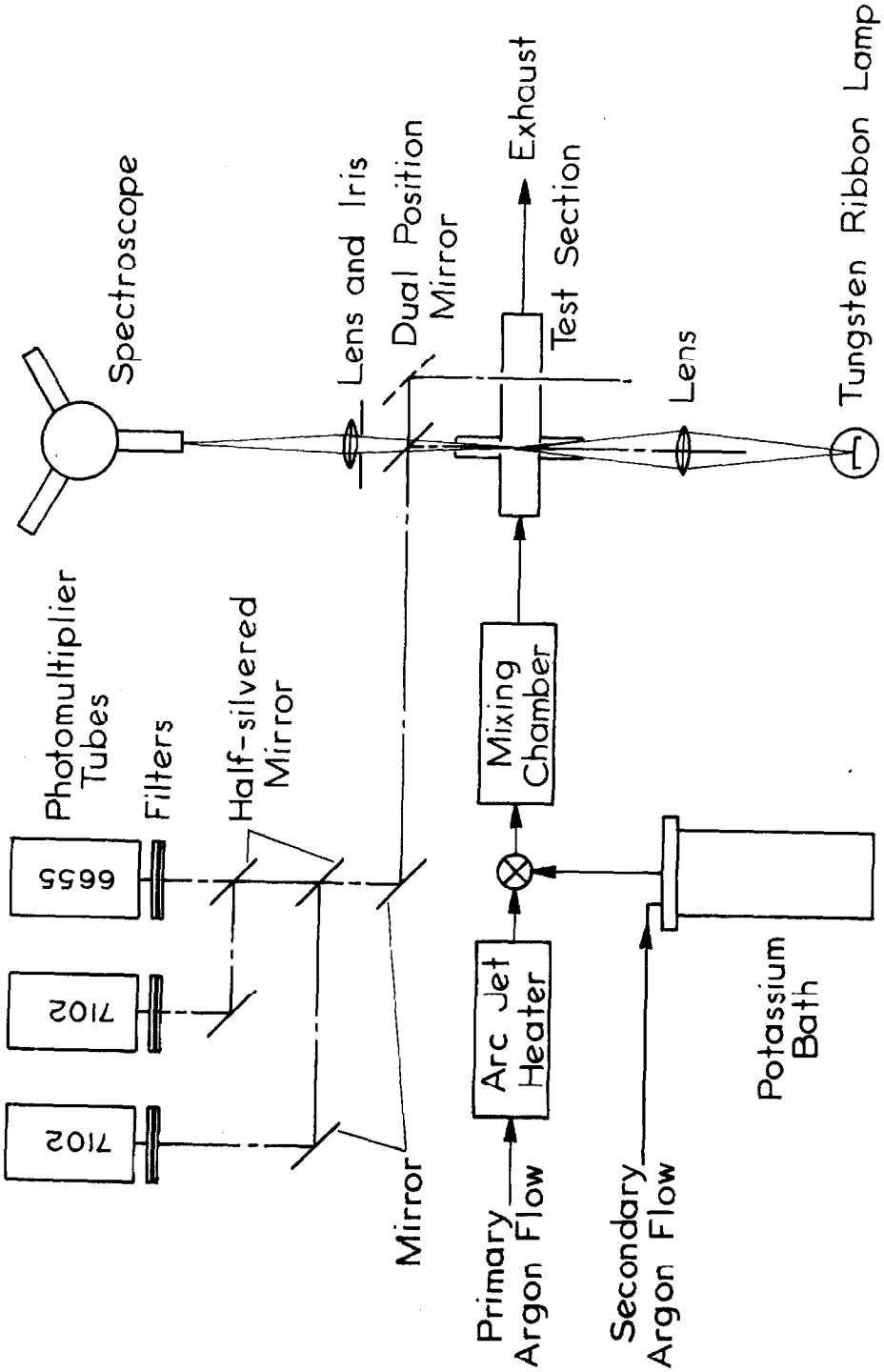

FIG. 7 SCHEMATIC DIAGRAM OF APPARATUS

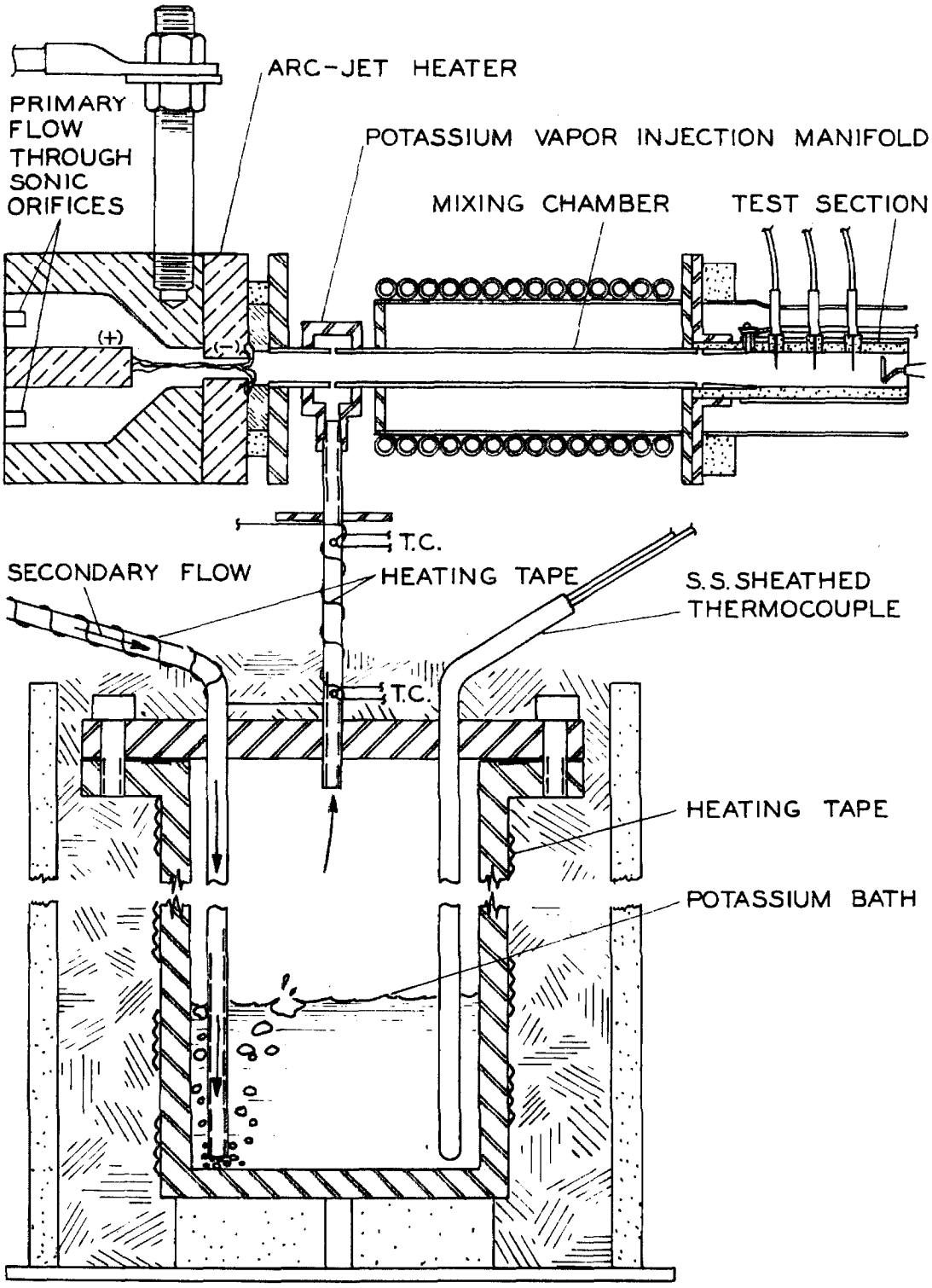

FIG. 8 SCHEMATIC DIAGRAM OF ARC-JET HEATER AND FLOW MIXING APPARATUS

A typical test section is shown in Figure 9 . Electrons are emitted thermionically from a spiral tungsten cathode immersed in the flow at the downstream end of the cylindrical test chamber and flow axially to a cylindrical stainless-steel anode imbedded in the boron nitride insulating wall. Typical dimensions in inches are given in Figure 9 . Thin tungsten-wire voltage probes were located as shown to measure the electric field in the plasma column. It was established that the electric field was constant along the duct by inserting as many as six probes into the flow, as is discussed in Appendix A.

A simpler test section configuration was found adequate for the study of ionizational relaxation processes and the determination of quasi-steady properties at the end of the ionizational relaxation period. Figure 10 shows a schematic diagram of this test section. In addition, much longer test sections were tried with various probe configurations, and diameters ranging from .430" to .500". All test sections gave similar results, and thus the short, simple test section in Figure 10 was adequate for ionization processes.

For recombination , however, the observed relaxations lasted somewhat longer than did the ionization relaxations, and thus use was made of the downstream set of probes in a long test section like that shown in Figure 9 to obtain longer test times.

The insulating cylinder used as the test section wall was made of boron nitride, and it was thermally shielded (shield not shown in Figs. 9, 10) so that the inner wall temperature was above

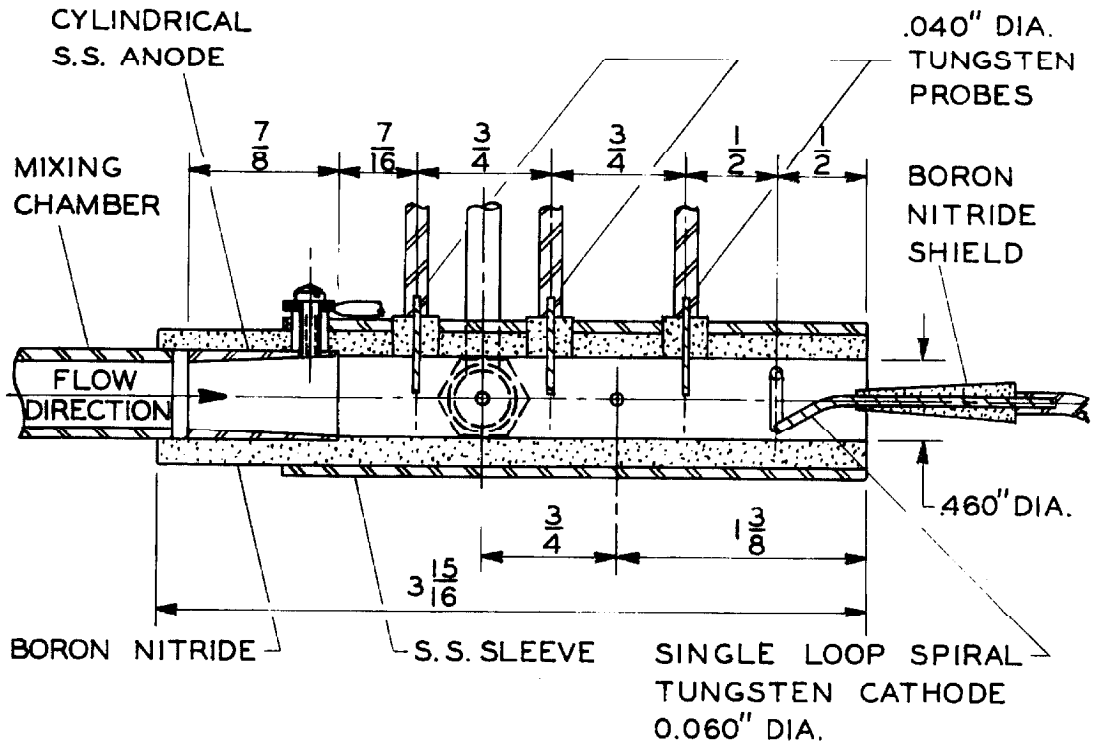

SIDE VIEW

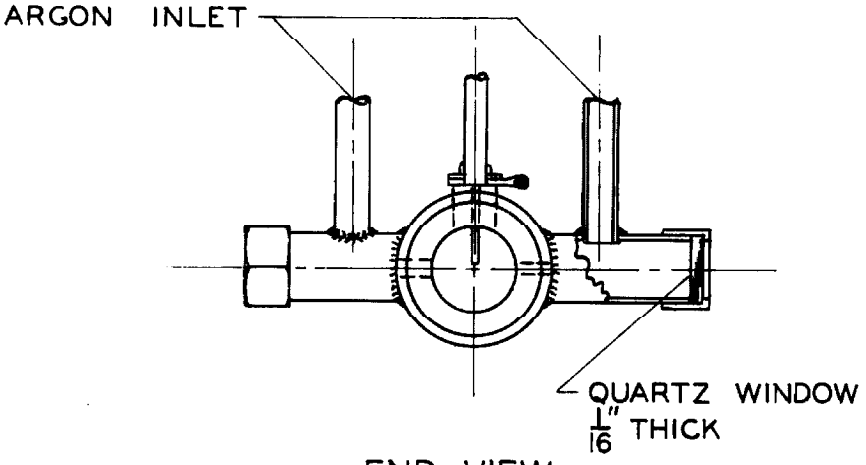

END VIEW

FIG. 9 SCHEMATIC DIAGRAM OF TEST SECTION

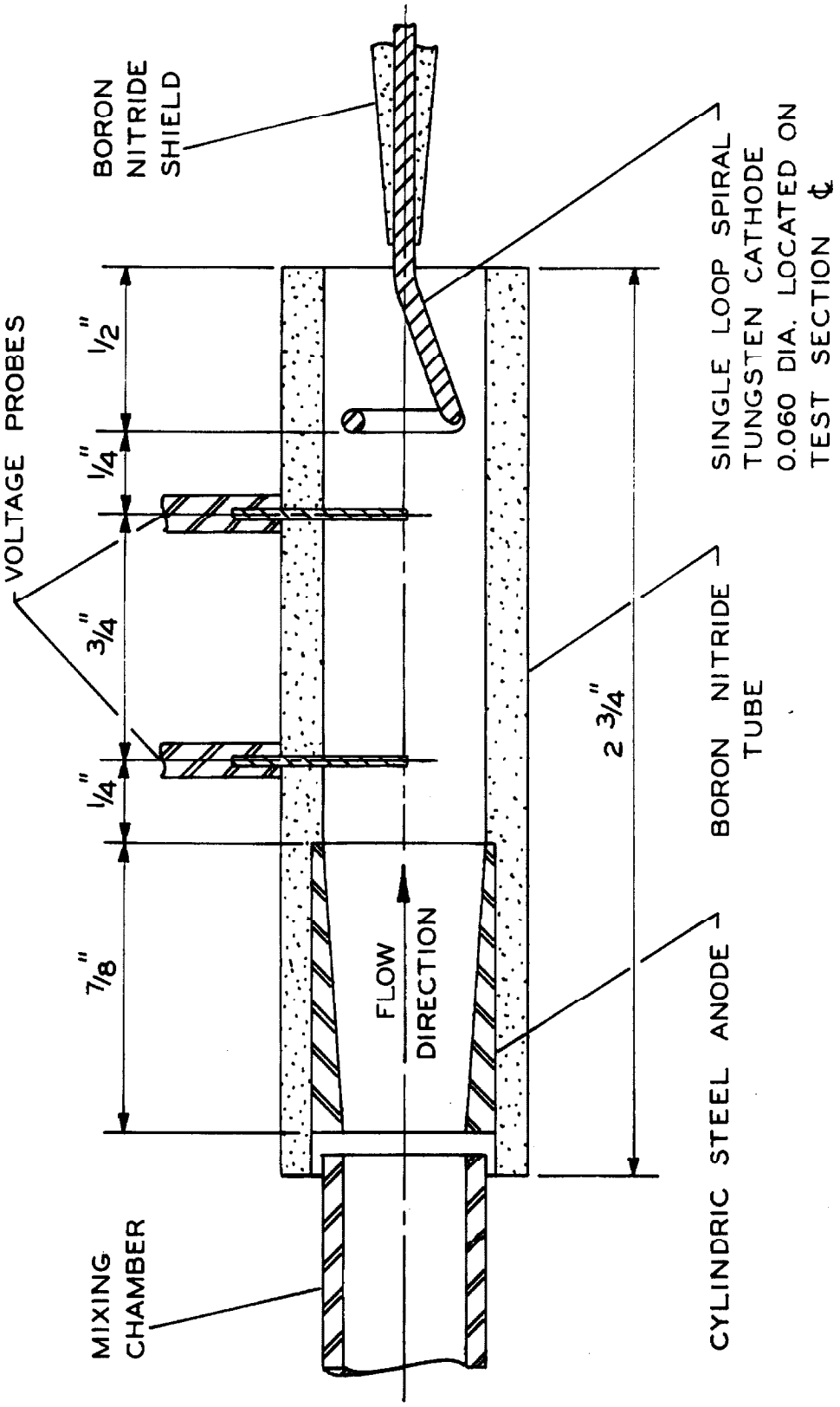

FIG. 10 SCHEMATIC DIAGRAM OF TEST SECTION

1250°K. The two sets of ports shown in Figures 7 and 9 were used in making spectral intensity measurements. The upstream set was equipped with a cell which could be purged with an auxiliary flow of argon gas. This prevented the condensation of potassium vapor on the quartz windows as well as the effusion of a plasma plume from the ports. Without this special cell arrangement, a cloud of cool potassium vapor was formed which led to undesirable absorption effects upon the spectrometric measurements. The auxiliary argon flow rate used to purge the ports was kept below $1\frac{1}{2}$ per cent of the total flow rate of the plasma and had no observable effects on measured values of the conductivity. The downstream set of ports was used exclusively for relative light intensity comparisons during transient periods, as is discussed in Appendix A.

A schematic diagram of the electric circuit used for the various experiments is shown in Figure 11. This diagram shows the circuits employed to perform experiments in any one of three possible fashions. First, a constant electric field could be applied between the discharge electrodes to obtain a constant current discharge in the test plasma. This steady discharge could then be abruptly interrupted by closing the upper mercury switch and thus reducing the electric field to either a very low value or to zero. Finally, by using only the lower portion of the circuit in Figure 11, it was possible to establish a step function increase in electric field between the discharge electrodes from an initially zero value to any desired final value up to several volts/cm. In this manner, the circuit of Figure

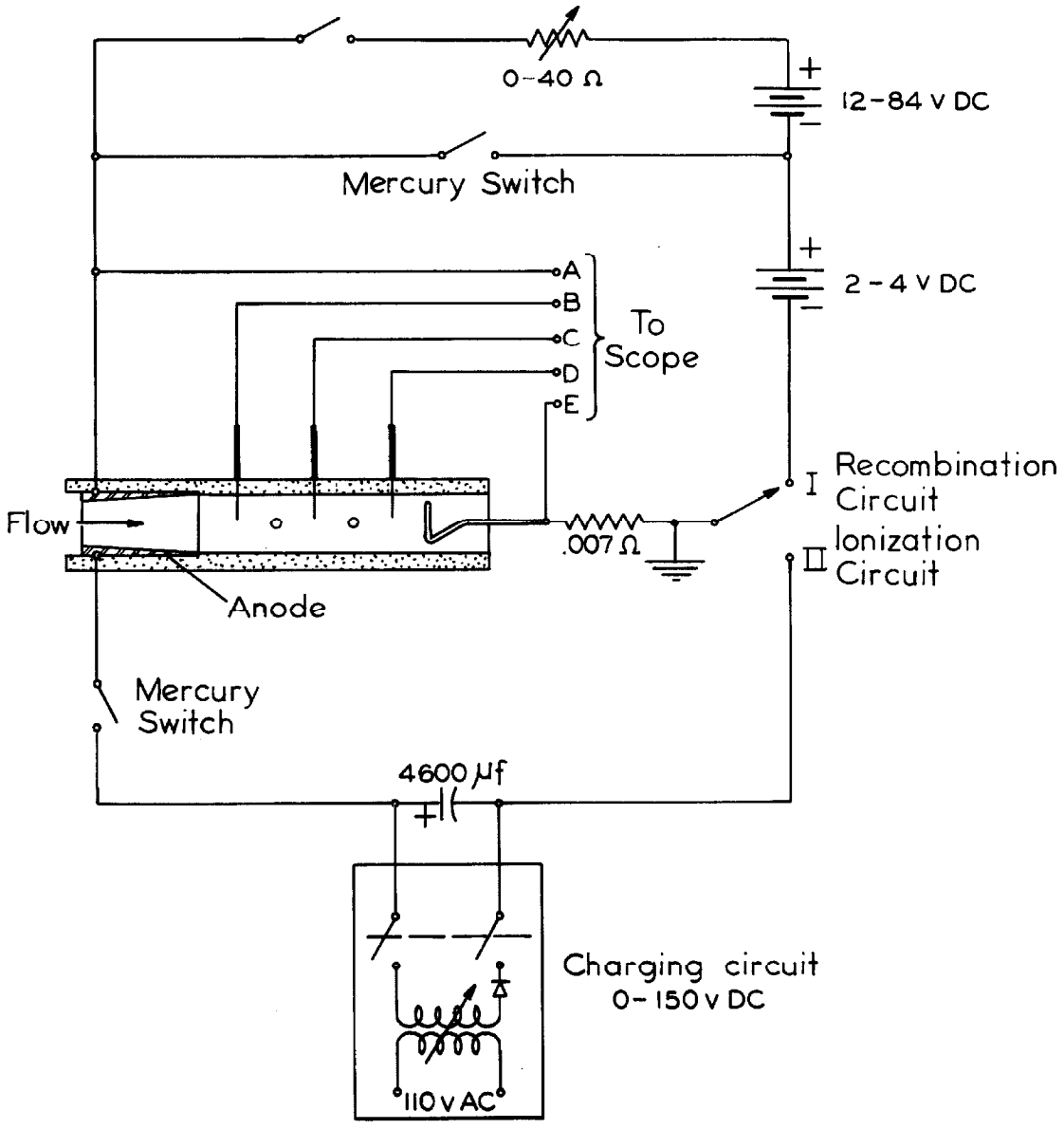

FIG. 11 SCHEMATIC DIAGRAM OF ELECTRIC CIRCUIT

11enabled the study of plasma behavior either under the action of a steady electric field or during the relaxation periods immediately following either the abrupt increase or reduction in electric field.

The schematic physical arrangement of the photomultiplier apparatus and the spectroscope used to make spectroscopic measurements of plasma characteristics is given in Figure 7. Photomultiplier tubes and optical filters were selected to isolate various regions of the spectrum containing three principal transitions between low-lying states of potassium, as well as the sodium-D transition which was observable because of the addition of a trace of sodium to the total flow. The photomultiplier tubes were cooled to dry-ice temperatures to eliminate thermal noise from the tube outputs, and condensation in the optical system was prevented by purging with dry, high-purity nitrogen.

The electrical circuitry associated with the photomultiplier measurements was conventional. For transient observations, the rise time for pulses observed with the photomultiplier tubes was less than a microsecond. In order to make precise light-intensity measurements for steady-state discharges, it was found necessary to use an electrical filter to smooth the high-frequency, random characteristics of the photomultiplier output.

The optical equipment was arranged so that it was possible to make as many as three simultaneous spectral observations. By rotating the light path to the photomultipliers out of the line of sight of the spectroscope, it was also possible to use the same port to make steady-state sodium line reversal temperature measurements. De-

tails on the optical system and associated circuitry, as well as a discussion of calibration procedures, are included in Appendix A.

Measurements of gas temperature were made either with thermocouples or fine tungsten wires immersed in the flow. Measurements of total discharge current in the test section were made by measuring the potential drop across the very small ($\approx .007\ \Omega$) resistor shown in Figure 11. Alternatively, in the steady-state case, currents could be measured with a conventional ammeter placed in the circuit. The potentials of the various probes, and occasionally that of the anode, were measured with respect to the cathode. All transient measurements and most steady-state measurements were recorded by photographing an oscilloscope display of the various probe potentials, the voltage drop across the current measuring resistor, and the photomultiplier outputs as a function of time.

The electrical conductivity was determined by measurements of the total current and voltage gradients in the plasma column. The floating potential difference between the thin tungsten wire probes placed at known locations in the plasma column gave the average electrical field strength in the column. For these experiments, the potential differences between the probes were typically of the order of 5 volts, and thus any possible differences in floating sheath potentials for the probes were negligible. The average current density flowing axially through the cylindrical plasma column was obtained by dividing the measured total current by the total cross-sectional area of the duct. The average electrical conductivity is then given by

$$\sigma = (I/A)/(\Delta V/\ell) \ , \qquad (26)$$

where ΔV is the floating probe potential difference, ℓ is the probe separation, I is the measured total current, and A is the cross-sectional area of the duct.

A final comment on the experimental pulse technique used here should be made. The pulse technique allows the measurement of electrical conductivity immediately following the ionizational transient period and thus eliminates gas heating effects for the data to be presented here. For very high current densities ($\sim$100 amp/cm^2), the effects of gas heating on conductivity could be observed. This is shown in the sketch below. For very high current densities, the electrical conductivity continues to slowly increase immediately after the initial ionizational transient period. The conductivity eventually flattens out and remains steady for times longer than those corresponding to the transit times for the flow through the test section. This type of behavior was most pronounced for the helium-potassium plasma, no doubt due to the relatively large elastic energy loss rate for these plasmas, as discussed in Section VII-A.

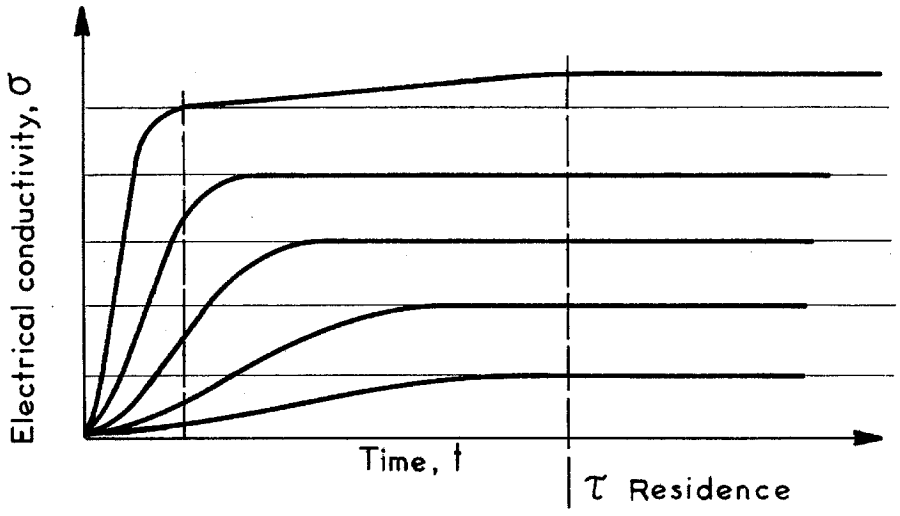

VII. EXPERIMENTAL RESULTS

A. Steady-State Electrical Conductivity

Measurements of the electrical conductivity of argon-potassium and helium-potassium seeded plasmas were made over a wide range of variation of experimental parameters. These conductivity values were determined from measurements of voltage gradients and total currents in the plasma column as described in the preceding section. The measurements were made immediately following the initial ionizational relaxation period after a step application of electric field. Since the ionizational relaxation was completed in times much shorter than the characteristic times for both the appreciable increase in the translational temperature of the heavy species and the flow of plasma through the test section, the plasma could be regarded as stationary with a constant translational heavy-species temperature fixed by initial conditions.

Consider first the conductivity measurements made in the argon-potassium system. Seed concentrations for measurements in argon-potassium plasmas were defined by the ratio, n_K/n_A, specified for the initial plasma conditions with zero applied field. The seed concentration was varied between .001 and .008, that is, the potassium seeding ranged from about .1 to 1 mole per cent of the flow. Initial gas temperatures, T_a, were varied between 1250 and 2000°K. Measurements of T_a are discussed in Appendix A. The accuracy of the gas temperature measurement depends on the accuracy of the measuring technique as well as the characterization of the

gas temperature by a bulk value averaged over the cross-sectional area of the duct. Values of T_a at about 1500°K are probably accurate to within ± 40°K, and those at 2000°K to about ± 100°K. An experimentally determined gas temperature profile is included in Appendix A , see Figure 33. The total gas pressure was maintained at 1 atmosphere. Measurements were made over a wide range of current densities extending from about .02 to 90 amps/cm^2, with applied field strengths from about 1 to 12 v/cm.

Figures 12 to 15 show typical experimental results for the argon-potassium seeded plasma, where the measured electrical conductivity is plotted as a function of the current density. Note that over the extensive range of current densities that the electrical conductivity increases one hundred fold, a substantial increase of much interest in connection with MHD power generating devices. The data are plotted along with theoretical curves as calculated in the manner discussed in Section IV-B. Note that the agreement between experiment and theory is quite good at the very high current densities. In this region, electron-ion interactions are predominant in determining the elastic energy losses as well as the electrical conductivity; this good agreement indicates that the use of the Spitzer conductivity expression and the inclusion of the electron-ion energy exchange in the theoretical calculations appears to be substantially correct.

For lower current densities, down to a few tenths amp/cm^2, the data fall somewhat below theoretically calculated curves which treat only the elastic collision energy loss mechanisms from the electrons to the neutral and ionized heavy species and neglects ine-

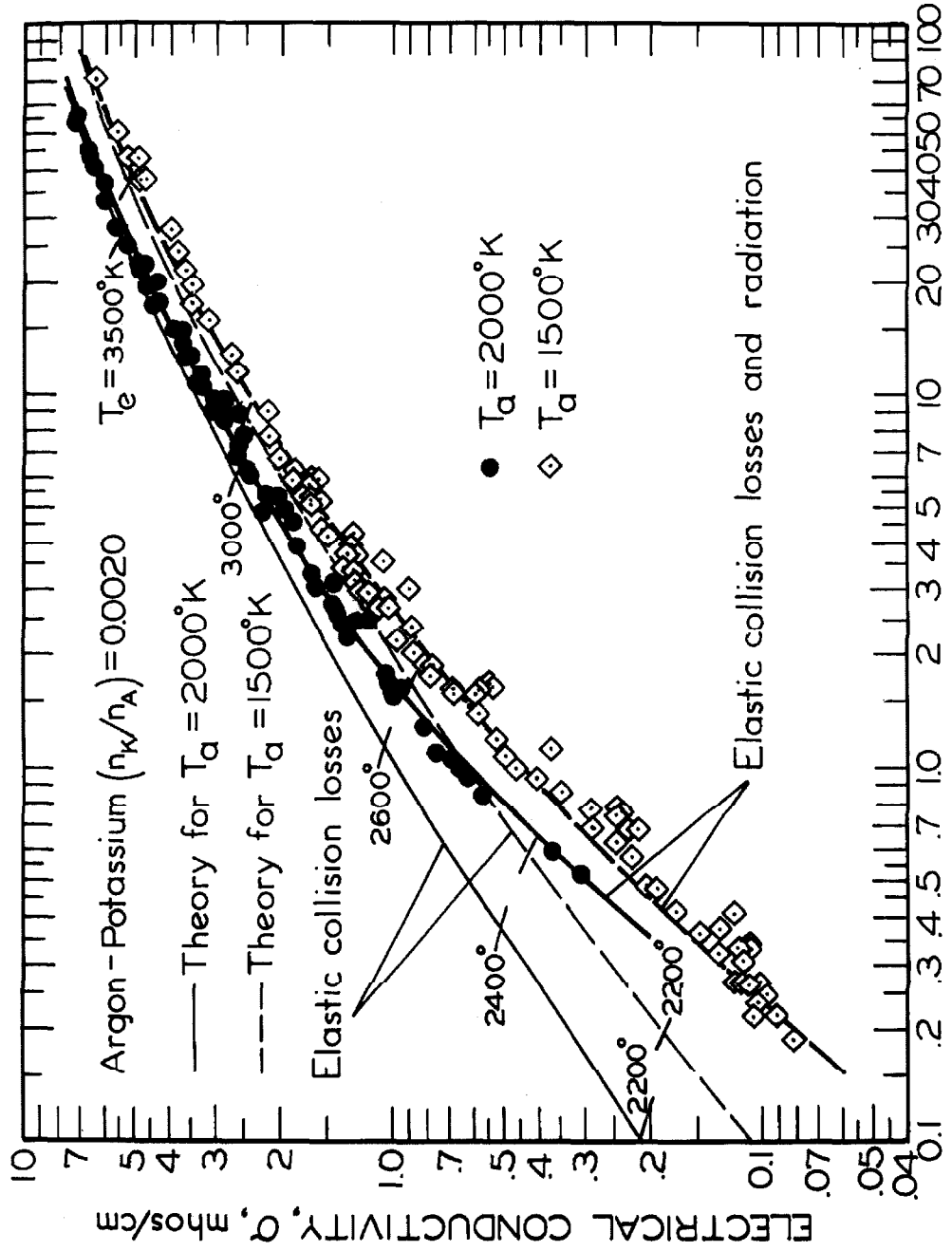

FIG. 12 DEPENDENCE OF STEADY STATE CONDUCTIVITY ON CURRENT DENSITY

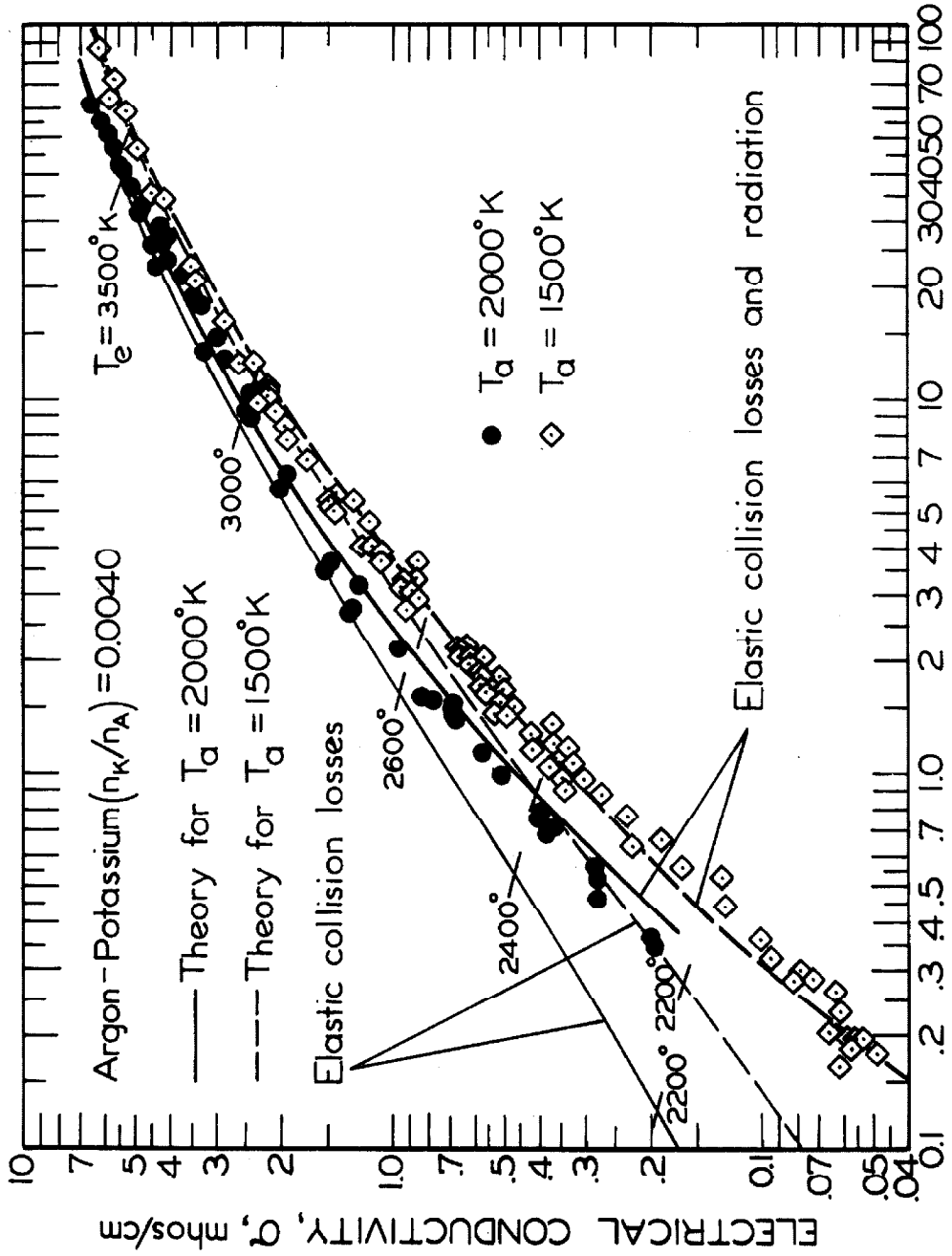

FIG.13 DEPENDENCE OF STEADY STATE CONDUCTIVITY ON CURRENT DENSITY

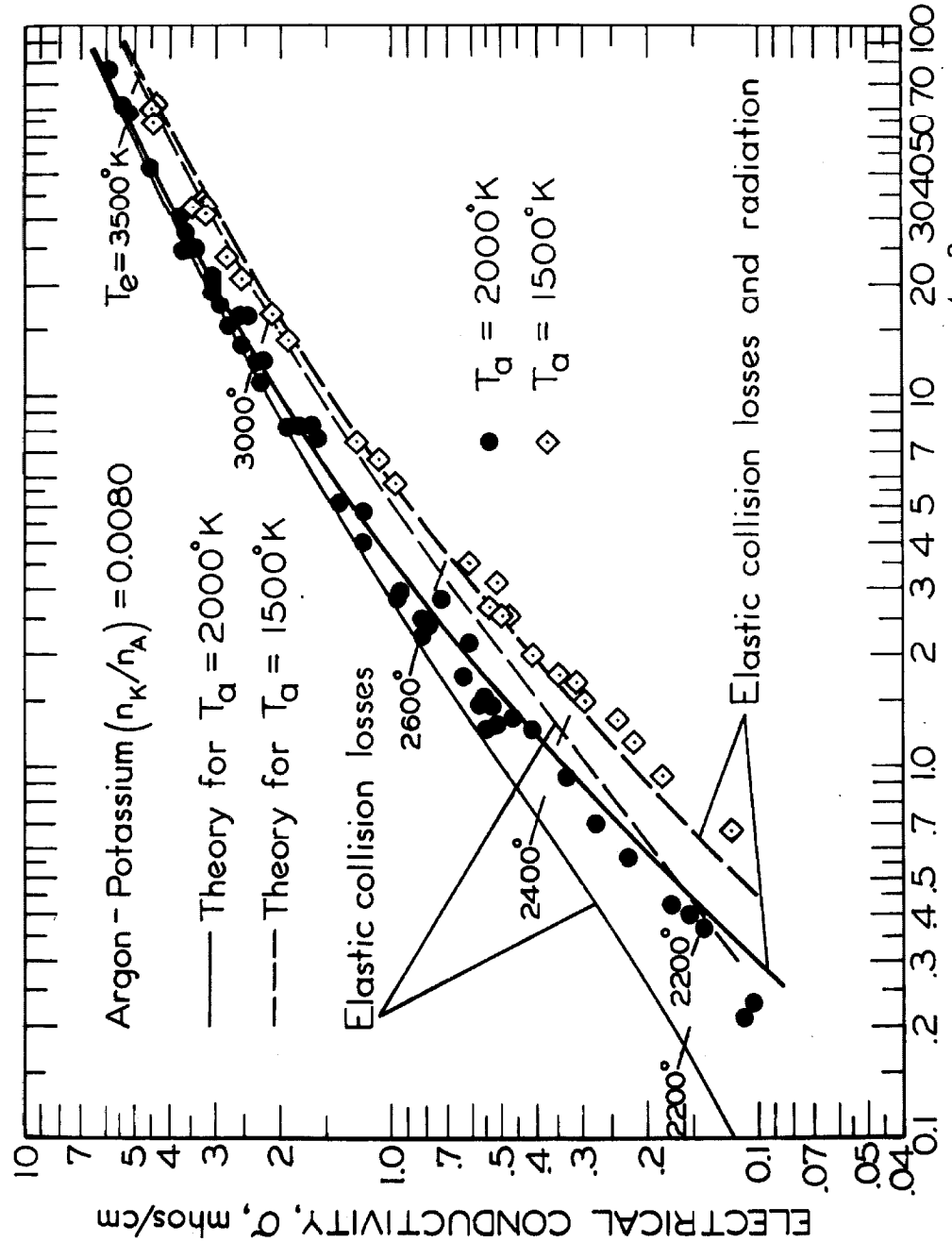

FIG. 14 DEPENDENCE OF STEADY STATE CONDUCTIVITY ON CURRENT DENSITY

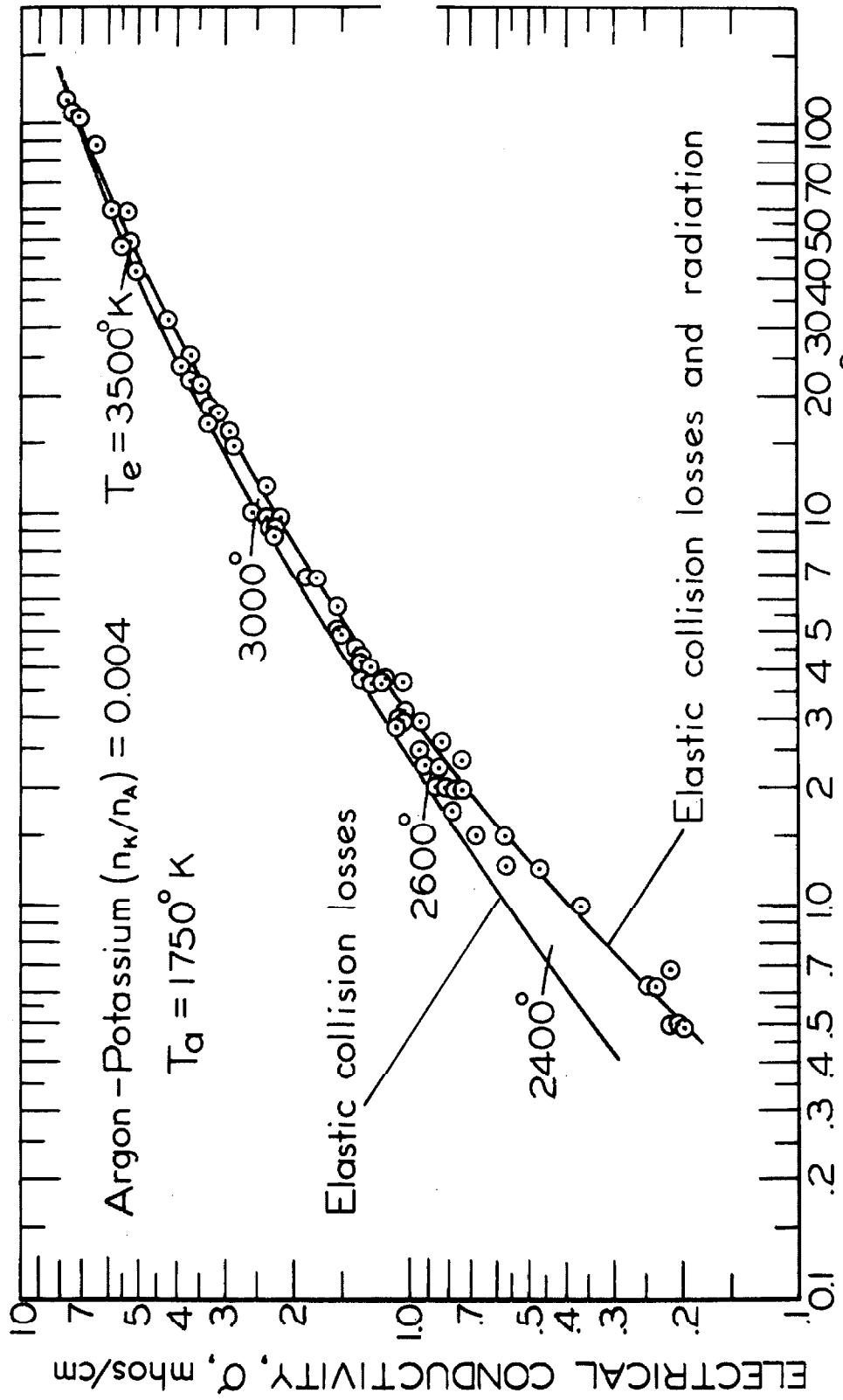

FIG.15 DEPENDENCE OF STEADY STATE CONDUCTIVITY ON CURRENT DENSITY

lastic energy losses completely. The inclusion of inelastic losses by the estimation of the steady-state radiative energy losses from the plasma has been considered for the lower theoretical curve with each set of data. The data are in excellent agreement with this complete theory down to very low current densities, about 0.2 and 0.4 amp/cm^2 for the 1500 and 2000°K gas temperatures, respectively,

The electron temperature elevation above the translational temperature of the heavy species becomes very large for high current densities; at 80 amps/cm^2, the electron temperature is larger by about a factor of 2. As the electron temperature is increased, the radiative losses increase very roughly as T_e^4, but the elastic energy loss, eqn. (16), is a very strong function of electron temperature since the electron density increases approximately as $\exp\{-4.34/2kT_e\}$, and thus the ratio of elastic to inelastic energy losses increases rapidly with increasing current density. Thus, radiation is the dominant loss mechanism in the low current range, e.g., for $T_a = 2000°K$, $n_K/n_A = .004$, the inelastic energy loss is comparable to the elastic energy loss at about a current density of 2 amps/cm^2.

Low Current Density Data

The typical data shown in Figure 16 illustrate that for very low current densities, below about .3 amp/cm^2, that the experimental values break away rather sharply from the theoretical curve which includes the radiative loss term in the electronic energy balance. The conductivity data show a smooth transition from this cur-

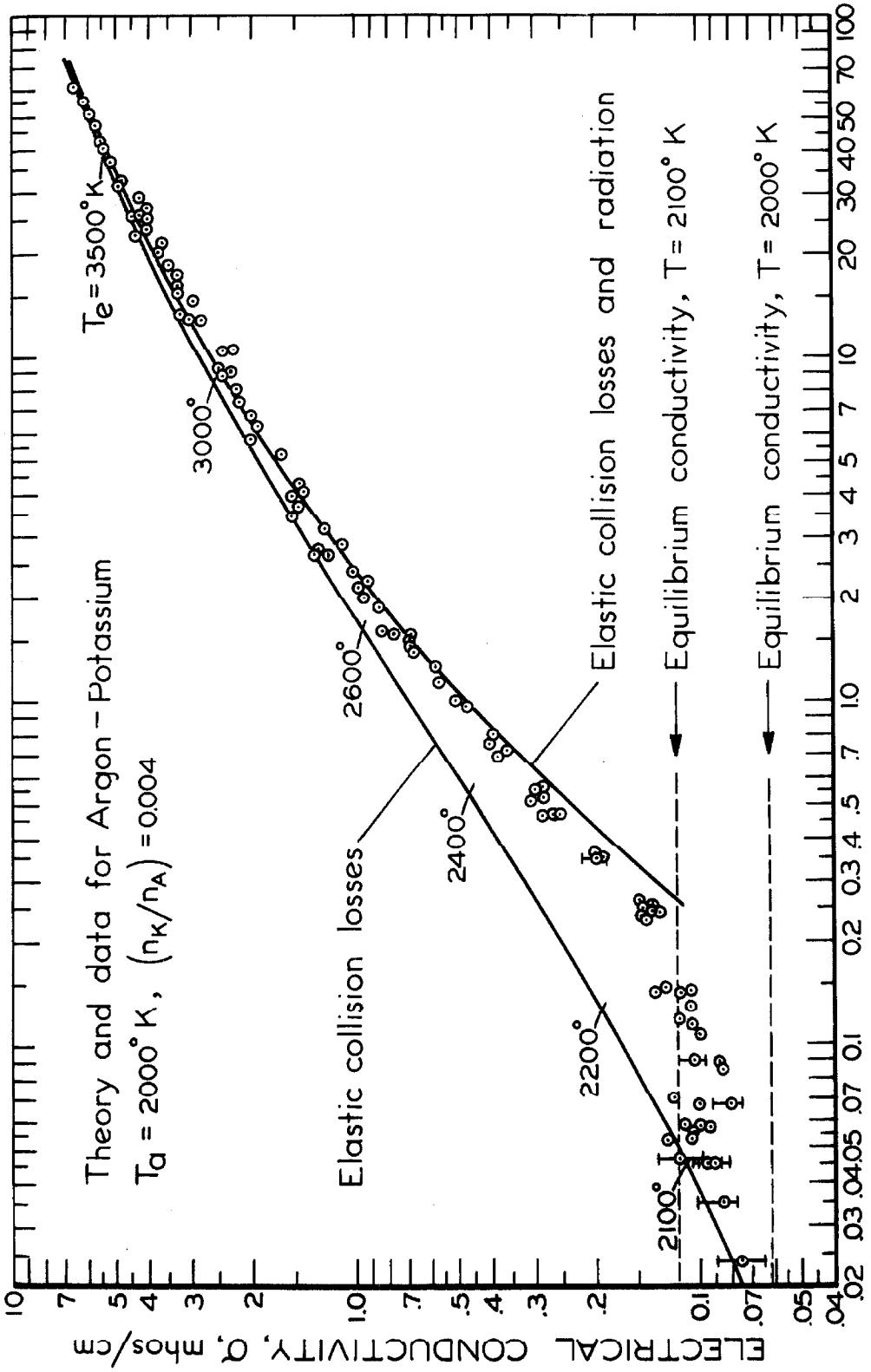

FIG.16 DEPENDENCE OF STEADY STATE CONDUCTIVITY ON CURRENT DENSITY

rent density down to the lowest currents investigated ($\cong .02$ amp/cm^2) and appear to level off at these lowest currents to a conductivity value approximately corresponding to the translational temperature of the gas, $T_a = 2000 \pm 100^{\circ}K$ for this case. Plausible explanations for this behavior may be connected with the energy balance for the first few excited states which account for the majority of the radiant energy loss. For high electron densities, electron-atom interactions are sufficient to maintain these states in thermal equilibrium with the free electrons. However, as the electron density falls, the frequency of electronic collisional de-excitation of these levels will no longer be large compared with the net radiative de-excitation rate, and the populations of these states will not be in thermal equilibrium with the free electrons. Under these conditions, the calculated values of radiant energy loss given here will be too large. See also Section III-F.

A second and perhaps more important effect is that there is an essentially constant rate of excitation of these low-lying states by atom-atom interactions. Hence, at low enough electron density, the atom-atom interaction will become the dominant excitation mechanism and the population levels of the excited states will tend to approach thermal equilibrium at the translational temperature of the heavy species.

Both of these processes would mean that the calculated inelastic energy loss from the free electrons, as estimated by the radiative transfer calculations, has been over-estimated; the measured values would thus be expected to be larger than calculated values, as

is demonstrated in Figure 16. A more complete discussion of this very low current region and of these two effects is given in Appendix C.

The measurements of conductivity for $T_a = 2000 \pm 100^{\circ}K$ and $T_a = 1500 \pm 40^{\circ}K$, shown in Figures 12 to 15, were terminated at about 0.4 and 0.2 amp/cm^2, respectively. Measured values of conductivity below these current densities tended to remain almost constant with decreasing current (not shown in the figures). In most cases, the constant value was considerably above the equilibrium value of the conductivity, corresponding to the translational temperature of the gas. Similar anomalous behavior was also reported by Kerrebrock[46] at very low current densities. This behavior was investigated for the apparatus used in this study, and was found to be the result of a thin, poorly-conducting film which builds up on the walls of the test section and which apparently shunts the voltage probes. This film appears to the eye to be a shiny surface which covers the entire test section wall. If tests are carried out with new boron nitride test sections before this film appears, low current density measurements such as those shown in Figure 16 can be made. This "dry" wall data of Figure 16 corresponds to the range $.025 \leq J \leq 0.40$ amp/cm^2. When the wall was slightly conducting, the plateau conductivity was about 0.2 mho/cm, extending below about 0.4 amp/cm^2. In contrast, the conductivities shown in Figure 16 decrease in a smooth way toward the equilibrium value. The data shown in Figure 16 are thought to be correct, and the correct behavior for the earlier experimental work of Figures 12 to 15 should be

qualitatively similar in this low current region.

Low Current Instabilities. The low current results also throw some light on a practical problem. A curve has been drawn through the data points of Figure 16 and is shown as the solid curve in Figure 17b . Figure 17a shows the variation in electric field strength represented by this data. Examination of Figure 17a indicates that the field strength increases monotonically with current density, but that between 0.4 and 1.5 amp/cm^2 the field strength is almost constant at about 2 v/cm. In this region, the current density and conductivity are very sensitive to small changes in field strength. Similar unstable regions were observed at other potassium concentrations and for temperatures in the argon-potassium plasmas. Under some conditions, this unstable region can extend over a fairly large current density range. This is illustrated by the data of Figure 18, taken in argon-potassium with $T_a = 1250^{\circ}K$ and $n_K/n_A = .002$, which show an unstable region extending from about .2 amp/cm^2 to 2.5 amp/cm^2 (between arrowheads). However, the helium-potassium data discussed below (Figure 20) had only a very small region of apparent instability in the neighborhood of 1 amp/cm^2.

In the unstable range, $d(\ell n\sigma)/d(\ell nJ)$ is approximately unity, and consequently the field strength is almost constant. However, if the radiation correction had been larger, as it would be in a smaller apparatus, the value of $d(\ell n\sigma)/d(\ell nJ)$ would increase above unity, and consequently the field strength would have a local maximum in this region. This type of behavior is illustrated by the dashed curves of Figures 17 a and b . These curves roughly would correspond to a

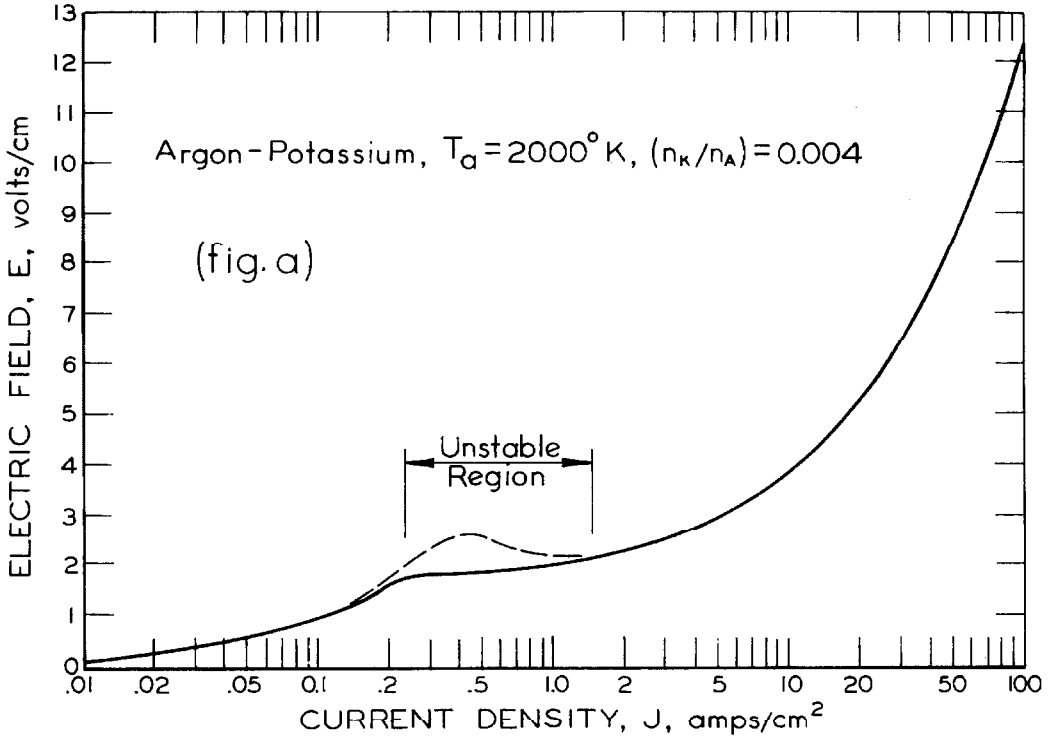

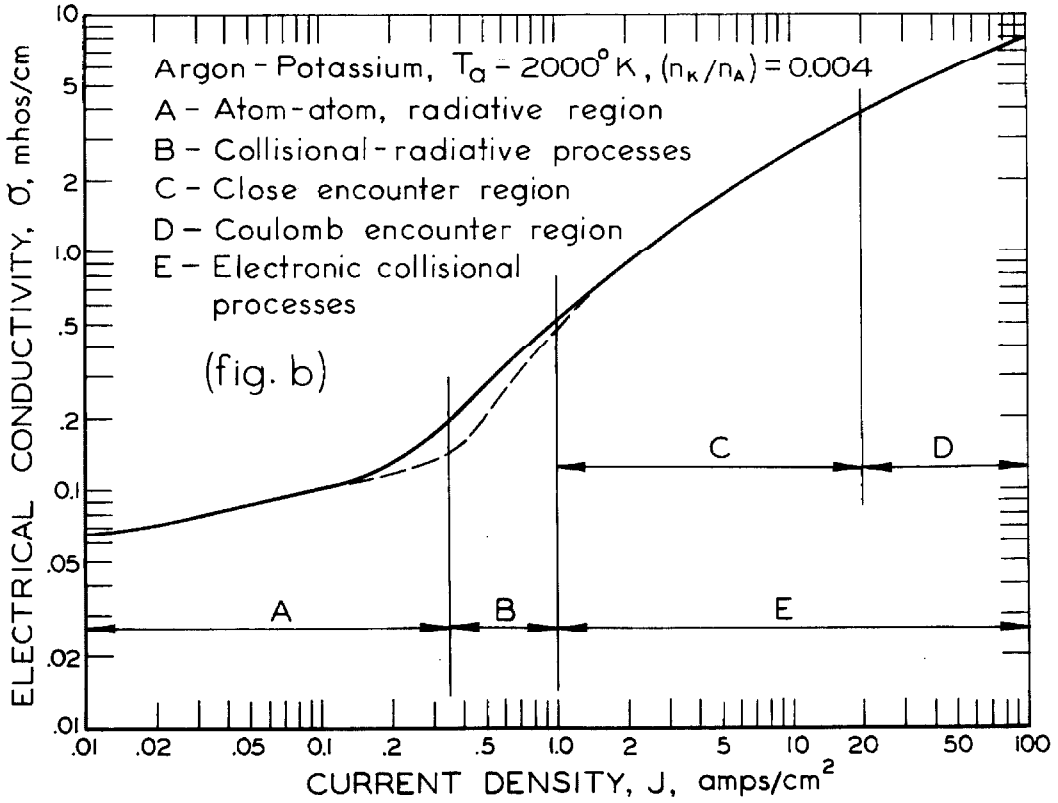

FIG. 17, a & b TYPICAL ELECTRIC FIELD AND CONDUCTIVITY VARIATIONS WITH CURRENT DENSITY

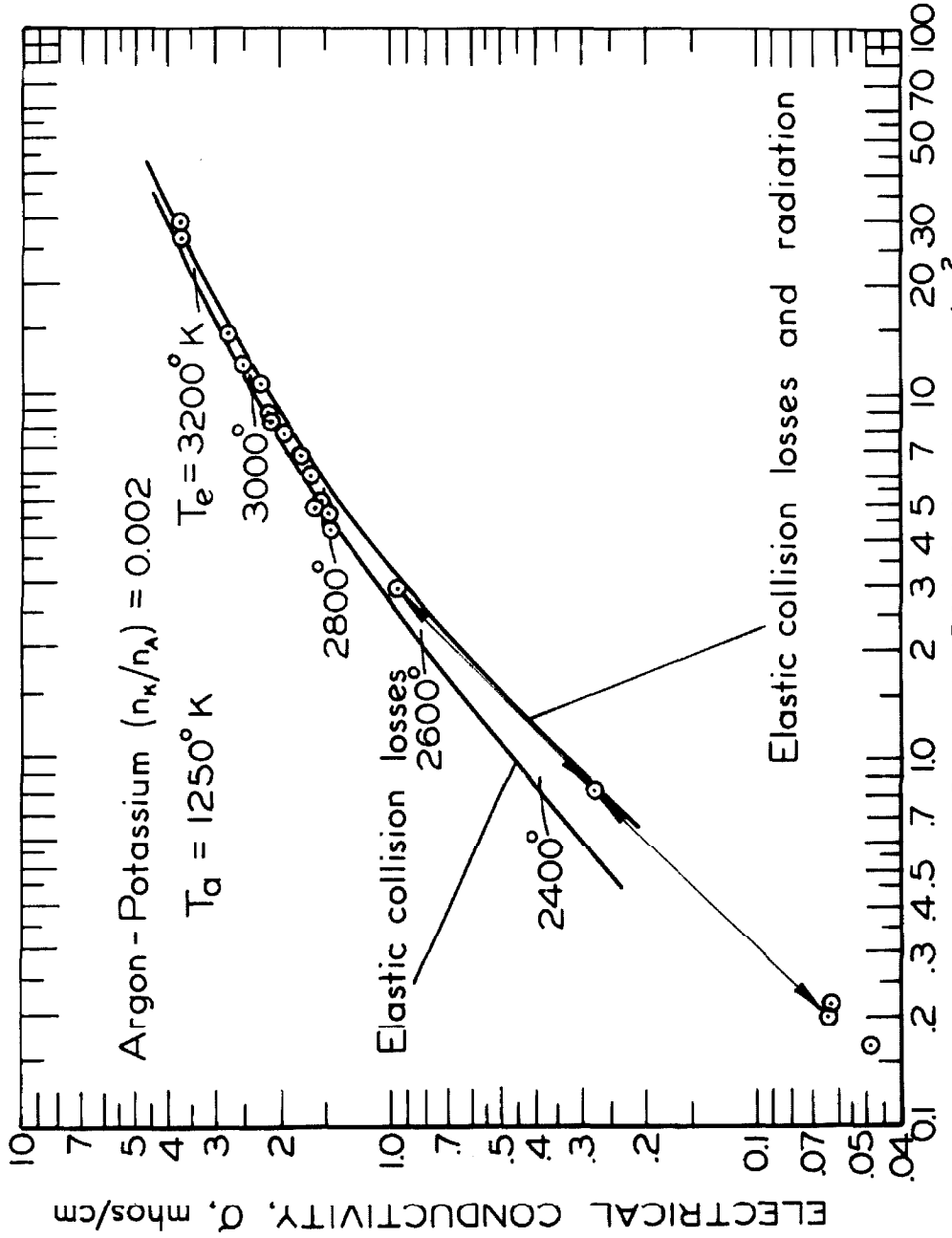

FIG. 18 DEPENDENCE OF STEADY STATE CONDUCTIVITY ON CURRENT DENSITY

system of about one half the diameter of the plasma studied here, which would exhibit a larger radiative loss effect. Such a maximum in the local field strength is indeed observed by Kerrebrock and Hoffman[46], who worked in an apparatus with a diameter about 60 per cent of that used in the present experiments. If the foregoing explanation is correct, this maximum is a result of the more important radiation loss in their smaller system and will not exist in a larger device in which radiation effects will be much less important.

The experimental observations of this work were done by a pulsed application of an essentially constant field strength, as has been discussed in Section VI, in order to record conductivity values immediately following the ionizational transient to eliminate undesirable gas heating effects. For this type of experiment, the measurements of current density clearly show the unstable region. The current density was generally observed to undergo an unstable transition from initially low current values to higher values at essentially constant field strengths, or in response to small fluctuations in field strength. For current densities above and below these unstable regions, the current density was steady at a constant value immediately following the ionizational transient and did not show the subsequent unstable behavior that was characteristic of the unstable regions.

The measurements of Kerrebrock and Hoffman were performed at current densities below about 10 amp/cm^2 in a steady-state system utilizing an external ballast resistor in their electric circuit. This type of experiment would not reveal the instability

except as a region where the observed conductivity - current density characteristic had a slope $d(\ell n\sigma)/d(\ell nJ) \gtrsim 1$.

As a final comment on the various current density regions, note that Figure 17b illustrates the current density regions over which the various phenomenological effects occur, under typical conditions in the argon-potassium system. For example, at a current density of 20 amp/cm^2, the Coulomb interactions become comparable to the close encounter interactions; above this current density, the Coulomb effects dominate, etc.

Additional Unstable Behavior. An interesting phenomenon has been reported by other authors[30, 38] in connection with similar experiments both in argon-potassium and helium-cesium plasmas. Two modes of current conduction have been observed. The first of these is encountered at low current densities, and under this condition the plasma emits a uniform diffuse glow from the entire volume. However, at a higher current density, a transition is observed to a second mode of conduction in which the discharge constricts to a relatively narrow, arc-like discharge. The critical value of the current apparently depends on the temperature of the plasma and the seed concentration. The author has never observed the second type of behavior in his experiments. Visual observation indicates that the discharge always gives rise to a diffuse, uniform glow which fills the entire cross section of the duct and which increases in intensity with current density.

This unstable behavior is probably that associated with complete ionization of the seed mentioned in Section IV-B and also dis-

cussed by Kerrebrock[46].

Figure 19 shows a difficulty encountered when the seed concentration was reduced to very low values. These data are for the argon-potassium system with $T_a = 2000^{\circ}K$, $n_K/n_A = .001$. As discussed by Pinchak[37], the large thermionically-emitted cathode currents which one achieves in seeded plasmas of this type are due to the reduction in surface work function caused by the absorption of potassium atoms on the tungsten cathode surface. When the potassium seed concentration is reduced sufficiently, a substantial reduction in surface emission occurs, which is illustrated by the fact that data in Figure 19 only extend up to about 12 amp/cm^2 for $n_K/n_A = .001$. These data were obtained after several attempts; usually only current densities in the neighborhood of 1 - 5 amp/cm^2 were obtainable at this concentration. Attempts to obtain data for concentrations lower than .001 failed due to insufficient surface emission.

Helium-Potassium Data. Electrical conductivity measurements were also made in the helium-potassium system at $2000 \pm 100^{\circ}K$ and 0.32 mole per cent ($n_K/n_{He} = .0032$) and are presented in Figure 20. The data are compared with the calculated curves which were discussed in Section IV-B.

The purpose of changing the carrier gas from argon to helium was to provide a sensitive check on the steady-state theoretical formulation by using a gas with a markedly different mass and electron-atom momentum transfer cross section. The mass of helium is one tenth as large as that of argon, and thus the corresponding electronic elastic collision energy loss term (eqn. (16)) is increased a factor

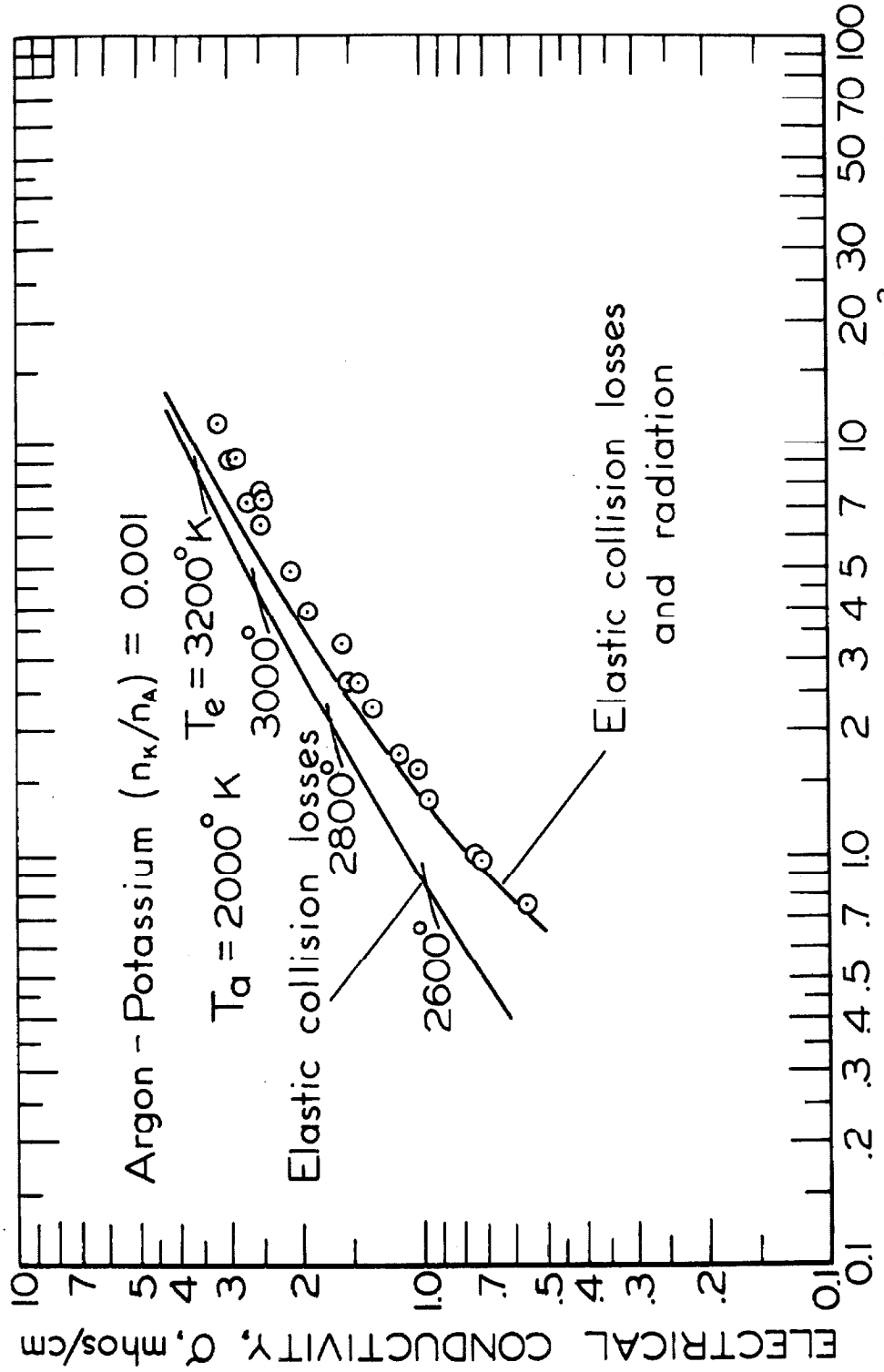

FIG. 19 DEPENDENCE OF STEADY STATE CONDUCTIVITY ON CURRENT DENSITY

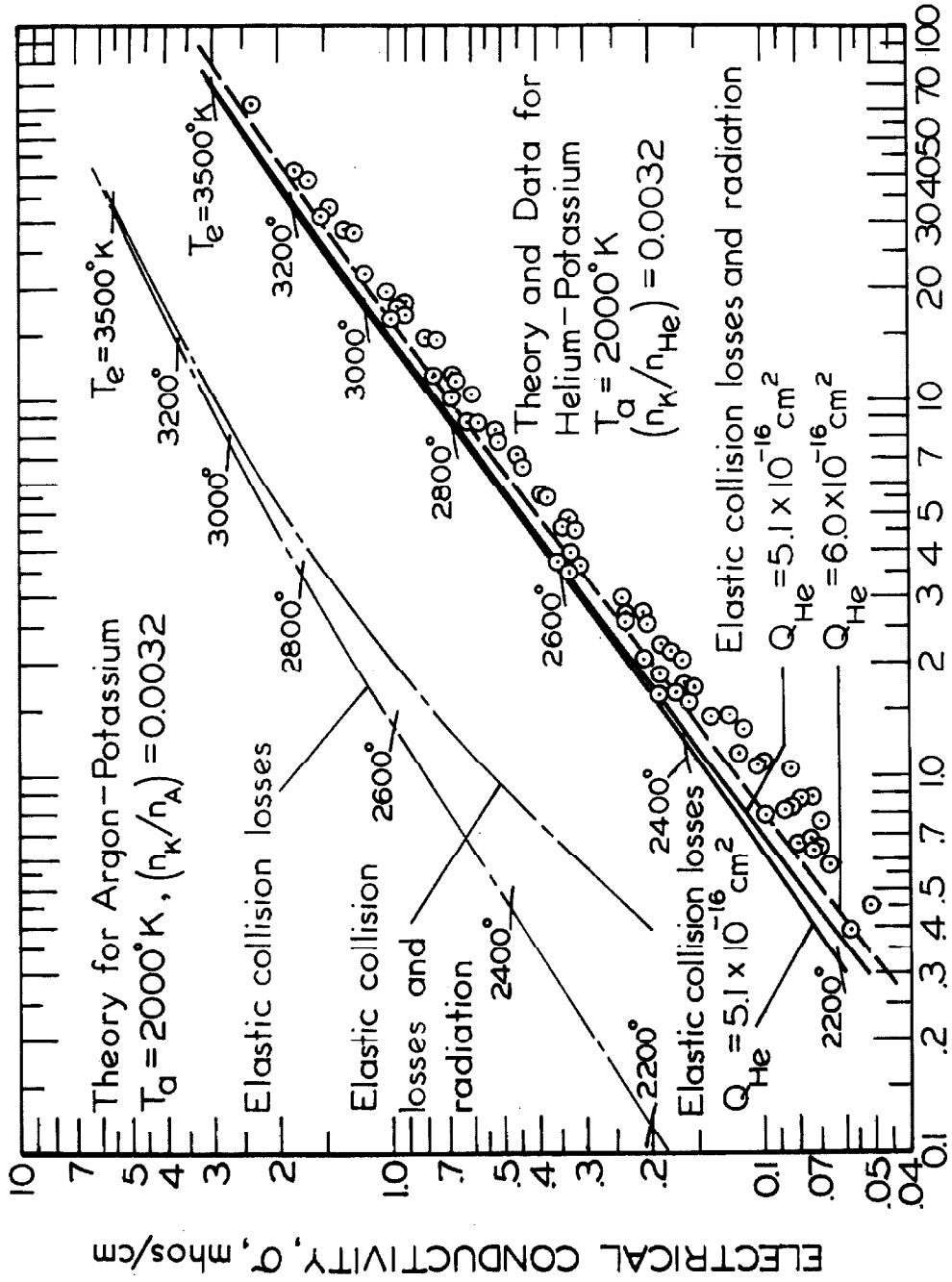

FIG. 20 DEPENDENCE OF STEADY STATE CONDUCTIVITY ON CURRENT DENSITY

of ten due to this fact. Further, the momentum transfer cross section is roughly about eight times as large for helium as for argon in the energy range of interest here, and does not exhibit the pronounced Ramsauer minimum that is observed for argon. These factors increase the elastic energy transfer rate substantially. Also, the larger cross section for helium produces a corresponding reduction in electrical conductivity (eqn. (8)). These factors produce the large differences between the two plasma systems illustrated in Figure 20. The electrical conductivity for a given current density is reduced considerably for the helium-potassium system compared to the argon-potassium case. Thus, the electric field necessary for a given current density is increased substantially for the helium-potassium case, the field strengths ranging here from about 7 to 25 v/cm. Note that the agreement between calculated curves and the measured values is good down to the 0. 4 amp/cm^2 low current limit shown here. Again, as in the argon-potassium case, the conductivity values showed the anomalous plateau behavior extending from 0. 4 amp/cm^2 down to . 08 amp/cm^2, the lowest current densities investigated (data not shown in Figure 20). This is probably again due to the existence of a shunting film on the test section walls, as was discussed above.

The relative radiation correction for the helium-potassium system is much smaller than that for the argon-potassium system. For example, at 1 amp/cm^2, the radiation correction produces a reduction in conductivity in the helium- and argon-potassium systems of about 5 per cent and over 30 per cent, respectively. This differ-

ence is produced by the increase in elastic energy transfer between electrons and neutrals resulting from the greatly increased momentum transfer cross section and the reduced atomic weight of helium as compared with argon, as is the case for the large decrease in conductivity discussed above.

Summary of Steady-State Conductivity Measurements

Let us now summarize the experimental and theoretical findings for the steady-state measurements of electrical conductivity. The agreement between experimentally measured values of the electrical conductivity as a function of current density with calculated values based upon the two-temperature model presented here is excellent over a wide range of experimental parameters and experimental conditions.

The dependence of the measured electrical conductivity upon changes in seed concentration, gas temperature, current density, electric field strength, and carrier gas characteristics has been that predicted by theory, and appears correct quantitatively as well as qualitatively. The measurements have been made under conditions where either electron-atom interactions or electron-ion interactions, or both, are important in defining the electron energy loss mechanisms as well as the electrical conductivity.

This good agreement between experiment and theory extends over the range of current densities from about 0.4 amp/cm^2 up to about 90 amp/cm^2. In this region, the electron densities predicted by theory are high enough that the key assumption of electronic col-

lisional equilibrium is probably valid; for lower electron densities, radiative depopulation effects and atom-atom excitation mechanisms appear to be important (see Appendix C). Further, energy losses from the free electrons due to inelastic collisions have been shown to be an important effect for the small scale experiments discussed here. This effect has been included in the theoretical formulation by properly treating elastic and inelastic processes separately in a formulation which depends only on fundamental atomic properties and employs no adjustable parameters.

Given this good agreement, we have a demonstration of the utility of this formulation in calculating nonequilibrium electrical conductivities for practical engineering systems utilizing these dense seeded plasmas. The theory used here should be equally valid for any other monatomic gas - alkali vapor plasma under similar conditions. The existence of the potentially large enhancement in ionization caused by electronic collisional processes has been conclusively demonstrated experimentally over the wide range of experimental conditions covered here. Note that, for example, the electrical conductivity at 10 amp/cm^2 in the potassium-argon system for $T_a = 1500^{\circ}K$, $n_K/n_A = .002$ (see Figures 2 and 12), is about 2500 times the value one would calculate for equilibrium at the gas temperature.

A more critical examination is needed, however, to establish the validity of the key assumption in the theoretical formulation, i.e., that the populations of free and bound states are given by the condition of thermal equilibrium maintained by electronic collisional pro-

cesses and hence defined by the electron temperature. As indicated in Appendix C , this assumption appears justified theoretically, but the foregoing experimental results do not provide a sensitive check upon this fundamental assumption.

This fact may be illustrated by considering the effects upon the measured electrical conductivity versus current density characteristic if the electron density were somewhat lower than that corresponding to equilibrium of the electron temperature. Physically, this is the situation that would exist if radiative depopulation effects were important[1]. To get a rough indication of this effect, consider an example. Suppose the electron density corresponding to a given electron temperature were lower by a factor of two than that predicted by the equilibrium relation of eqn. (6); then ask what the experimentally measurable electrical conductivity - current density relationship would be over the whole range of current densities. The results of this calculation for a typical case with $T_a = 2000^{\circ}K$, $n_K/n_A = .004$, in the argon-potassium system are shown in Figure 21 . The solid curve corresponds to thermal equilibrium at the electron temperature. The dashed curve is the result if the actual electron density were only one half that corresponding to equilibrium at the electron temperature. Note that no measurable difference in the conductivity - current density characteristic is obtained. The reason for this is that for the lower current densities, where close encounters dominate, both the current density and the electrical conductivity are nearly directly proportional to the electron density. Further, at higher currents where Coulomb encounters dominate,

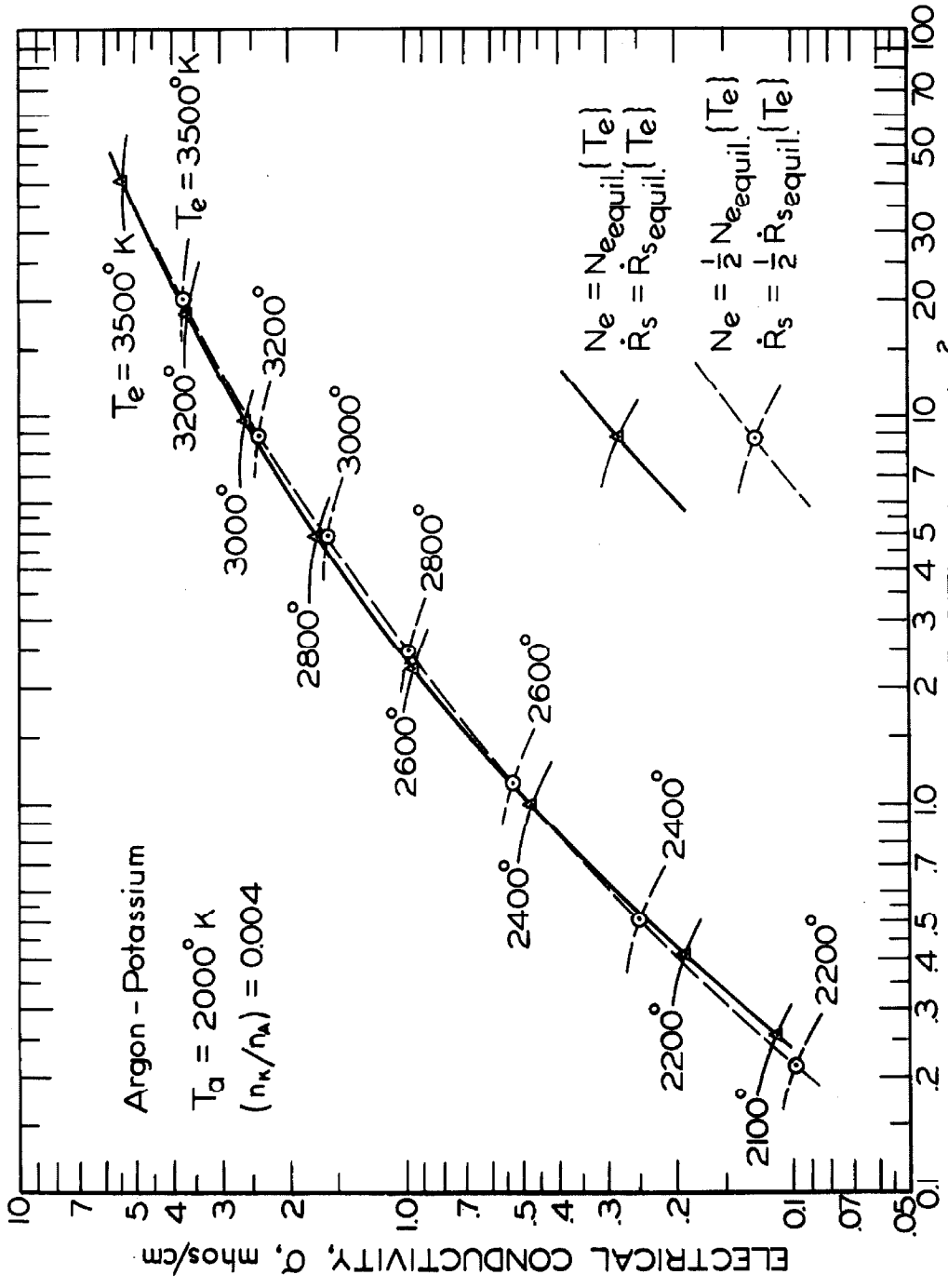

FIG. 21 INFLUENCE OF RADIATIVE DEPOPULATION ON CONDUCTIVITY - CURRENT DENSITY CHARACTERISTIC

the electrical conductivity is a much less sensitive function of electron density, and thus changes in density still result in a shift falling essentially along the somewhat less steeply sloping equilibrium curve.

Note, however, that a reduction in electron density for a given electron temperature results in a higher electron temperature for a given current density. For example, in Figure 21, at 20 amps/cm^2, a measurement of electron temperature would be too high by about 300°K if the actual electron density were only one half of the equilibrium value. Thus, a sensitive check on the theoretical formulation would be the experimental measurement of the electron temperature. Further, if the physical model is correct, the populations of the various excited states in the seed atom and the number density of the free electrons must correspond to electronic collisional equilibrium at the electron temperature.

B. Electron Temperature Measurements

The above discussion suggests that a precise verification of the model requires a more direct measure of electron temperature or density. In this section, a description is given of the experiments used to obtain a measure of the electron temperature with the direct measurement of populations of various excited states in potassium and sodium. Following this, the results of recombination measurements will be presented which additionally provide an estimate of the free electron density.

Two spectroscopic techniques were used to determine popu-

lation temperatures* of electronic states of neutral sodium and potassium atoms. In order to obtain the electron temperature from these data, it is necessary to show that these states are in thermal equilibrium with the electron gas. Calculations for the argon-potassium system of the total probability of electronic collisional de-excitation and also the total probability of radiative decay (see Appendix C), including the effects of absorption, were made for the low-lying levels of potassium up to and including the 4F level at an electron temperature of 2600°K and an electron density of about $10^{14}/cm^3$. The results showed that the ratio of probability of radiative decay to that of collisional de-excitation by electrons is of the order of 1:100 for these states. Hence it seems reasonable to expect that for this electron density, the lower excited states and the electron gas are in equilibrium. For higher excited states, equilibrium is even more likely. Note that for a current density of 2 amp/cm^2, the calculated value of electron density in the plasma under study is greater than 10^{14}. For current densities below 2 amp/cm^2, the electron density drops off, and calculations indicate that the equilibrium assumption becomes questionable for current densities around $\frac{1}{2}$ amp/cm^2. In summary, it appears to be reasonable to assume that thermal equilibrium does exist between the electronic excited states and the electron gas when current densities above 2 amp/cm^2 or electron densities above 10^{14} are used. Hence, in this range, it is also

---

* The population temperature of an observed state density in a not necessarily equilibrium system is defined as the temperature one would associate with an equilibrium system possessing this same state density value.

reasonable to equate population temperatures and electron temperatures.

Previous attempts have been made by the author and others[8, 30, 46, 48, 49] to obtain spectroscopic measurements of excited state populations in seeded plasmas to determine the electron temperature. These early results did show a substantial electron temperature increase, and provided a qualitative check on the two-temperature theory, but did not possess the quantitative accuracy desirable for a precise check on the theory. The data presented in this section do provide this essential quantitative check.

The difficulties in the author's early spectroscopic measurements, reported in reference 48, were traced to the existence of undesirable self-absorption effects which caused measured population temperatures to appear about 10 per cent lower than those predicted by theory. These effects were eliminated by purging the viewing ports, as discussed in Section IV and Appendix A.

The data presented in this section have been recently reported[50]. On this same date, the results of similar measurements in argon-potassium plasmas (using a potassium line reversal technique) were reported by Brederlow, et al.[51], which also substantiate the quantitative conclusions which can be drawn from the following discussion.

The first spectroscopic technique used to determine a population temperature was the sodium line reversal, or SLR, method which utilizes the $3p \rightarrow 3s$ transitions of neutral sodium. This tech-

nique is well known, e. g. reference 52, and provides an absolute measure of the population of the 3p level, and hence an absolute measure of the population temperature. However, since the light source used in the experiments was a tungsten ribbon lamp, the measured values were limited to temperatures below about 2950°K.

The second technique was a relative method based on the use of the change in light intensity resulting from a given transition in response to a change in the applied electric field. The intensities of the $3p \rightarrow 3s$ transitions of neutral sodium, and the $4p \rightarrow 4s$ and $5p \rightarrow 4s$ transition of neutral potassium were measured before and after an electric field was applied to the plasma.

Since the intensity of a transition is proportional to the population density of the upper state, one can determine the population temperature of the upper state by measuring this intensity. The absolute intensity observed depends in detail on absorption of the plasma and the apparatus used to measure the intensity. However, relative changes in intensity can be used to infer relative changes in population temperature, provided the absorption of the line does not change.

For the conditions of the present test, the line spreading is due to Stark and collision broadening as well as Doppler broadening.

However, calculated values of the Stark broadening are negligible compared to the other two effects, and thus changes in electron density should have no effect on absorption. In addition, resonance lines were employed, and thus slight changes in number density of atoms in the ground state have a negligible effect for the conditions discussed here. Consequently, the absorption does not change as a function of current or electron density. In the absence of changes in absorption, the intensity ratio for a given line can be written as

$$\frac{I\{T_2\}}{I\{T_1\}} = \exp\left[\frac{\Delta E_i}{kT_1} - \frac{\Delta E_i}{kT_2}\right] \quad . \tag{27}$$

Here, **I** is the intensity of the i^{th} transition, T is the temperature, k is Boltzmann's constant, and ΔE_i is the energy difference of the i^{th} transition. The subscript 1 refers to conditions when the electric field is zero, and 2 to conditions when a field is applied. This equation can be solved for the temperature ratio to give:

$$\frac{T_1}{T_2} = 1 - \frac{kT_1}{\Delta E_i} \ln\left(\frac{I_2}{I_1}\right) \quad . \tag{28}$$

Equation (28) was used to obtain temperatures from intensity data for the $3p \rightarrow 3s$ transition in neutral sodium. The measurements were made up to temperatures of about $3000^{o}K$, and for these calculations the value used for T_1 was obtained from the SLR measurements. These data and that obtained from the SLR technique are shown as the solid points in Figure 22. The two sets of data agree reasonably well in the region between 6 and 8 amp/cm^2, where they overlap. This indicates that the relative method and the use of equation (28) is consistent with the SLR method and gives confidence in

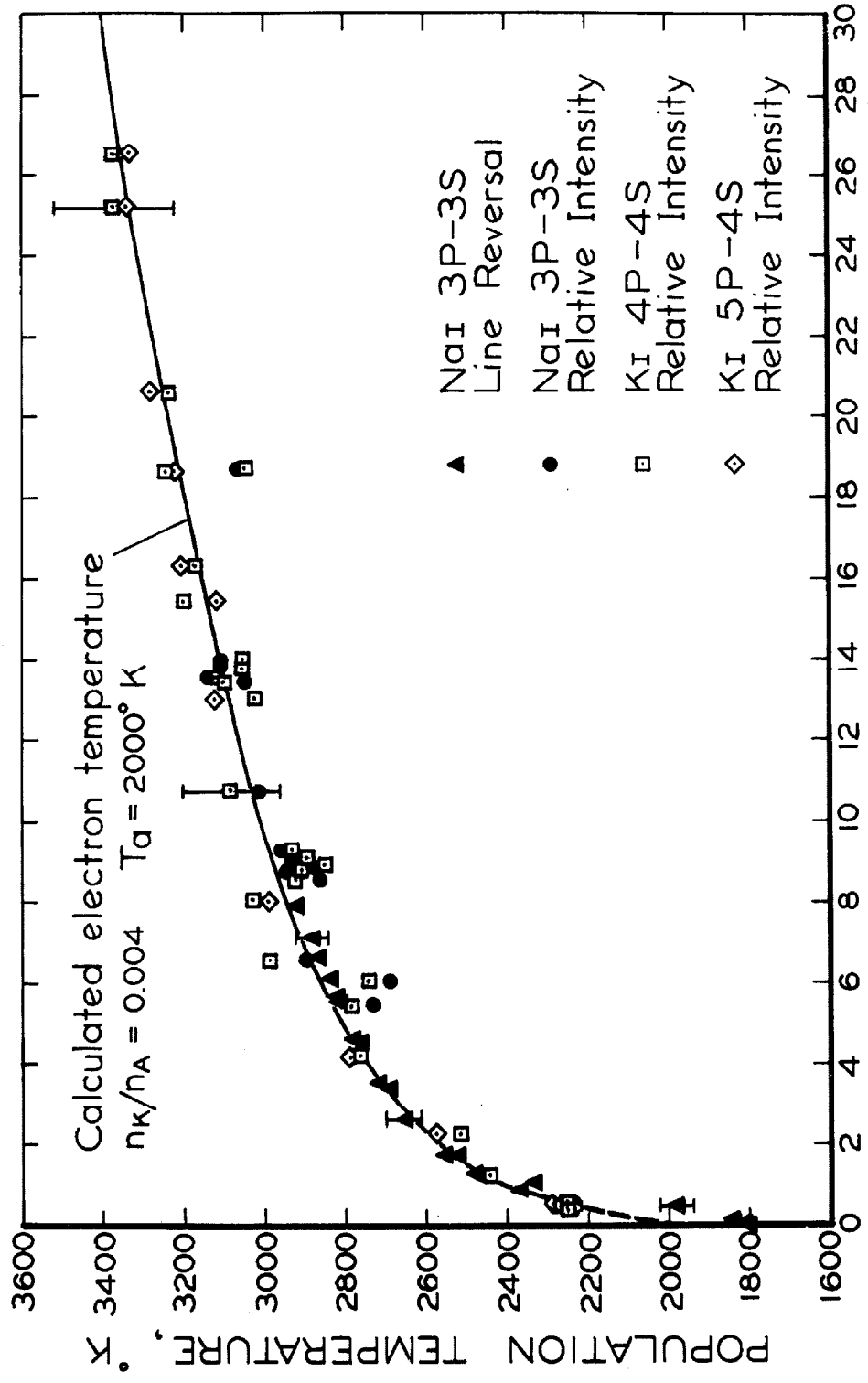

FIG. 22 DEPENDENCE OF POPULATION TEMPERATURES ON CURRENT DENSITY

the relative method as it is used here.

In addition to the sodium measurements, data were obtained with two transitions in potassium. However, in order to use equation (28) with this data, it is necessary to determine the values of the temperatures in the zero field case. This is a non-trivial problem, because radiation losses keep the various excited states out of thermal equilibrium and because no absolute technique such as the SLR method was readily available.* The method used to obtain the initial temperatures was as follows. Relative intensity data were obtained simultaneously for the 3p → 3s sodium transition and the 4p → 4s potassium transition. The value of T_1 for the potassium transition was picked to minimize the squared deviations between T_2 values calculated from equation (28) for the two transitions. (This calculation is based on the assumption that the various lines will be in thermal equilibrium when the electron density is high.) In another set of experiments, simultaneous measurements of the 4p → 4s and 5p → 4s potassium transition intensities were made. The value of T_1 for the 5p → 4s was picked to minimize the squared deviations between the two sets of data.

The zero field temperatures calculated by this technique for an 1800°K temperature of the 3p → 3s sodium transition were 1790°K for the 4p → 4s potassium transition and 1865°K for the 5p → 4s potassium transition.

Use of these values of zero field population temperatures for

---

* Reference 51 reports successful use of a potassium line reversal technique.

the two potassium lines gives the values of population temperature shown in Figure 22 as the open points. The data agree very well with each other and with the values obtained from the sodium data for the whole range of current densities investigated. This good agreement indicates that the equilibrium assumption made in interpreting the intensity data is justified.

In Figure 22, brackets have been placed on some of the SLR data and on some of the potassium data to indicate the maximum errors. The maximum uncertainty in the SLR data is about $\pm$ 40°K, and this uncertainty is due to errors in technique and drift in operating conditions for the arc-jet heater. The larger uncertainty for relative measurements reflects this $\pm$ 40°K maximum uncertainty in the zero-field SLR temperature for these data.

The 10°K difference between the initial population temperatures for the Na_I 3p → 3s and K_I 4p → 4s transitions is not significant within the accuracy of the techniques. The close agreement in these temperatures would be expected due to the similarity between the corresponding energy levels in the two atoms. The higher initial temperature obtained for the 5p → 4s K_I transition is significant, since detection of a 65° difference is within the capabilities of the technique. This difference indicates a lack of thermal equilibrium in the zero field case, and suggests that the electron temperature is somewhat higher than the "temperature" of the lowest excited state (if electronic collisional processes are still dominant over atom-atom processes). Note that these measurements indicate the temperatures corresponding to these low-lying states are about 200°K

(4p → 4s) and 135°K (5p → 4s) below the mean translational gas temperature of 2000 ± 100°K.

The solid curve shown in Figure 22 represents the calculated value of electron temperature for the experimental conditions used in these experiments. Although the data are somewhat scattered, they clearly fall along the curve, and hence are in excellent agreement with the calculated values. As was pointed out earlier, there is good reason to expect that for currents of 2 amp/cm^2 or higher, all of the excited states studied were in equilibrium with the electron gas. Hence, the comparison of measured and calculated temperatures, shown in Figure 22, does constitute a check on the electron temperature calculation. It is evident that the calculation gives a satisfactory estimate of electron temperature except at very low current densities.

C. Recombination Rate Measurements

This section deals with measurements which were made of electron-electron-ion recombination rates and with their comparison with values calculated from a model utilizing the classical inelastic collision cross-section expressions of Gryzinski[8].

The apparatus and electric circuit used to measure recombination rates are shown in Figures 7, 9, and 11. The measurement technique consisted of first establishing a steady initial discharge in the argon-potassium plasma. The field strength was then abruptly reduced to a very low value, and during the relaxation period immediately following the reduction of the electric field, measurements were made of the electrical conductivity and the relative

populations of several of the excited states of potassium. From these measurements, it is possible to deduce electron densities, temperatures, and recombination rates.

The range of current densities used in the initial discharge was between 2 and 17 amp/cm^2, which corresponds to field strengths of about 2.5 and 5 v/cm and to initial electron densities of about 1.5 and 8×10^{14}/cm^3. A very small electric field was maintained during the relaxation period so that the plasma conductivity could be monitored. The final field strengths used were between 0.3 to 0.8 v/cm.

A typical set of experimental data is reproduced in Figure 23. Here, light intensity data from two consecutive tests are presented as a function of time. Also shown on the figure are the probe voltages used in obtaining the conductivity values and the values of the electron density calculated from the conductivity values. Figure 24 shows additional typical electron density variations. The transient in the applied field dies out within two microseconds and the probe voltage difference remains essentially constant thereafter.

Light intensity data are shown for the 5p → 4s and 4p → 4s transitions in K_I. The 5p → 4s light intensity initially decays slightly more rapidly than the electron density, and the 4p → 4s light intensity, reaching a relatively low value by about 20 μsecs, then changes more slowly thereafter. A similar behavior was noted for the non-resonance 6s → 4p transitions of K_I (not shown). Interpretation of data for the latter transition must include consideration of the effect on absorption due to changes in the populations of the 4p level with time.

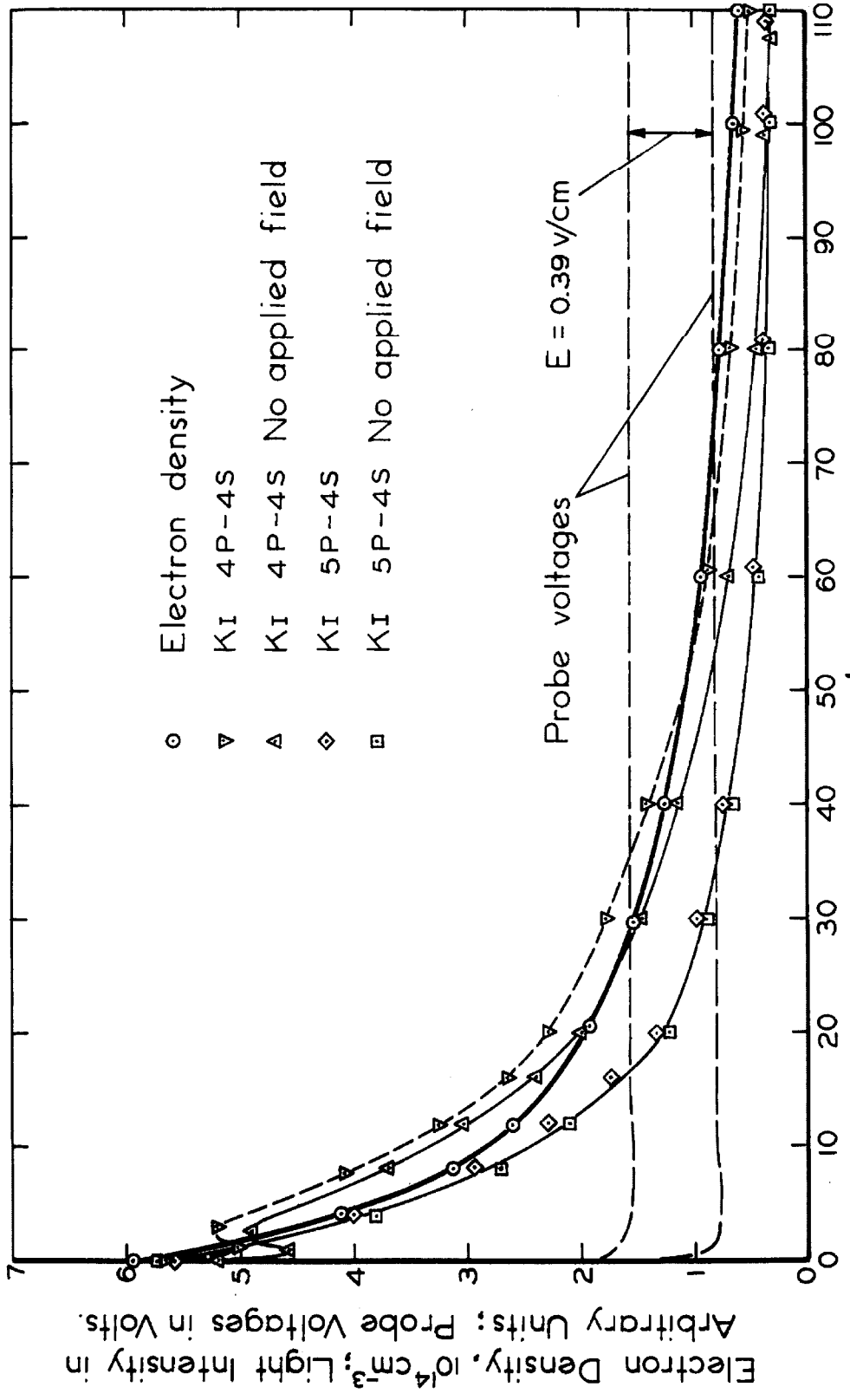

FIG. 23 TYPICAL RECOMBINATIONAL RELAXATION DATA

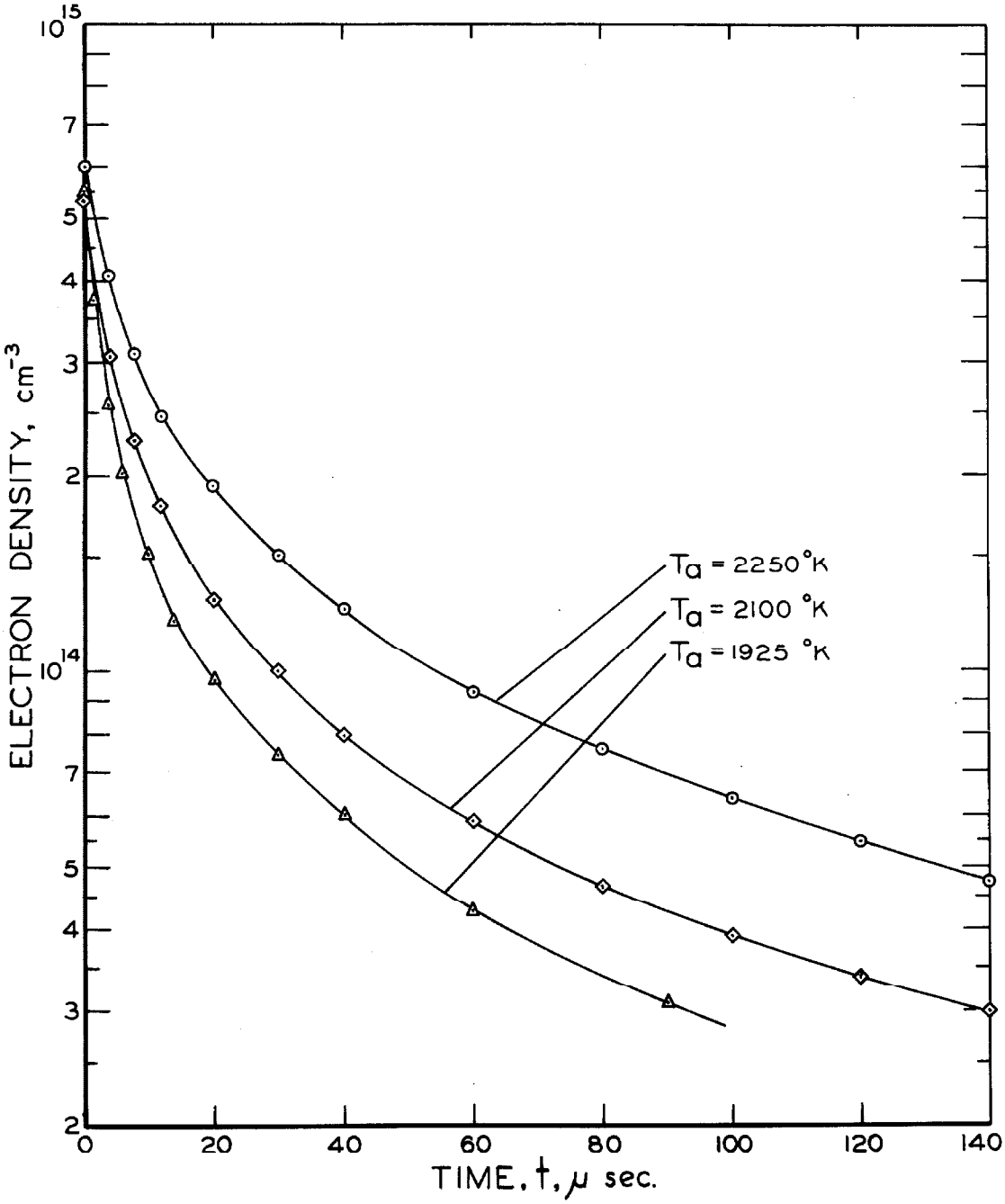

FIG. 24 TYPICAL VARIATION OF ELECTRON DENSITY DURING RECOMBINATIONAL RELAXATION

Note in Figure 23 that the measurements of the decay of the light intensities have been made for nearly identical initial conditions, but for final conditions both with and without a small applied electric field. The values for the 4p → 4s transitions appear slightly displaced in the vertical direction. This reflects the small random fluctuation in initial light intensity commonly observed and is of no importance in interpreting the results. The important thing to note is that the relative changes in population for the 4p and 5p levels appear to be nearly identical with or without an applied field. The effect on the decay rates due to the presence of the small field (0.39 v/cm for this case) is negligible and shows that the relatively small energy input to the free electrons by this field during the relaxation process probably has no important effect on the free-electron recombination rate.

Also note the initial lag in the decay of the first excited state population (4p → 4s light intensity) which is probably due to the initial downward cascading from higher states to the 4p level, as will be discussed later in this section.

Data Reduction. The data reduction procedure used to analyze the recombination data was discussed in Section V-A, and more details will be given here.

Detailed calculations of the radiant energy losses from bound states of potassium at steady state for the argon-potassium system have been performed and are discussed in Appendix B . These calculations show that about 70 per cent of the total radiation loss is accounted for by the 4p → 4s transition in K_I for temperatures of 2000

to 3000°K. Thus, in the quasi-steady relaxation case, the measurement of the relative population of the 4p state in time allows a calculation of the radiation loss from the 4p state, since the initial steady-state intensity and radiation loss are known. The remaining, less than 30 per cent, of the radiation loss can be determined if the general behavior of the relaxation of the various higher contributing transitions is known. This is afforded by the observation of the 5p→4s transition.

Calculation of the contributions of the various terms to the sum, $\Sigma V_i(dN_i/dt)$, show that the only term of appreciable magnitude is that of the 4p level, whose variation in population has been determined as stated above. This fact is due to the relatively large populations of the 4p level. Finally, calculation of σE^2 is done directly from the instantaneous experimental data. In this manner, instantaneous values of all the terms in equation (20), except that for $\mathring{\Omega}$, are calculated directly from the experimental data, and thus equation (20) can be used to determine the variation of $\mathring{\Omega}$ with time during the relaxation period. The first approximation to the instantaneous electron temperature can be obtained from values of $\mathring{\Omega}$ by use of equation (16a).

The results of calculations for the intermediate set of data given in Figure 24 are shown in Table II on the following page. Here, the various terms in equation (20) are evaluated for a number of times during the relaxation period. The last three rows of the table give the final values for the electron density and temperature,

TABLE II.

1	time, t (μsec)	0	2	8	16	20	30	60	100	140
2	$-1.61\ (dN_{4p}/dt)$ watts/cm^3	-	-	1.0	.38	.26	.11	.03	.02	.02
3	$-(V_o+\frac{3}{2}kT_e)\frac{dN_e}{dt}$ watts/cm^3	77.0	41.9	11.9	4.78	3.25	1.82	.58	.24	.14
4	$\mathring{R}$ watts/cm^3	8.4	8.1	5.4	3.06	2.55	1.45	.64	.38	.32
5	σE^2 watts/cm^3	.63	.55	.39	.29	.27	.22	.14	.12	.10
6	$\mathring{\Omega}$ watts/cm^3	69.2	34.4	7.9	2.39	1.43	.70	.11	0	-.02
7	$-(E^*+\frac{3}{2}kT_e)dN_e/dt$ watts/cm^3	21.4	11.7	3.3	1.33	.91	-	-	-	-
8	T_e^* ^oK	2850	2710	2480	2370	2330	-	-	-	-
9	N_e 10^{14}/cm^3	5.3	4.0	2.27	1.51	1.28	1.0	.59	.40	.30
10	T_e ^oK	>3500	>3500	$\gtrsim$3000	2580	2470	2370	2180	2100	2000
11	α 10^{-10}cm^3/sec	3.64	3.47	3.05	2.78	2.60	2.46	2.23	2.06	2.06

and the recombination coefficient, $\alpha \equiv (-1/N_e^2)dN_e/dt$. Values of the collisional recombination rate coefficient, $(-1/N_e^3)dN_e/dt$, are shown in Figure 25 as a function of the electron temperature. The data taken from the table appear as the solid circles, and other data obtained from a number of different tests are also included in this figure.

Discussion. The values of the recombination coefficient calculated for times greater than 20 microseconds after the beginning of the relaxation are shown as the dark data points in Figure 25. These data are in fair agreement with points (open circles) calculated from the theory described in Section V-B, although they are scattered by about 60 per cent for the range investigated.

The agreement is at least as good as one would expect when considering the possible uncertainty in the estimated values of the electron temperatures and those uncertainties connected with the theory. In particular, note that the theoretical rates are directly proportional to the constant γ, which could easily be 50 per cent higher or lower than the value used here. The theory is probably good to within a factor of 2, judging by the agreement of experimental measurements in cesium with calculated values,[40] and the classical cross sections used are thought to be valid to within about a factor of 2[53]. The principal uncertainties in the estimated electron temperatures are the result of possible errors in the gas temperatures as well as errors in the electron energy balance. These possible errors give a probable uncertainty in the data themselves of about a factor of 2.

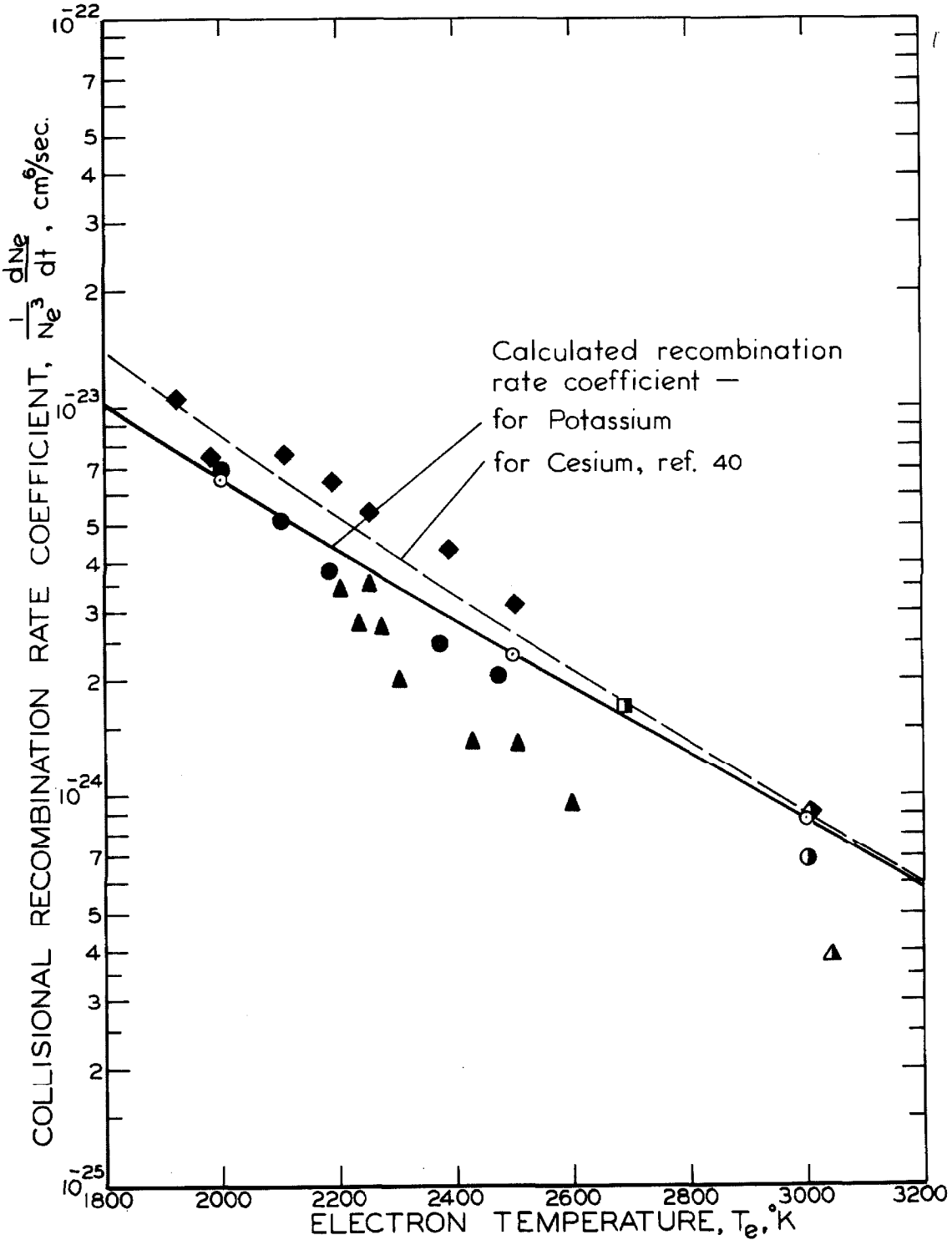

FIG. 25 COLLISIONAL RECOMBINATION RATE COEFFICIENT

The half-filled data points of Figure 25 are those calculated for times as close to the time origin as possible, and in reducing this data it has been assumed that the electron temperature is at its initial value. Though these data would not be expected to show good agreement with the calculated values, since the quasi-steady populations did not have time to develop, it can be seen that fair agreement is obtained. At the other end of the temperature scale lie data obtained some 100 microseconds after the initiation of the relaxation process. Here, the electron temperatures are close enough to the gas temperatures to reduce substantially the uncertainties in electron temperature. Thus, the data for temperatures in the 1900 to 2300°K range are probably relatively more accurate.

Note that the 60 per cent scatter in the collisional recombination rate coefficients about the theoretical values would only correspond to a 30 per cent variation in electron density, even if all the scatter were due to errors in calculated electron density. Given this good agreement between experiment and theory, one can conclude that the electron densities as given by the two-temperature model are reasonable estimates of the actual plasma electron densities. Further, the recombination rates measured here for potassium appear to be in good agreement with present electron-electron-ion recombination rate theory.

The results given in Table II illustrate a difficulty encountered in determining the electron temperature with the quasi-steady energy balance as written in equation (20). The calculations have

been performed starting backward from 140 microseconds after the voltage decrease was initiated, and seem to give reasonable electron temperatures until about 20 microseconds. From this point back to the time origin, the calculated electron temperatures appear to be unreasonably high, and as the origin is approached closely, the calculated values exceed the measured initial temperature of 3000°K for this example. Thus, it appears that a true quasi-steady condition does not exist until after times of about 20 microseconds and that the population levels take at least this much time to distribute themselves in a true quasi-steady fashion.

Thus the term $-(V_o + \frac{3}{2}kT_e)dN_e/dt$ is probably too high to be a valid estimate of the rate of energy input to the free electrons during this early phase, since most of the electrons will recombine first into the uppermost levels, and then these levels must be further collisionally de-excited to the ground state. Hence, the average rate of energy transfer to the free electrons in this phase would be more adequately defined in terms of an expression of the form $-(E^* + \frac{3}{2}kT_e)dN_e/dt$, where the term in the parentheses represents the average energy released to the free electrons for each electron recombination into the higher states. The value of E^* would be approximately equal to the binding energy of the level immediately above the critical gap if de-excitation to lower levels by electronic collisions is negligible. It is interesting to solve for the electron temperature during this short period at the beginning of the relaxation process by simply equating this expression to the elastic energy loss term $\dot{\Omega}^{(10)}$. If E^* is chosen to be 0.94 ev, as calculated for

the range of electron temperatures between 2000 and 3000°K, then calculated electron temperatures, T_e^*, fall somewhat lower than before, as shown in rows 8 and 10 in Table II. These temperatures look about right, since the steady-state value before relaxation is about 3000°K. This may be regarded as somewhat fortuitous, since it is not obvious that the remaining terms in the energy balance will exactly cancel under these conditions.

Finally, some speculative evidence that a quasi-steady state is not reached until about 20 microseconds is given by the light intensity data given in Figure 23. The 5p → 4s transition decays quite rapidly at first, but reaches a low value by about 20 microseconds and decays slowly thereafter. The initial rapid decay would be expected in response to the initial drop in electron density, and the relatively slow variation indicates that after 20 microseconds the quasi-steady state may have been reached. The population of the 4p state does not begin to decay rapidly until after times ranging from 4 to 10 microseconds for various initial conditions. This indicates the relatively long times necessary for the 4p state to reach a quasi-steady state condition. This behavior is consistent with the fact that for these experiments, populations of the first excited state are not small compared to the density of free electrons, and that calculated de-excitation rates for these low-lying levels are not much faster than the rate of de-excitation across the critical gap.

D. Ionization Rate Measurements

This section discusses experimental measurements made during the ionizational relaxation period which occurs in response to the step function application of an essentially constant electric field to the plasma. Electrical conductivities and light intensity data were recorded during this transient as discussed in Section IV. Typical sets of observations are shown in Figures 26 to 28. Figure 26 A shows a typical set of electrical measurements as a function of time during the ionizational transient period obtained in a test section of the type shown in Figure 9 . The upper trace gives the anode potential measured with respect to the cathode potential represented by the lower trace. Also shown are the potentials of the two downstream probes, also measured with respect to the cathode. The difference in floating potential of these two probe traces divided by their separation distance gives the electric field E . The total current trace rises sharply during ionization and then flattens out at the end of the transient. The zero reference for the current trace coincides with the lower trace giving the cathode potential. The average current density is given by dividing the total discharge current by the cross-sectional area of the duct. Figures 26 B and C , 27 A and B, and 28 A, B, C, D show additional sets of data showing the behavior of various spectral transitions in potassium as a function of time.

For all these data, the total discharge voltage is applied at the time origin and remains approximately constant for the duration of the test. After a short initial transient, the probe potential difference remains essentially constant. The probe traces illustrate a

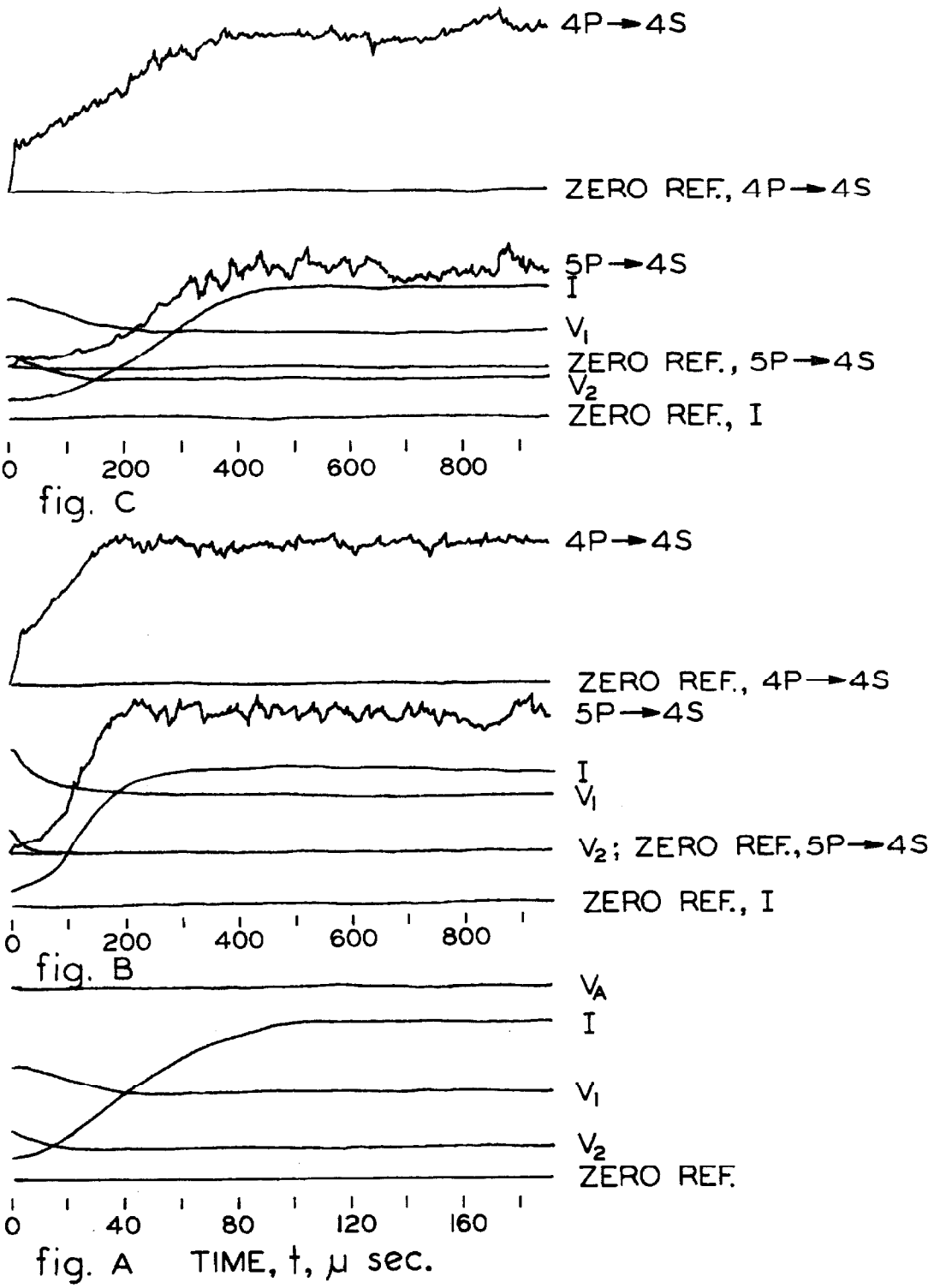

FIG. 26 TYPICAL IONIZATIONAL RELAXATION DATA

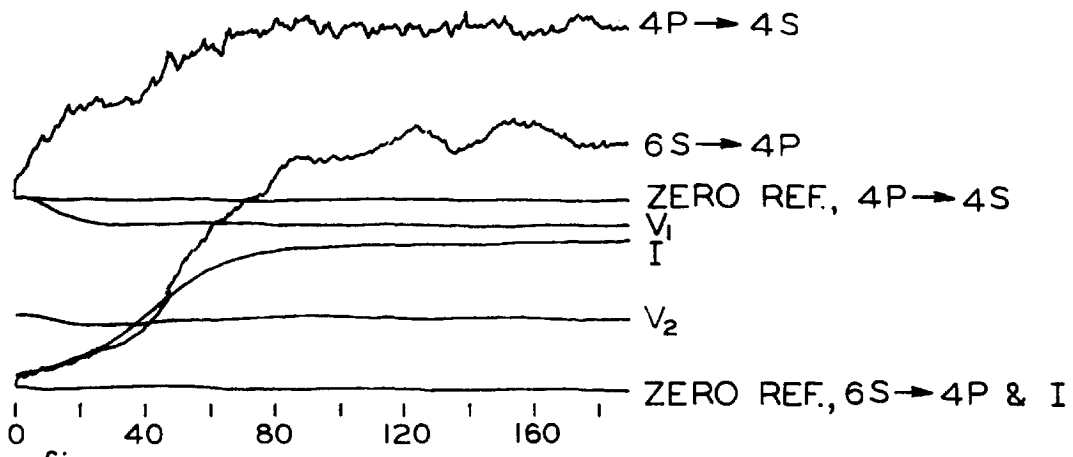

fig. B

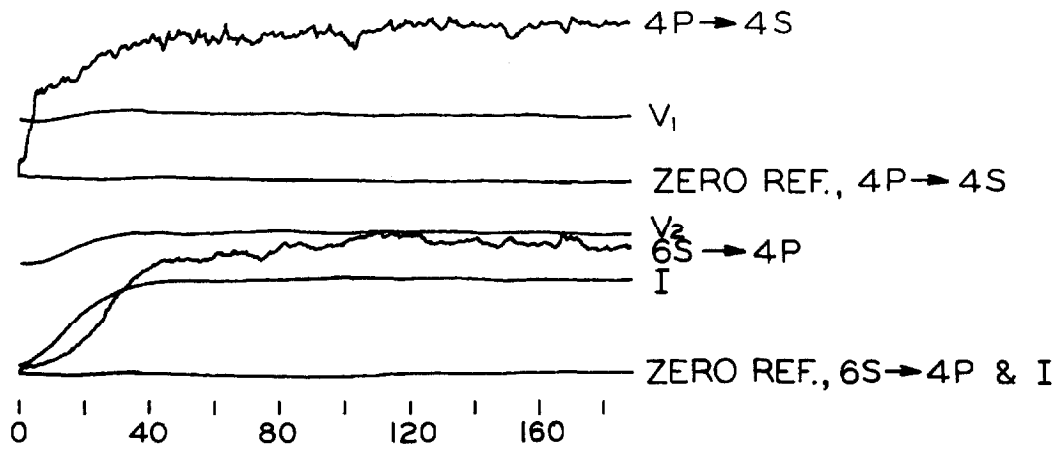

fig. A TIME, t, μ sec.

FIG. 27 TYPICAL IONIZATIONAL RELAXATION DATA

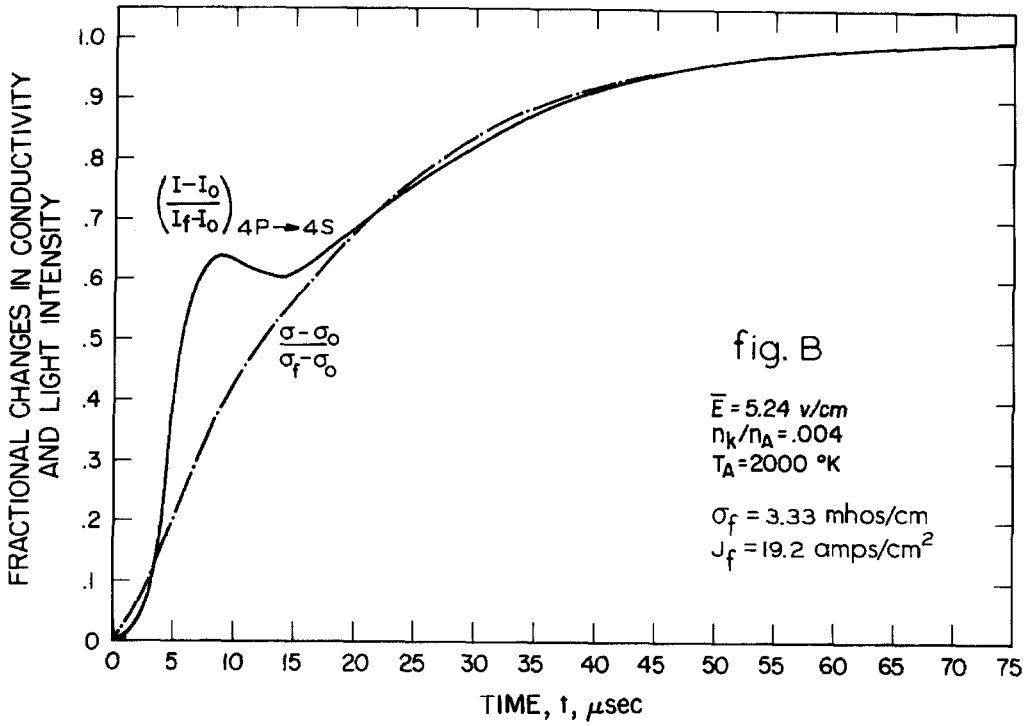

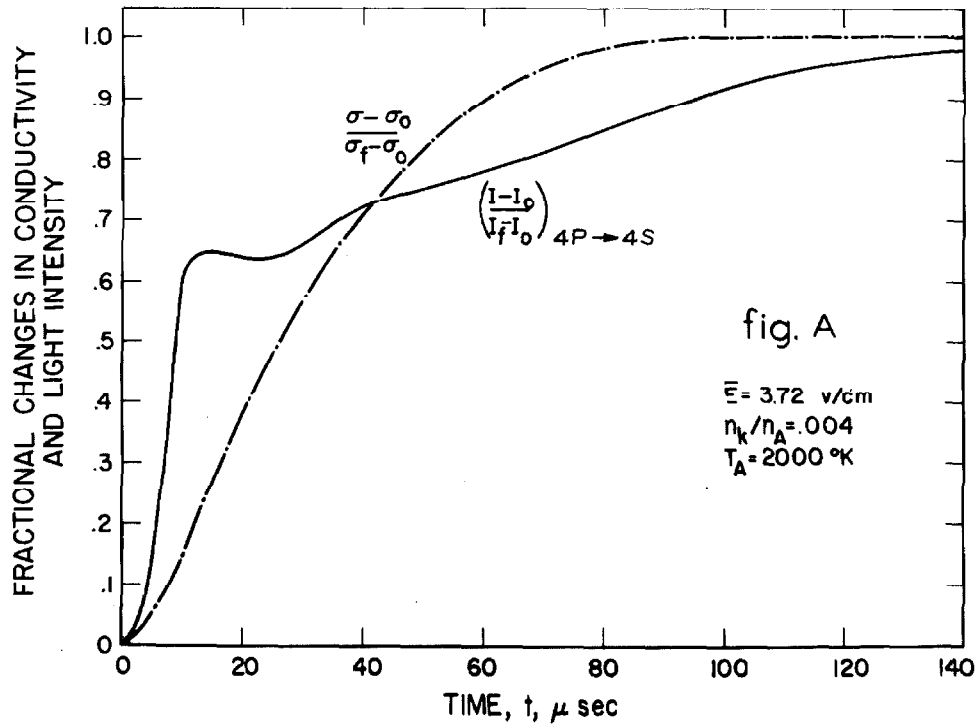

FIG. 28 A & B VARIATION OF INTENSITY AND CONDUCTIVITY WITH TIME

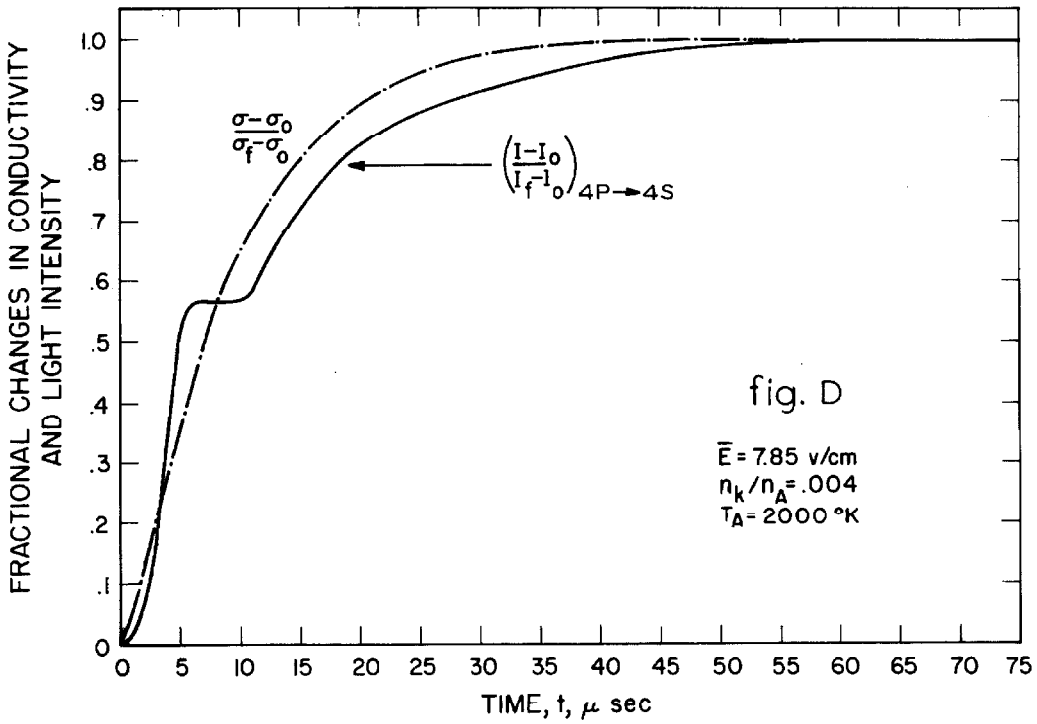

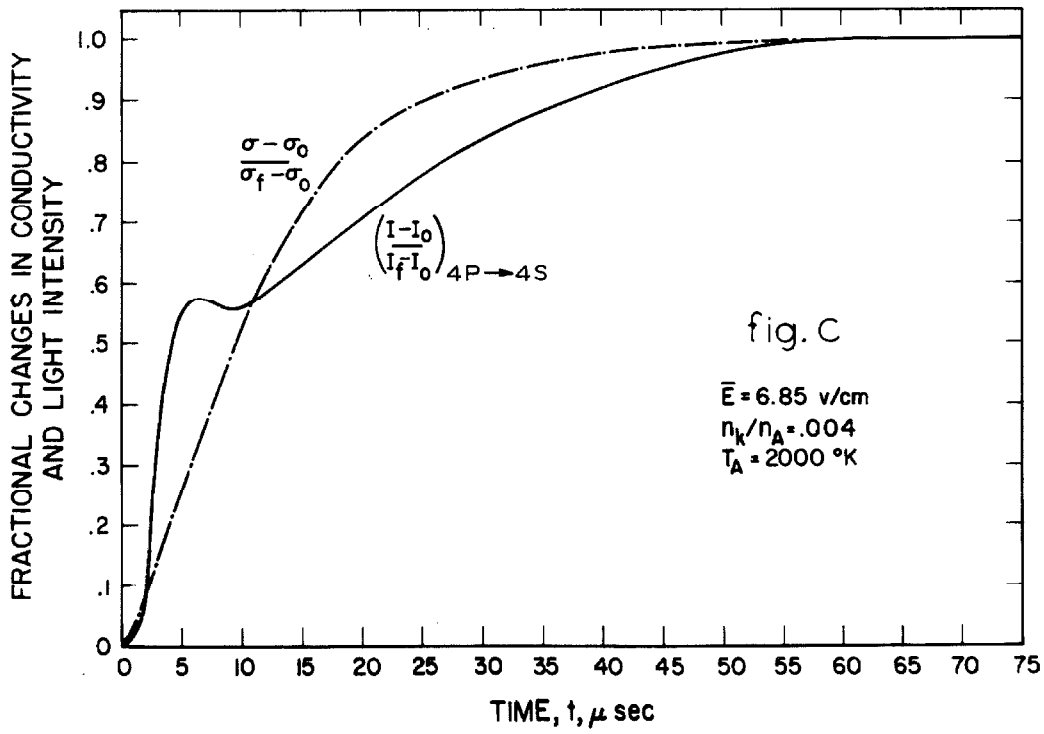

FIG. 28 C & D VARIATION OF INTENSITY AND CONDUCTIVITY WITH TIME

difficulty encountered in attempting to analyze the data. Ideally, one would hope that the probe potential difference would be constant during the entire ionizational transient period. Actually, it is generally larger toward the beginning and decreases somewhat as the end of the transient period is reached. Thus, in analyzing the data, the ionizational transient has been characterized in terms of an average E value during the transient. This is somewhat unsatisfactory for a quantitative analysis, and this fact must be considered in trying to analyze the data. For this reason, the emphasis of this discussion will be primarily upon the qualitative features of the ionizational process. It is believed that the variations in probe potential as measured with respect to the cathode are the result of transient changes in the nature of the discharge near the electrodes, but the varying probe potential difference has not been satisfactorily explained, or eliminated.

Note that the light intensity corresponding to the 4p → 4s transitions in potassium exhibits a marked qualitatively different transient behavior from that of the current density. The light intensity of this resonance transition can be interpreted as corresponding to the relative changes in population density of the 4p state in time. The distinctive feature of these data is the rapid initial rise of the 4p → 4s radiation to a plateau value and then, after a delay, the relatively slower increase in intensity as the end of the ionizational transient is completed. This behavior is even more apparent at lower field strengths, as is shown in Figures 28 A, B . The intensity of the 6s → 4p transitions (nonresonance) shows a delay until after the plateau for the 4p → 4s transitions occurs and then seems to rise in a manner

quite similar to that of the current density. The light intensity of the resonance 5p → 4s transitions seems to follow the rise in current density very closely.

The behavior of the 4p → 4s light intensity data (cf. Figures 26 to 28) indicates that the population densities of low-lying states do increase very rapidly to elevated quasi-steady values in times short compared to those associated with the changes in electron density as indicated by the changes in conductivity. Further, as shown in Section VII-C, when electron densities are high enough, one can relate relative changes in light intensity from resonance transitions to relative changes in electron temperature. These relations will be valid over the latter portions of the ionizational transient; for example, the light intensity data shown in Figures 28 A, B, C, D can probably be interpreted in this manner back from the end of the transient up to the plateau region. An analysis of the typical data shown in Figure 28B shows that the electron temperature at the plateau is within 10 per cent of its final value, i.e., at the plateau $T_e \cong 2920^\circ K$ and $T_{e\,final} \cong 3150^\circ K$. Thus the behavior of the 4p → 4s light intensity data indicates that the electron temperature must rise very rapidly to a relatively high value and then flatten out, or perhaps decrease for a time, then finally increase relatively more slowly as the ionizational transient is completed. This is just the type of behavior one would expect from the theoretical considerations of Section V-B (see Figure 6). These data thus give experimental justification for the theoretical formulation of the ionizational transient given in Section V-B. That is, the populations of low-lying states do increase very rapidly in re-

sponse to a substantial initial electron temperature elevation, and that this increase in electron temperature and population density occurs much more rapidly than does the increase in current density, and hence electron density. The conclusion from this is that the ionizational relaxation period proceeds at a rate limited by the rate of ionization and not the rate of increase of electron temperature.

Examination of the 5p → 4p resonance transitions show that the population density increases at a rate more nearly that of the rate of increase of the free electron density. The excitation energy of the 5p state is 3.06 ev and is located slightly below the calculated critical gap discussed in Section V-B. This state would be expected to show a rate of increase equal to or faster than that of the free electrons due to the existence of this critical gap. It also should populate at a rate somewhat slower than that of the 4p state due to the large energy separation between the 5p and 4p states. The data of Figures 26 to 28 show this behavior. However, the initial differences in rates of population of the 4p and 5p states are large enough that the assumption of quasi-equilibrium of all the levels below the critical gap with respect to the ground state may not be valid over the initial portion of the transient. The lag in the 6s → 4p light intensity data until the plateau for the 4p state has been reached partially reflects the fact that the 6s → 4p transitions are non-resonance transitions, and thus the radiation escaping the plasma changes with the relatively large changes in the density of atoms in the 4p state, the emitted radiation tending to increase as the number density of absorbers increases.

Typical measurements of electrical conductivity as a function

of time, for various average applied electric field strengths, are shown in Figure 29. These data are for the argon-potassium system with $T_a = 2000^\circ K$ and $n_K/n_A = .004$. It is clear from this figure that as the field strength is increased, the steady state values of electrical conductivity increase and the time required to reach these values decreases. The information most directly obtained from these data is the relaxation time, τ_r, required for the change in electrical conductivity $(\sigma-\sigma_o)$ to reach $(1-\frac{1}{e})$ of the final value $(\sigma_{max}-\sigma_o)$. In analyzing the data, it is convenient to give the results as a function of a characteristic time for the process, $\tau_c = \frac{N_{eo} V_o}{\sigma_o E^2}$. Note that $\frac{1}{\tau_c}$ is just the initial rate of energy input, per electron, to the free electrons when $\varepsilon_e \ll V_o$, as mentioned on page 63, and that energy balance considerations (see Section V-B, pp. 66-68) suggest this quantity is an appropriate one with which to correlate observed relaxation times.

Values of τ_r are given in Figure 30 for a range of values of potassium concentration and as a function of the characteristic time, $(N_{eo} V_o/\sigma_o E^2) \equiv \tau_c$. The data lie roughly along a straight line through the origin with a slope of about 8. For the experimental conditions used here, a field of 4 v/cm and $n_K/n_A = 0.0042$ gives a characteristic time of about 30 μsec. Higher fields correspond to much shorter times, and, for strengths as high as 10 v/cm, the relaxation time is less than 10 μsec. It is evident, then, that relaxation times for field strengths of interest will be in the range of tens of microseconds or less.

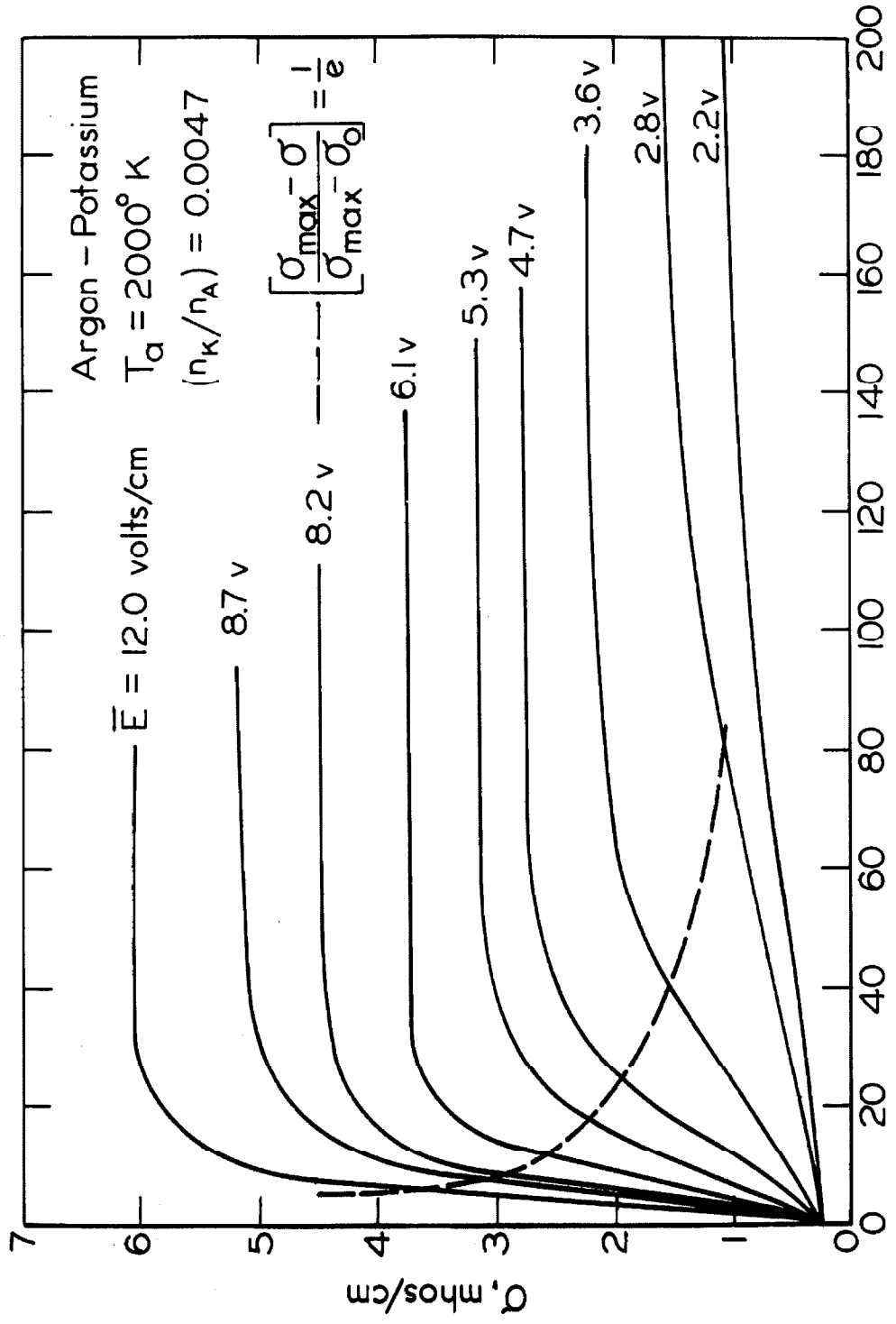

FIG. 29 VARIATION OF CONDUCTIVITY WITH TIME

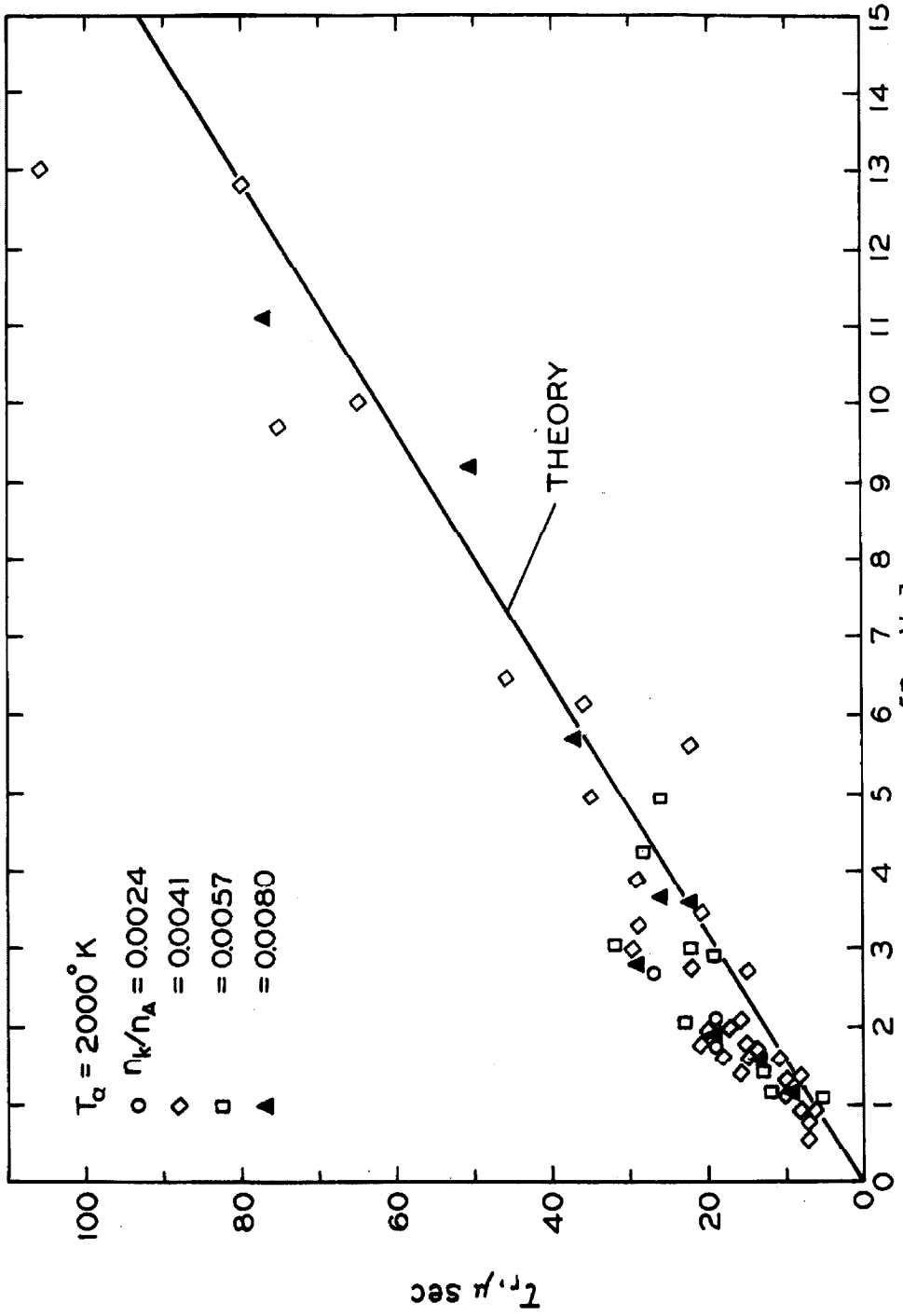

FIG. 30 VARIATION OF RELAXATION TIME WITH CHARACTERISTIC TIME

For a given field strength, the characteristic time changes by about a factor of 3 over the range of potassium concentrations covered by the experiments. The good correlation of the data of Figure 30 suggests that the dependence on potassium concentration is correctly accounted for by use of the characteristic times as the variable.

Before discussing the theoretically calculated curve appearing in Figure 30, let us briefly consider the data in terms of the qualitative discussion below equation (24) of Section V-B. Recall that this discussion indicated that the ionization rate could be approximately estimated from energy balance considerations. Note that, for large fields, measured values of relaxation times are almost identical with the theoretical values found in the preceding section when the assumption was made that all available power went into ionization. Both depend linearly on τ_c , and both are about 8 times larger. Thus, it appears that most of the power input from the electric field to the free electrons goes into the ionization process for field strengths above about 4 v/cm.

For field strengths less than 4 v/cm, the experimentally determined relaxation times are larger than those predicted from the assumption that all the power goes into ionization, and it is evident that, for these low fields, elastic energy and radiation losses are important sinks for power during the ionization period.

The small values found for the relaxation times imply that no transient conductivity problems will be encountered at the entrance of an electric generator using a seeded plasma. For example, with

a field strength of 3 v/cm, the relaxation length for a flow with a Mach one inlet speed, $n_K/n_A = 0.0028$, and $T_a = 2000^{\circ}K$, is about 4 cm. Normal fringing of the electric field should obscure the presence of such a relaxation length and make its effects negligible.

Comparison of Measured Ionization Rates with Theory. Equation (23) contains an expression for the rate of ionization in terms of the instantaneous electron temperature and density. Equation (25) gives the approximate simplified electronic energy balance which enables one to relate the instantaneous electron temperature and density subject to the assumptions discussed in Section V-B.

The above considerations enable the determination of $T_e = T_e\{N_e\}$ and thus $N_{eq}\{N_e\}$. Therefore, all the quantities in eqn. (23) can be put in terms of the instantaneous electron density, and the resulting equation can, in principle, be integrated numerically to determine N_e as a function of time.

If we consider the electric field to be characterized by an average value during the ionizational transient, then we can use the constant E results shown in Figure 6 . Note that for this case the electron temperature is so nearly constant during the first 63 per cent of the ionizational transient that we can consider the ionizational process to occur at a constant average T_e to get a rough estimate of the ionizational relaxation times.

The results shown in Figure 4 show the ionizational profiles for the constant T_e case as determined by integrating eqn. (23). That is, integrating equation (23) for constant T_e gives

$$2\varkappa(t-t_o) = \ell n \left\{ \frac{\left(\frac{N_e}{N_{e_f}}\right)^2 \left(\frac{N_{e_f}}{N_{e_o}}\right)^2 \left[1 - \left(\frac{N_{e_o}}{N_{e_f}}\right)^2\right]}{\left[1 - \left(\frac{N_e}{N_{e_f}}\right)^2\right]} \right\} \qquad (29)$$

where $\varkappa$ is defined as $\frac{1}{N_e}\frac{dN_e}{dt}$ given from eqn. (22) and is constant for a constant T_e. N_{e_f} is defined as $N_{e_{equil}}\{T_e\}$, and is also constant for this simple case. Equation (29) has been used to calculate the results shown in Figure 30.

Thus we can roughly estimate the relaxation time for the constant E case. For example, from Figure 6, we see that for E = 3.0 v/cm that $\overline{T}_e \cong 2770^oK$. Now, from Figure 4, we see that 63 per cent of the change in N_e occurs in τ_r = 47 microseconds. For E = 3.0 volts, τ_c = 7.6 microseconds. In this manner, the theoretical curve shown with the data of Figure 30 was estimated.

Note that the agreement between the theory and the data shown in Figure 30 is surprisingly good. The agreement is probably much better than one would expect in view of the approximations that have been made. Expression (22) is probably valid to within a factor of 2, as was the case for the theoretical recombination rates (Sections V-B, VII-C). The most serious difficulties are probably those connected with the important simplifying assumptions that have been made to relate experiment and theory:

(a.) $E \cong \text{const} = \overline{E} \Rightarrow T_e \cong \text{const} = \overline{T}_e$,

(b.) $\mathring{R} \cong 0$,

(c.) quasi-steady lower state populations; $\Sigma V_i \frac{dN_i}{dt} \cong 0$.

Also, as in the recombination case, errors in electron temperature

estimates cause significant errors in relaxation rate estimates.

Figure 31 shows a roughly approximate theoretical curve compared with the badly scattered data points for the helium-potassium plasma that were observed in this study over a small range of the characteristic time τ_c. Note that the agreement between experiment and theory here is not nearly as good as for the argon-potassium case. An important difference exists in the experimental conditions under which the two sets of data were obtained. The average transit time for the flow through the test section for the argon-potassium case was typically about 400 microseconds, but for the helium-potassium case it was only about 150 microseconds. For this reason, little confidence can be placed in data with τ_r longer than 50 microseconds for the helium-potassium case. Therefore, no data points for longer τ_r appear in this figure.(54)

A portion of the scatter on both sets of data probably reflects the uncertainty in assigning an average E value to the ionizational transient period. No great quantitative confidence should be placed in the data, as experimental errors could be $\pm$ 50 per cent for individual points for the argon-potassium case, and probably much higher for the helium-potassium data.

Discussion. The approximate ionization rate theory discussed here explains, at least in a qualitative way, some important phenomena which have been observed in the ionizational transients in high-pressure gas discharges. As pointed out in reference 55, observed ionizational transients have generally been one or two orders of magnitude faster than conventional calculations based upon one-step ioni-

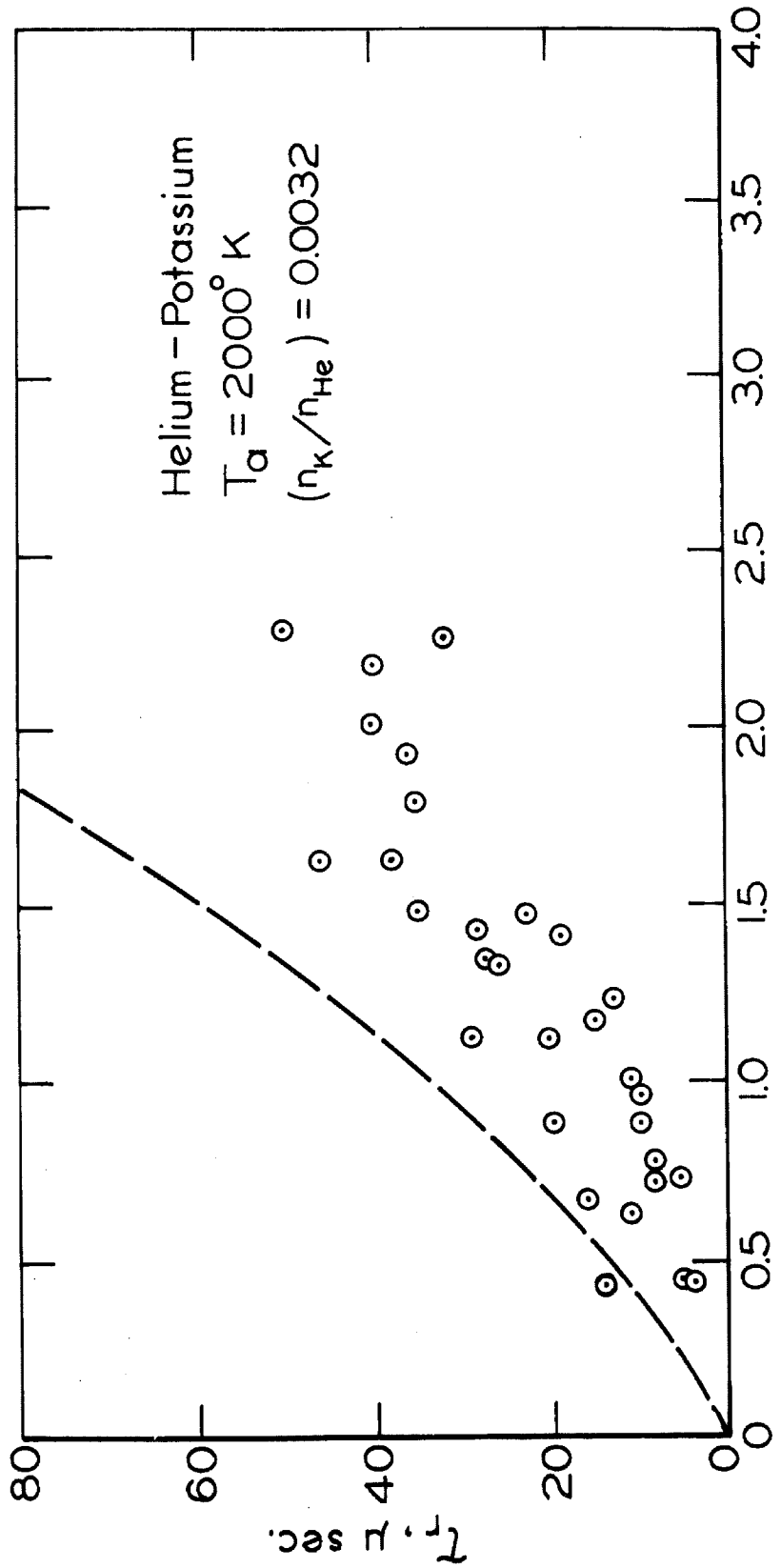

FIG. 31 VARIATION OF RELAXATION TIME WITH CHARACTERISTIC TIME

zation mechanisms would indicate. This fact has been verified by the experimental results presented here (see also reference 48). The theory discussed here shows that the effective activation energy for the ionizational process is approximately the energy difference separating the state immediately above the critical gap from the ground state.

Some additional interesting information concerning this point was found by the author in the early stages of this study. In an attempt to understand the ionizational transient, a correlation between observed initial ionization rates was made with the electron temperature occurring at the end of the ionizational transient. This was done in the following manner. An estimate of $\frac{1}{\sigma}\frac{d\sigma}{dt}\Big|_o$ for various transient data was made near the time origin of the transient period. Then, to a good approximation, $\frac{1}{\sigma}\frac{d\sigma}{dt}\Big|_o \simeq \frac{1}{N_e}\frac{dN_e}{dt}\Big|_o$, which then gave an estimate of the initial rates of ionization. Then, not knowing the details of the electron temperature variation, it was hoped that the actual electron temperatures could be roughly characterized as some constant fraction of the final electron temperatures at the end of the ionizational transients which could be determined from the measurement of the final electrical conductivities. A plot of $\log \frac{1}{\sigma}\frac{d\sigma}{dt}\Big|_o$ versus $1/(kT_{e_f})$ then gave a straight line whose slope could be defined in terms of an "activation energy" which turned out to be very nearly $3.5 \pm .20$ ev for a wide range of seed concentrations. In view of the foregoing theoretical discussion, this result is not surprising, since equation (23) gives an effective activation energy of 3.4 ev, and as indicated in Figure 6 , the electron temperature predicted by theory

does in fact remain at about 90 per cent of the final value over most of the transient for a wide range of field strengths.

The qualitative behavior of the light intensity from the $4p \rightarrow 4s$ transition, as discussed here, indicates that the electron temperature does rise qualitatively in a fashion predicted by the theory. Further, the reasonable agreement between the experimentally measured relaxation times for the argon-potassium system and the simplified theory gives a very rough quantitative check on the theory. This agreement is not felt to be as significant as the agreement between measured recombination rates and theory because of the somewhat greater difficulty in comparing the ionizational experiments to theory due to the experimental difficulties in achieving a constant E field as well as the various approximations in the theory.

A precise quantitative check on the ionization rate theory must await the performance of careful experiments done under accurately controlled conditions where either the electron temperature or applied electric fields are maintained strictly constant in time.

Finally, the theory and data presented here indicate that the ionization rate does determine the relaxation times for conditions of practical interest in connection with MHD devices. The theory discussed here appears to be a reasonable one to apply to the calculation of ionizational transients in large scale MHD devices.

VIII. SUMMARY

It is useful to summarize here the principal conclusions and results of this study in relation to previous work in the field. As mentioned in introduction, the two-fold purpose of this work has been to contribute both useful engineering data and calculation methods concerning the determination of the electrical conductivity and ionizational relaxation characteristics of seeded plasmas, and also to gain an insight into the important physical processes describing the behavior of such plasmas. This work has considered the description of both steady and transient plasmas under the action of applied electric fields.

Consider first the study of the steady-state plasma. This careful and detailed experimental investigation has provided extensive measurements of nonequilibrium electrical conductivity over a wide range of parametric variations. The electrical conductivity, and the influence upon it by variations in gas temperatures, seed concentrations, atomic cross sections, current densities, electric field strengths, and energy loss processes have been investigated here and found to be accurately and simply described theoretically, over a wide range of conditions of engineering interest, in terms of a simple physical model. Experimental measurements of electron temperatures have provided the first conclusive and quantitative verification of the validity of this physical model and the key assumptions in the theoretical formulation.

The careful experimental work performed in this study has led to important modifications of the existing theory. It was found

essential to include inelastic as well as elastic electronic collisional energy losses in the theoretical formulation to accurately describe the measured experimental results. This revised formulation accurately reflects the physical differences between these two processes in terms of fundamental atomic properties and employs no adjustable parameters. The consideration of the detailed energy dependence of the atomic cross sections and the inclusion of both electron-ion and electron-atom interactions has been essential in describing the experimental results. Phenomena occurring at very low current densities have been investigated, and identified and qualitatively described in terms of their probable physical origins.

Experimental measurements of transient electronic ionizational and recombinational relaxation characteristics have been performed for potassium seeded plasmas. Use has been made of existing theoretical formulations of electronic inelastic collisional rate processes to describe the experimental observations of this study in terms of simple physical models. This simple description has been demonstrated here to be reasonably accurate and useful for the determination of the ionization and recombination relaxation processes of importance in MHD power generation.

The electronic recombination rate coefficients measured for potassium in this study show good agreement with the theoretical formulation, as had previously been demonstrated by measurements in cesium, hydrogen, and helium. The simple ionizational relaxation formulation employed here adequately explains the observed relaxation characteristics and ionization rates, and demonstrates that

the rate of ionization determines the inlet relaxation length in practical MHD devices, and shows that these rates are probably rapid enough to cause no practical difficulty in this regard.

APPENDIX A

This section includes a detailed description of the experimental apparatus and experimental techniques utilized throughout this study. Each major portion of the apparatus and the techniques employed in its use will be discussed individually.

Arc-Jet Heater

Figure 8 gives a schematic diagram of the arc-jet heater. The primary flow of argon or helium gas is injected tangentially through sonic orifices to produce a spiralling flow about the anode. This flow then produces vortex stabilization of the arc, which heats the flow and which extends between cathode and anode as shown. Operation is begun by establishing the desired gas flow rate, then applying a potential across the anode and cathode and temporarily shorting them with a very fine copper wire to initiate the arc. It was experimentally determined that the arc ran more efficiently and stably with the downstream electrode chosen as the cathode[37].

All metal surfaces of the arc-jet heater were made of copper, and suitable cooling was effected by numerous water jacket passages. A 3/16" thick quartz insulator was placed between the cathode and the mixing chamber to ensure that the arc was confined to strike only on the water-cooled copper cathode. It was found necessary to recess the exposed face of the cathode in the manner shown to ensure only very small rates of erosion of the cathode surface. The recessed surface allowed operation of about 2 hours before the exposed cathode surfaces showed any significant erosion. Upon operating for

longer periods of time with a given cathode, the surfaces would finally show signs of erosion; the centermost portion would erode away, and then deterioration of the cathode surface proceeded somewhat more rapidly. By carefully changing cathodes at appropriate intervals, it was possible to eliminate copper contamination of the flow almost entirely.

Electrical power to the arc jet was provided by a remotely-located, conventional motor-generator set. This unit could supply D. C. voltages of up to 270 volts at power levels ranging from about 1 to 10 kw as needed for these experiments. The volt-ampere characteristics of the arc could be controlled by the suitable choice of air-cooled ballast resistors in the arc heater circuit.

The power input to the arc could be varied continuously by adjusting a rheostat placed in the field coil circuit of the motor generator set used to supply D. C. power to the arc. Typical operating conditions with argon and with helium are given below:

Gas	Primary Flow Rate	Arc Voltage	Arc Current	Mean Gas Temperature at Test Section
argon	2.23 gm/sec	72 volts	68 amps	2000°K
helium	.6 gm/sec	172 volts	58 amps	2000°K

The primary argon or helium flow was measured with a calibrated tapered-tube, rotating metal-flow flowrator (Fischer and Porter series 10A 2700) with a maximum error of about 3 per cent.

Arc initiation was difficult to achieve in pure helium and generally required an applied total arc voltage of at least 260 volts.

Difficulties were also encountered in achieving a stable arc when starting the arc on pure helium. For these reasons it was found desirable to start the arc in a pure argon flow and then progressively reduce the argon flow while gradually increasing the helium flow and simultaneously increasing the power input to the arc. In this manner, it was possible to achieve a pure helium flow with a stable arc at the approximate operating conditions listed above.

Potassium Bath and Secondary Gas Flow

Potassium vapor was entrained in a small secondary flow of either argon or helium by bubbling the flow up through $\frac{1}{2}$ to $2\frac{1}{2}$ lbs. of liquid potassium at 793°K in the bottom of a stainless-steel cylinder of 4" I. D. and 16" height, as illustrated schematically in Figure 8 The space above the liquid potassium was maintained at a total pressure of slightly over one atmosphere and contained a partial pressure of potassium vapor of about .054 atmosphere, which corresponds to vapor pressure equilibrium at the liquid temperature. The secondary flow has a calculated minimum residence time of 2 seconds in the potassium bath and is thus thoroughly mixed with potassium vapor in this region before being combined with the primary flow. Measurements of the potassium concentrations entrained in the secondary argon flow were performed to establish the degree of entrainment of the potassium vapor in the secondary flow. This was done by condensation of the potassium vapor from a known quantity of the secondary flow and dissolving this vapor in distilled water. A titration was then performed to determine the quantity of dissolved

potassium that was recovered from the secondary flow sample.

These measurements showed that the seed concentration of the flow passing through the potassium bath was within at least 90 per cent of the value calculated assuming the flow to be completely saturated with the equilibrium potassium concentration. Hence all calculations of potassium concentration in these experiments were based on the assumption that the secondary gas flow was saturated with the potassium vapor in an amount corresponding to the equilibrium concentration of potassium vapor above the liquid potassium at 793^{o}K; and therefore, the maximum error in these calculated potassium concentrations in the secondary flow is taken to be less than 10 per cent.

Small amounts of sodium were also placed in the bath along with the potassium. The vapor pressure for sodium is low enough compared to that of potassium at 793^{o}K to cause no significant error in the calculated potassium concentrations in the flow and, in addition, the small amounts of sodium introduced into the total flow were not enough to cause any measurable changes in any of the plasma properties.

All portions of the potassium bath except a thin copper sealing gasket were made of stainless steel. The entire bath was wrapped externally with electrical heating tapes and was thermally insulated to ensure a fairly uniform wall temperature. In addition, stainless steel tubing wrapped with separate electrical heating tapes ensured that the potassium vapor in the secondary flow did not con-

dense before being mixed with the primary flow. Two stainless steel shielded thermocouples extended into the liquid potassium and the output of one of these was used to activate an automatic temperature regulator (Brown Instruments) controlling the power to the heating tapes. The temperature of the potassium bath was also continuously monitored from the thermocouple readings with a millivolt meter (Hewlett-Packard model 425A).

Flow rates in the secondary gas flow were determined with floating-ball type flowrators (Fischer and Porter "Tri-Flat" series) which were precisely calibrated for both argon and helium by measuring volume flow rates at operating pressures and temperatures utilizing a simple water displacement technique, as recommended by the manufacturer. The maximum error in secondary flow settings was about 3 per cent for all seed concentrations employed in these experiments.

The entire secondary flow system, including the potassium bath, was kept filled with argon or helium at all times, including periods between runs, during which the system was kept at 5 psig in either argon or helium. These precautions prevented any possible contamination of the system by atmospheric gases.

Mixing Chamber

The mixing chamber used for flow equilibration is illustrated schematically in Figure 8 . The purpose in utilizing this chamber was to allow time for the secondary flow to become thoroughly mixed with the hotter primary flow, to allow sufficient time for the relaxa-

tion of initial electron temperatures and electron concentrations produced in the primary flow by the arc, and to allow time for ionization levels of the potassium seed to be increased to their steady value in the mixed flow. The objective was to obtain a uniform, homogeneous, seeded plasma at the test section with a uniform heavy-particle temperature (except very near the walls) and electron temperatures and densities corresponding closely to the gas temperature (exactly equal to the gas temperature except for the influence of radiation loss from the plasma).

The average residence time for the flow in the mixing chamber was typically about 2 milliseconds for these experiments. Measurements of ionization relaxation times for potassium done in connection with these studies, as described in Section VII-D , indicate 2 milliseconds to be quite adequate to ensure full ionization relaxation of the potassium seed. Similarly, recombination rates in argon at these temperatures[11] are sufficiently fast to allow full relaxation of any high electron-ion concentrations built up in the arc region in times of less than one millisecond. The time for electron temperature equilibration due to elastic collisions with the heavy species is easily faster than 10^{-5} seconds. Finally, characteristic diffusion times of potassium in argon are sufficient to give complete mixing of the flows in the 2 milliseconds provided.

It should be noted that all portions of the inlet manifold exposed to the flow operated with a visible red-orange glow, and in fact, during helium runs the inlet manifold had to be cooled with an external auxiliary air flow to prevent the manifold from burning up.

Thus, there were no problems encountered with potassium condensation anywhere in the system. Further evidence of this fact was the observation that upon termination of the potassium flow, the electrical conductivity in the test section dropped essentially to zero in a few seconds.

Cooling for the stainless-steel mixing chamber walls was provided by an external air flow. The air flow was then cooled by heat exchange to a water flow in copper tubing surrounding the air flow as is illustrated in Figure 8.

Measurement of the rise in temperature of the cooling water used to cool the arc jet and the mixing chamber was provided by a series connection of 16 chromel-alumel thermocouples. This was done only to obtain a gross check on operating conditions. Attempts to determine mean gas temperatures by an enthalpy balance on the system were not accurate enough to give more than a crude upper bound on gas temperatures, since it was impossible to recover all heat losses from the system with the cooling water.

Gas Temperature Measurement

Two techniques were found to give results of sufficient accuracy for the experiments performed. For gas temperatures near 1500°K, chromel-alumel thermocouples of .005" diameter were employed to determine gas temperatures. In this range, a radiation correction of about 50°K was added to the measured wire temperatures to obtain the gas temperature. The thermocouple arrangement is shown in Figure 32. It was found that a .005" diameter tungsten

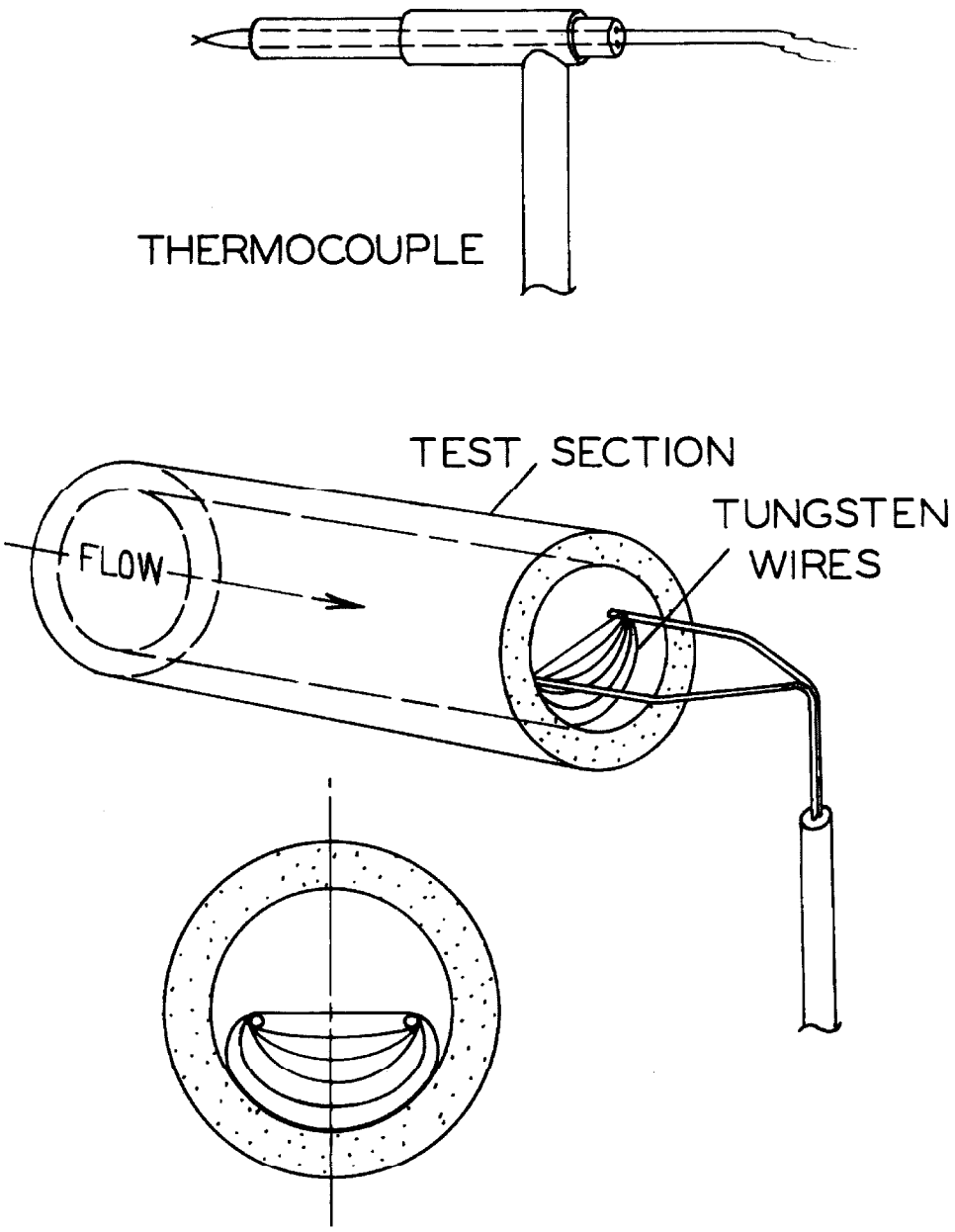

FIG. 32 GAS TEMPERATURE MEASURING DEVICES

wire could be utilized to obtain gas temperatures in this range with an accuracy comparable to that obtained with the thermocouples. For this case, a single tungsten wire stretched between supports like those shown at the bottom of Figure 32 was utilized.

A conventional optical pyrometer (Leeds and Northrup model 8622-C) was used to measure the brightness temperature of the tungsten wires at 6500Å. Emissivity values for tungsten are known as a function of temperature for this wavelength[52] and enabled calculation of the true wire temperature. Radiation corrections could then be made to obtain the gas temperature.

For higher temperatures, near 2000°K, use was made of the tungsten wire technique. For these higher temperatures, the magnitude of the radiation correction made the accuracy of its determination of some concern. In order to reduce uncertainties in this correction, the temperatures of a graded series of wires of diameters ranging from .012" down to .003" were measured. These measurements were found to give a linear plot of the logarithm of wire diameter as a function of wire temperature. This plot was extrapolated to .001" diameter thickness and a radiation correction of about 40°K was then calculated for this diameter. It was then possible to relate the temperature of the various sized wires to the gas temperature. Thus, to determine the gas temperature for a given run, it was only necessary to know the temperature of a tungsten wire of convenient size (about .005" diameter) from which the gas temperature could be determined.

The specification of the gas temperature was actually more complicated than this, however, because the gas temperature was not constant across the test section, but dropped off to about 1250 - 1300°K at the wall. In order to determine the gas temperature profile, measurements were made with a fine network of .006" diameter tungsten wires as shown in Figure 32. Readings of wire temperatures of the various wires were made at the intersection of each wire with the vertical plane containing the centerline of the duct. The associated gas temperature at each point in the flow was then determined as described above. A typical gas temperature profile is shown in Figure 33. The gas temperature, T_a, as referred to throughout this work, was then taken to be the bulk or average temperature obtained by averaging over the cross-sectional area of the duct. That is,

$$\frac{T_B}{T_{C_L}} = 2 \int_0^1 \xi T^*(\xi) d\xi \ ,$$

where $\xi = r/R$; r is the radial coordinate, and R is the radius of the duct; T_{C_L} is the temperature determined at the centerline of the duct; T_B is the bulk temperature $\equiv T_a$; and $T^*(\xi) = \frac{T(\xi)}{T_{C_L}}$ where $T(\xi)$ is the temperature determined at the position ξ . The bulk temperature, T_a , is shown in Figure 33 for this typical profile.

Finally, a further approximate test was made in order to roughly check the tungsten-wire temperature readings. Very thin platinum wires (.005" diameter) were placed in the flow and were observed to melt at about their melting point of 2047°K as ascertained

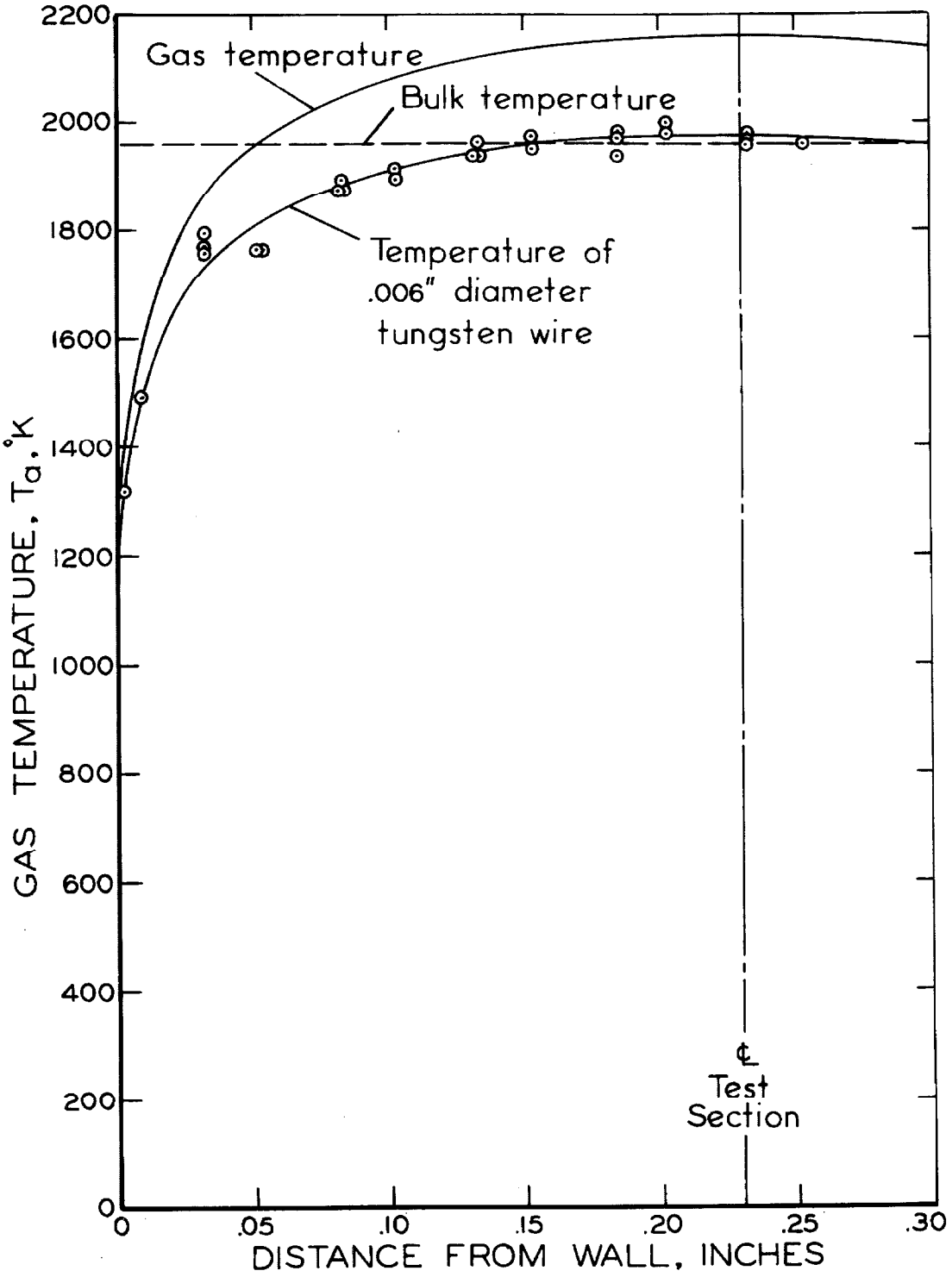

FIG. 33 TYPICAL TEMPERATURE DISTRIBUTION ACROSS TEST SECTION

by estimating the platinum wire temperature based upon simultaneously measured temperatures for tungsten wires.

The above methods gave estimates of average gas temperatures which were probably accurate to within $\pm$ 30 to 40^{o}K at 1500^{o}K and $\pm$ 100^{o}K at 2000^{o}K.

Spectroscopic Apparatus and Measurements

The optical system was designed to provide, first of all, sodium line reversal, or SLR, measurements of the population of the 3p state in neutral sodium, Na_I. Secondly, it provided relative population measurements of various low-lying states of neutral potassium, K_I, in addition to relative measurements of populations of the 3p state in Na_I. A schematic diagram of the optical system has been shown in Figure 7. The entire optical system was mounted on a specially designed optical bench which allowed three degrees of freedom motion and precise adjustment of the optical system. The SLR measurements will be discussed first, and then detailed information on the relative measurements will be given.

The SLR measuring apparatus was conventional, and the general technique is fully described in ref. 52. The principal components used here were the following: two double convex lenses of 3.75 cm diameter and 20 cm focal length, a Gaertner 474-AV spectroscope, and a General Electric type 18A tungsten ribbon lamp. Variable electrical power was supplied to the lamp with a Variac transformer unit, and lamp voltages were measured with a Simpson model 29 A. C. voltmeter.

Figure 9 shows the special test cell which allowed argon purging of the viewing ports and thus prevented the formation of a cloud of cool potassium vapor which would cause undesirable absorption effects. It was found that the auxiliary flow needed to eliminate these absorption effects was less than $1\frac{1}{2}$ per cent of the total flow . This auxiliary flow produced no measurable effects upon experimentally measured conductivity values.

As the auxiliary flow was increased from zero to about one per cent of the total flow, the measured SLR temperature steadily increased. Increasing the auxiliary flow from about 1 per cent up to as large as 5 per cent of the total flow produced no further change in the measured SLR temperature, thus indicating that the cool absorbing layer had been effectively eliminated.

The port closest to the lamp was of 3/32" diameter, and the port nearest the spectroscope was 1/16" diameter. The optical system was precisely aligned so that light passing through the first port completely and uniformly filled the second port. The center of focus between the two lenses was precisely located at the centerline of the test section. The light beam emerging from this hole then completely filled an iris-type aperture placed immediately in front of the lens closest to the spectroscope, as is illustrated in Figure 7 . The beam was then focussed accurately to cover the slit of the spectroscope.

The SLR lamp was calibrated by reading its brightness temperature at 6500 Å with a precision optical pyrometer placed so as to view the lamp through the test section from a point between that side

of the test section closest to the spectroscope and the lens immediately in front of the spectroscope. During this calibration, the quartz window covering the port on this side of the test section was removed to ensure that the brightness of the lamp as read by the pyrometer would correspond to the intensity used as a comparison with the intensity of the sodium transition. The brightness temperature at 6500 Å was corrected to the brightness temperature at 5893 Å with the standard calculation outlined in ref. 52 . Thus, the brightness temperature at 5893 Å was determined as a function of the lamp voltage to obtain a calibration curve for SLR measurements.

It should be mentioned that calibration curves as obtained with the above calibration procedure were not significantly different from those obtained by a simpler approximate procedure, as outlined in ref. 52 , in which direct readings of the brightness temperature of the tungsten filament are corrected for reflection losses at the surfaces of the lens nearest the lamp to determine the brightness temperature as seen at the center of focus in the plasma.

The optical pyrometer used for these measurements (Leeds and Northrup model 8622-C) had been calibrated by checking against an NBS standard lamp.

A second set of optical apparatus was designed to measure relative changes in light intensities from various transitions in the lower states of potassium and sodium. The schematic diagram given in Figure 7 shows the system of mirrors, filters, and phototubes necessary to study these transitions experimentally. Photomultiplier tubes and optical filters were selected to provide a means by which

spectral bands containing the various transitions could be isolated for individual study. Second-order interference filters were chosen to give second-order transmittance bands with average half widths of about 90 Å centered at the particular transition of interest. Additional Kodak Wratten filters were carefully chosen to exclude the first-order transmittance bands. The phototubes were chosen to give good response in the spectral region of interest, but to have negligible response in the third- and higher order transmittance bands. In addition, the spectral regions of investigation contained no transitions of significant intensity of any other species in the flow besides the atom of interest. The tubes and filters used to monitor each transition are shown in the following table:

Transition	Bausch and Lomb 2nd-Order Interference Filter No.	Kodak Wratten Filter Number	RCA Phototube Number
K_I 4p → 4s	33-79-76	89B	7102
K_I 5p → 4s	33-79-40	0	7102
K_I 6s → 4p	33-78-69	29(F)	6655-A
Na_I 3p → 3s	33-79-58	22	7102

The photomultiplier tubes were electrostatically shielded by placing them inside both brass and stainless steel liners, and all electrical leads were carefully shielded and grounded. During operation, they were sealed off and immersed in a mixture of dry ice and ethyl alcohol to cool the tubes below 200°K. These precautions eliminated spurious electrical pick-up and thermal noise from the photomultiplier output signals. The entire photomultiplier tube -

mirror system was completely purged with dry, high-purity nitrogen which prevented all condensation in the optical system. Care was taken to eliminate light leaks from external sources during the tests.

The light path for incoming light to the phototubes was adjustable and could be connected to either of the two pairs of observation ports in the test section. When connected to the upstream port, the light inlet was aligned snugly against the quartz window and light leakage was prevented. When the inlet was connected snugly against the downstream port, the light pipe contained a celluloid seal about 4 inches from the port which provided a region between port and seal of dead gas space and eliminated the vapor plume which would have been present at the inlet, had the seal not been present. This second port arrangement was used exclusively for ionization and recombination transient measurements.

Precise light intensity comparisons could be made between two steady-state discharge conditions by utilizing the photomultiplier optical system and the upstream pair of ports. In order to measure the ratio of intensities accurately, it was necessary to connect a .25 μfd capacitor between the oscilloscope input and ground, which smoothed the high-frequency, random characteristic of the light intensity trace from the phototubes. This provided relative light intensity comparisons accurate to within 2 per cent. The averaging of the random signal thus obtained could be checked by comparing traces resulting from fairly high light intensities (and thus possessing a fairly well-defined signal even without the filter), both with and without the filter. The result was that the filter gave a good time

average of the random signal.

The photomultiplier tube circuitry was conventional. The measured light intensities were within the linear range of phototube outputs (output current ≤ 1/10 bleeder current), and care was taken to provide sufficient capacitive coupling with the final dynode stages to ensure stabilization of dynode voltages. A Kepco model ABC 1500 M voltage-regulated D. C. power supply was employed to operate the phototubes.

The unfiltered phototube circuitry used in transient measurements showed a rise time of less than 1 microsecond in response to light pulses.

Additional Measurement Techniques

Brief mention should be made of the manner in which basic data were taken during these experiments. Transient ionization, relaxation, and steady-state measurements will be discussed first, followed by recombination relaxation measurements.

The lower portion of the circuit diagram in Figure 11, labeled ionization circuit, was used to establish a step function increase in the electric field between the discharge electrodes from an initially zero value to any desired final value up to about 30 v/cm. This was accomplished by charging a 4600 μfd electrolytic capacitor to any desired initial voltage by means of a D. C. voltage supply obtained by rectifying the output of a variable A. C. transformer with a silicon transistor. The charging was done by an external circuit. The capacitor was switched into the external circuit for charging and then

switched completely out of the external circuit into the test circuit before beginning the test. This switching arrangement prevented ground-looping between the charging circuit and the test circuit.

The test discharge was then initiated by closing the lower mercury switch shown in Figure 11. Since the time constant for discharge of the capacitor through the plasma was much longer than test times of up to about 400 microseconds, a nearly perfectly constant potential difference was applied between the discharge electrodes. Minor initial difficulties with slightly underdamped voltage pulses[48] were eliminated by reducing circuit inductance and resistance to very low values by using large no. 12 gauge copper wires for the leads and keeping them as short as was physically possible.

All probe potentials, current measurement potential and photomultiplier output signals were recorded with a Tektronix type 551 dual-beam oscilloscope equipped with a type M, 4-trace amplifier and a type D amplifier unit. Some preliminary experiments, with no light intensity measurements, were performed with a Tektronix type 535 single-beam oscilloscope and type M pre-amplifier. Very short, shielded leads for the voltage probe measurements were connected with Tektronix type P6000 10X compensated probes, carefully adjusted to give accurate high-frequency response. The current measurement circuitry had to be carefully shielded and grounded to remove external electrical noise, and the observed rise time for this circuitry, as well as that of the voltage probes, was less than two microseconds. The current measurement resistor and the oscilloscope amplifiers were periodically calibrated against the oscilloscope

square-wave generator to check all measurements. Average oscilloscope readings were accurate to within 3 to 4 per cent, but with careful calibration and photo measurements they could be made to within 2 per cent.

For very low current density measurements, it was convenient to operate the discharge in a steady state fashion by using a ballast resistor and battery voltages from 2 to 12 v D. C. These measurements were also recorded on the oscilloscope. Also, Simpson model 29 panel meters were included in the steady-state circuitry to afford qualitative observations of discharge characteristics over the range of current densities from 0 to 40 amp/cm in a fashion similar to that employed by Pinchak[37].

Recombination relaxation measurements were similar to those performed during the ionization relaxation period. The upper portion of the circuit shown in Figure 11 was utilized, and the relaxation was again initiated by closing a mercury switch. The mercury switches used for these experiments were of the conventional tilt-action type.

As an additional comment, some preliminary data were taken with alundum test section walls[48]. Most all of the data reported here were taken with boron nitride test sections. Boron nitride was found to have a much longer useful lifetime.

APPENDIX B

Plasma Radiative Transfer Calculations

In formulating the quasi-steady electronic energy balance as discussed in Section III, it was necessary to include energy losses from the free electrons due to radiative energy transfer from the plasma volume. Energy can be lost directly from the free electrons due to photon emission by a free electron moving in the electric field of an ion (Bremsstrahlung). Energy is also lost from the free electrons as a result of inelastic collisions with the various heavy species. That is, if bound or free states initially created by inelastic electronic collisions decay by the emission of radiation instead of by an electronic collisional de-excitation or recombination, then a net energy loss from the free electrons results. Thus, the total radiative energy transfer at the boundaries of the plasma can be calculated to estimate the magnitude of the rate of inelastic collisional energy loss from the free electrons, when electronic collisional processes and radiative transitions determine the populations of the various free and bound states.

This Appendix gives the details of the plasma radiative transfer calculation used to estimate the steady-state rate of energy loss from the free electrons due to inelastic collisions (see eqn. (3)).

An estimate of the total free-free emission rate (Bremsstrahlung) per unit volume from the plasma can be made with the formula of Spitzer[56]:

$$\mathring{R}_{f\text{-}f} = 1.435\times10^{-34} Z^2 T_e^{\frac{1}{2}} g N_e N_i \quad \text{watts/cm}^3 \qquad \text{(B-1)}$$

With an electron temperature of 3500°K and an electron density of 2×10^{15}, we find $\mathring{R}_{f-f} \cong .034$ watts/cm^3.

The total rate of emission per unit volume due to free-bound transitions is obtained by calculating the rate of radiative recombination to each bound level and multiplying by the energy difference between the free electrons and the bound level, and them summing over all possible transitions. However, in order to get an upper bound on the magnitude of this total rate, it is sufficient to multiply the total radiative recombination rate to all bound states by the energy difference between the free electrons and the ground state. The total radiative recombination rate coefficient for hydrogenic atoms can be written as (see Section V-A)

$$\alpha_r \equiv \frac{1}{N_e^2}\frac{dN_e}{dt} \cong 2.7\times10^{-13}/(kT_e)^{3/4} \text{ cm}^3/\text{sec}$$

and the rate coefficient for potassium should not be substantially different. Thus, an upper bound on the total rate of emission per unit volume due to free-bound transitions is

$$\mathring{R}_{f-b} \lesssim (V_o + \frac{3}{2}kT_e)\frac{dN_e}{dt}\Big|_r \cong V_o N_e^2 \alpha_r \ . \qquad \text{(B-2)}$$

With an electron temperature of 3500°K or .302 ev, and an electron density of 2×10^{15}/cm^3, we find $\mathring{R}_{f-b} \lesssim 1.9$ watts/cm^3.

As will be shown in the following, the total rate per unit volume of emission of radiation from bound-bound transitions in potassium is quite large compared to the above estimates of free-free and free-bound radiation rates, e.g., $\mathring{R}_{b-b} \cong 26$ watts/cm^3 at T_e = 3500°K, $N_e \cong 2\times10^{15}$/cm^3. This condition of electron temperature

and density is near the upper limit of conditions encountered in these experiments, and for lower temperatures and densities the bound-bound transitions dominate even more heavily. Thus, free-free and free-bound transitions will be neglected in this analysis.

The remainder of this section will be devoted to the detailed calculation of bound-bound radiation losses from the plasma volume, as shown in Figure 34.

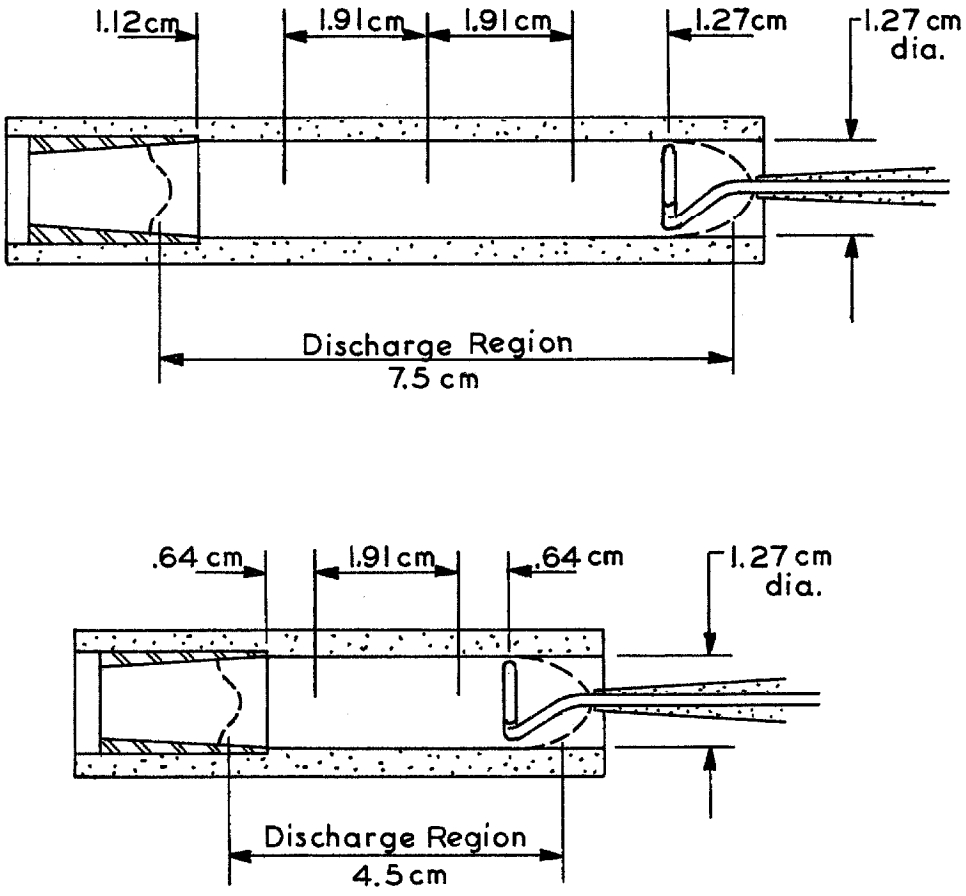

DISCHARGE CONFIGURATIONS

Figure 34.

Geometrical Considerations

For this calculation, it is convenient to use the concept of a mean beam length[57, 58]. The mean beam length is defined as the radius of an equivalent hemispherical plasma body whose radiation to a unit area at the center of its base is the same as the average radiation to the surface of the arbitrary plasma volume of interest. The utility of the mean beam length concept is that it allows one to calculate the total radiation from the arbitrary plasma volume of interest as if the path length for radiation were a constant equal to the mean beam length. Thus, once the mean beam length has been determined, the geometrical portion of the problem is solved and the remaining calculation depends only on the plasma properties. In general, of course, the mean beam length will depend upon the detailed absorption of the plasma, but for the relatively broad lines of primary importance, this dependence may be expressed quite simply and the mean beam length is readily determined.

In practice, one calculates the ratio of the mean beam length for the plasma volume of interest to the mean beam length for a transparent gas of identical geometrical configuration. This ratio and the relatively simple geometrical determination of the transparent gas mean beam length then give the desired mean beam length for the actual plasma volume.

The use of many probes inserted in plasma volumes with configurations similar to those shown in Figure 34 established that the electric field was essentially constant throughout except in the region very near the electrode surfaces. Visual observations revealed the

discharge glow to be uniform and to completely fill the duct. Thus, the assumption is made that the plasma volume is a cylinder of uniform properties extending in the region between the discharge electrodes. From Figure 34 we see that one could calculate the net radiation leaving the cylindrical region between the probes allowing for the fact that radiation from the ends can enter this volume. Alternatively, since the discharge region is uniform, one could regard the entire plasma between the discharge electrodes as the volume of interest and calculate the total radiative loss from this entire volume. Calculations have been performed in both ways and lead to equivalent results; however, only the latter method will be discussed here, since the use of the mean beam length concept is the most straightforward in this case.

The walls can be regarded as essentially transparent for all radiation leaving the plasma, since the wall temperatures are about 1200°K, whereas the population temperatures of the excited states are typically 2500°K or more.

As will be justified in the following, the lines which give the largest contribution to the total bound-bound emission rate have profiles whose widths are determined primarily by collision broadening. Olfe[59] shows that for an infinite circular cylinder of plasma with widely separated, collision-broadened lines,

$$\frac{L}{L^o} = \left[\frac{\Gamma(5/4)}{\Gamma(7/4)}\right]^4 = .942 \quad . \tag{B-3}$$

Here, Γ denotes the gamma function, and L/L^o is the ratio of the mean beam length of the plasma of interest to the mean beam length

of a transparent gas. This result should also be approximately correct for the finite cylinders of interest here, since L/L^o is quite insensitive to the length-to-diameter ratio of the cylinder[58]. Note also in this context that references 57, 58 indicate that an empirical rule that has been found useful under arbitrary conditions of absorption is $L/L^o \cong .85$.

It can be shown that when the mean beam length refers to radiation to the entire surface area A of the plasma volume, V, that L^o is given by $L^o = 4V/A$ [59]. Thus, to a very close approximation, the mean beam length for the cylindrical plasma of interest here is given by

$$L \cong 3.6 \frac{V}{A} = \frac{3.6\, d\ell}{2d + 4\ell} . \qquad \text{(B-4)}$$

Typical mean beam lengths for the plasma configurations used here were about 1.04 cm.

Line Broadening Calculations

Line broadening for the plasmas of interest here is due primarily to Lorentz (collision), Doppler, and Stark broadening effects, listed in order of decreasing importance. The natural widths of the lines are quite small compared to these added broadening effects. The calculation of the (half) half-widths for each of these broadening terms will be discussed in the following.

Lorentz (Collision) Broadening

The classical theory of collisional damping provides a description of the broadening of a spectral line caused by changes in the characteristics of the emitted radiation when the emitting atom

experiences an elastic collision with another (neutral) atom during the time of emission. The (half) half-width for this collisional broadening may be expressed as[60]

$$b_c = \frac{1}{2c} N' \vec{V} \sigma^2 \quad . \tag{B-5}$$

Here, N' is the number density of perturbing atoms, c denotes the speed of light, σ^2 is the cross section for broadening collisions (optical cross section), and $\vec{V}$ is the mean speed of the perturbing particles relative to the emitting atom given by kinetic theory to be

$$\vec{V} = \sqrt{\frac{8kT_a}{\pi\mu}} \quad ,$$

where μ is the reduced mass of the emitting atom - perturbing atom system.

More exact theories describing the interaction process are available, but the simple classical theory will be sufficient for the calculations performed here, and further, the presently available experimental data have been correlated in terms of the "optical collision cross section" defined in eqn. (B-5). The chief difficulty with the use of the classical collisional broadening theory leading to equation (B-5) is that pronounced asymmetrical shifts of the line profiles, not predicted by the simple classical theory, occur at high densities. Though these shifts are not important at the densities of plasmas studied here, most of the collisional broadening data have been taken at fairly high densities where the asymmetry is large, causing the determination of effective half-widths to be rather difficult and inaccurate.

For the experimental conditions here, the principal source of

collsional broadening is that due to perturbations by the argon or helium atoms, since the amount of potassium seed never exceeded 1 per cent of the total flow.

Values of the optical cross section as defined by eqn. (B-5) have been determined experimentally for alkali emitters perturbed by various foreign gases. Several measurements of potassium line broadening by nitrogen exist, but little is known about broadening by argon and helium[61-63]. The broadening of sodium lines by nitrogen, helium, and argon has been measured by several authors. These data are rather incomplete, and the data taken by various investigators differ somewhat. With these difficulties, it was possible to estimate approximate values of optical cross sections for the potassium lines of chief importance broadened by argon and helium. Values of σ^2 thus obtained are shown in Table B-I. These values are based on the available measurements of potassium line broadening in nitrogen, argon, and helium, as well as the fact that the relative variation in the broadening of potassium lines by nitrogen, argon, and helium should be similar to that measured for sodium lines. The values of σ^2 thus obtained are thought to be accurate to within about 40 per cent. Also shown in Table B-I are values of the absorption oscillator strength (dimensionless) for a few important lines of potassium[22, 64, 65]. These values have been calculated with the Coulomb approximation to the transition integral as formulated by Bates and Damgaard[24], and show excellent agreement with the available experimental data.

TABLE B-I

Absorption Oscillator Strengths for a Few Important Transitions in Potassium

Designation lower state	Designation upper state	Absorption Oscillator Strength[22, 64, 65] $f_{\ell\text{-}u}$	Optical Cross Section, σ^2 $(\text{Å})^2$ [61, 62, 63] A-K	Optical Cross Section, σ^2 $(\text{Å})^2$ [61, 62, 63] He-K
$4s\ ^2S_{\frac{1}{2}}$	$4p\ ^2P^o_{\frac{1}{2}}$	.66	150	64
$4s\ ^2S_{\frac{1}{2}}$	$4p\ ^2P^o_{\frac{3}{2}}$	.33		
$4p\ ^2P^o_{\frac{1}{2}}$	$5s\ ^2S_{\frac{1}{2}}$	.17	200	85
$4p\ ^2P^o_{\frac{3}{2}}$	$5s\ ^2S_{\frac{1}{2}}$	.17		
$4p\ ^2P^o_{\frac{1}{2}}$	$3d\ ^2D_{\frac{3}{2}}$	.85	200	85
$4p\ ^2P^o_{\frac{3}{2}}$	$3d\ ^2D_{\frac{5}{2}}$	.70		
$4p\ ^2P^o_{\frac{3}{2}}$	$3d\ ^2D_{\frac{3}{2}}$	.08		
$3d\ ^2D_{\{\frac{5}{2},\frac{3}{2}\}}$	$4f\ ^2F^o_{\{\frac{7}{2},\frac{5}{2}\}}$	.76	290	125

Doppler Broadening

The Doppler broadening of a spectral line due to the random thermal motion of the emitting atom is expressed in terms of a (half) half-width given by[25]

$$b_d = \frac{1}{\lambda c}\sqrt{\frac{2kT_a \ell n 2}{m_a}} \quad . \tag{B-6}$$

Here, λ is the wavelength of the spectral transition of interest.

Stark Broadening

The theories describing Stark broadening due to interactions between the emitting atom and the electric fields of plasma electrons and ions are fairly elaborate. Interactions between the radiating atom and arbitrary perturbing atoms can be treated very generally quantum-theoretically, the difference between what is referred to here as Stark broadening and the "collision" broadening discussed above being essentially the Coulomb potential produced by charged perturbers. There is no need to discuss these theoretical formulations here, since only an estimate of the line width associated with Stark broadening is needed.

Various approximate formulas for estimating these line widths depending on various plasma conditions have been given by Margenau[21]. More recently, Griem[22] has published the results of extensive Stark broadening calculations for many elements including potassium.

The approximate impact theory formula for the (half) half-widths for quadratic Stark broadening due to plasma electrons and ions, given by Margenau for the conditions of electron temperatures and densities of these experiments, is[21]

$$b_s = \frac{500}{2\pi c}\,\Omega_4^{2/3} T_e^{1/6}\left[1 + \frac{0.28}{M^{1/6}}\left(\frac{T_a}{T_e}\right)^{1/6}\right] N_e\,, \qquad \text{(B-7)}$$

where Ω_4 is determined experimentally or given approximately by $\Omega_4 \cong 3\times10^{-17}\, g^6$. In these expressions, M denotes the molecular weight (dimensionless) of the radiating atom, and g denotes the principal quantum number of the upper state of the radiating atom which is

assumed to have a hydrogenic energy level structure. T_e is in ^oK and N_e is in cm^{-3}.

Preliminary approximate calculations performed with eqn. (B-7) gave somewhat larger estimates of line widths than those calculated in detail by Griem for potassium. Calculated values of radiative loss did not differ appreciably, however, since for these plasma conditions the contribution of Stark broadening to the total broadening is small. The calculated Stark broadening widths of Griem show excellent agreement with experiment for radiation from cesium[65]. Since the energy level structure of potassium is quite similar to that of cesium, the calculations for potassium are also probably very good. Thus, the calculated Stark broadening parameters of Griem have been used in evaluating the experimental results.

Griem expresses the (half) half-widths for quadratic Stark broadening in the form[22]

$$b_s = [1 + 1.75\alpha(1 - .75r)]w , \qquad (B-8)$$

where α is the broadening parameter due to the influence of ions, w is the electron-impact (half) half-width, and r is the ratio of the mean distance between ions to the Debye radius (see reference 22). These parameters are tabulated for the transitions of primary importance in potassium in reference 22.

Spectral Line Profiles

The above discussion indicates that the broadening of the spectral lines of plasmas discussed here is primarily caused by dispersion broadening due to the Lorentz and quadratic Stark effects as

well as Doppler broadening. The shape of the line profile for combined dispersion and Doppler broadening effects has been considered by Voigt[66] and Rieche[67], and is also discussed by Penner[25]. The resulting spectral absorption coefficient has the form[25]

$$P_{|\xi|} = \frac{S}{b_d}\sqrt{\ell n\, 2/\pi}\,\frac{a}{\pi}\int_{-\infty}^{\infty}\frac{\exp(-y^2)}{a^2+(\xi-y)^2}\,dy \qquad (B-9)$$

where

$$a = \frac{(b_c+b_s)(\ell n\, 2)^{\frac{1}{2}}}{b_d},$$

$$\xi = \frac{\omega-\omega_o}{b_d}(\ell n\, 2)^{\frac{1}{2}},$$

and the integrated absorption, S, is given by

$$S = \frac{b_d}{(\ell n\, 2)^{\frac{1}{2}}}\int_{-\infty}^{\infty}P_{|\xi|}\,d\xi = \frac{\pi e^2}{mc}N_\ell f_{\ell-u}\left(1-\exp\frac{-h\nu_{\ell u}}{kT_e}\right)\cong\frac{\pi e^2}{mc}N_\ell f_{\ell-u} \qquad (B-10)$$

where $f_{\ell-u}$ is the absorption oscillator strength (dimensionless). For all transitions of importance, $h\nu_{\ell u} \gg kT_e$. The conventional practice of adding half-widths for dispersion broadening has been adopted.

The radiancy of a given spectral line, R_L, can then be expressed in the form

$$\frac{R_L(\ell n\, 2)^{\frac{1}{2}}}{2R\omega_o^o b_d} = \tfrac{1}{2}\int_{-\infty}^{\infty}[1-\exp(-P_{|\xi|}L)]d\xi, \qquad (B-11)$$

where L is the mean beam length for radiation from the plasma volume of interest (e.g. (B-4)), as has been discussed. $R\omega_o^o$ is the blackbody radiancy per unit reciprocal wavelength interval at the line center. Reference 68 contains a useful set of tables for the determination of this quantity (see Table III, page 79, reference 68). Penner

discusses the evaluation of these integrals in detail and presents the quantity on the left hand side of eqn. (B-2) as a function of $\frac{S}{b_d}\sqrt{\ell n\, 2/\pi}\, L$ for various values of the line width parameter, a , of eqn. (B-9). These curves are known as "curves of growth" as employed by van der Held[69].

Radiative Loss Calculations

The total rate of energy loss from the plasma per unit volume due to bound-bound transitions is given by

$$\mathring{R}_s = \sum_i R_{L_i} \frac{A}{V}, \qquad \text{(B-12)}$$

where the summation is taken over all bound-bound transitions. Here, R_{L_i} is the line radiancy of the i^{th} transition, as given by eqn. (B-11). For the electron temperatures of these experiments, the summation converges quite rapidly, with the principal contributions given by resonance transitions from the lowest lying states.

Equations (B-2) through (B-12) were used to calculate the average radiant energy loss per unit volume from the plasmas as discussed in Sections III-E and F. Enough lines were considered to establish the convergence of the summation in eqn. (B-12) and to be certain that omitted higher transitions were negligible. That is, the following emission series were considered: np → 4s, ns → 4p, nd → 5s, np → 3d, nf → 3d, ns → 5p, nd → 5p, 4f → 4d, and 5d → 4f. Here, n was taken over all emission lines giving an appreciable contribution. Values of n extending up to between 7 and 11 were usually sufficient in this regard.

Calculation of the radiant energy losses per unit volume, $\mathring{R}_s$,

due to bound-bound transitions was carried out as described above for $2200 \leq T_e \leq 3500^{\circ}K$ and values of initial potassium concentration $n_K/n_A = .002, .004, .006,$ and $.008$, for $T_a = 1500$ and $2000^{\circ}K$ for the argon-potassium system. These results were then simply extended by appropriate modification of the preceding equations to include the helium-potassium system. Typical results for the argon-potassium system at $T_a = 2000^{\circ}K$ are shown in Figure 35. Also shown are the contributions to $\mathring{R}_s$ given by only the $4p \rightarrow 4s$ transitions for $n_K/n_A = .004$. Note that 70 per cent of the total radiation loss is due to these transitions for the temperature range investigated.

Examination of a special case is of interest here. When the line width parameter, a, is large, the spectral profile is essentially determined by dispersion broadening effects. This condition holds fairly accurately for the $4p \rightarrow 4s$ resonance lines which account for most of the radiation loss (see Figure 35). When this is the case, and when the plasma can be considered optically thick $\left[\left(\frac{SL}{2\pi(b_c+b_s)}\right) >> \frac{2}{\pi}\right]$, then $R_L/R\omega_o^o \cong 2\sqrt{SL(b_c+b_s)}$. Under these conditions, the total rate of energy loss becomes

$$\mathring{R}_s = 2\sum_i \left[R\omega_o^o \sqrt{S(b_c+b_s)}\right]_i \sqrt{L}\,\frac{A}{V} . \qquad \text{(B-13)}$$

Thus, from eqn. (B-4), $\mathring{R}_s \sim \sqrt{A/V} \sim \sqrt{1/L}$, which shows that the dependence of the calculated radiation loss is not particularly sensitive to moderate changes in configuration of the plasma. This explains the fact that experimental results were insensitive to discharge length variations in the range from 4.5 to 7.5 cm, and indicates that

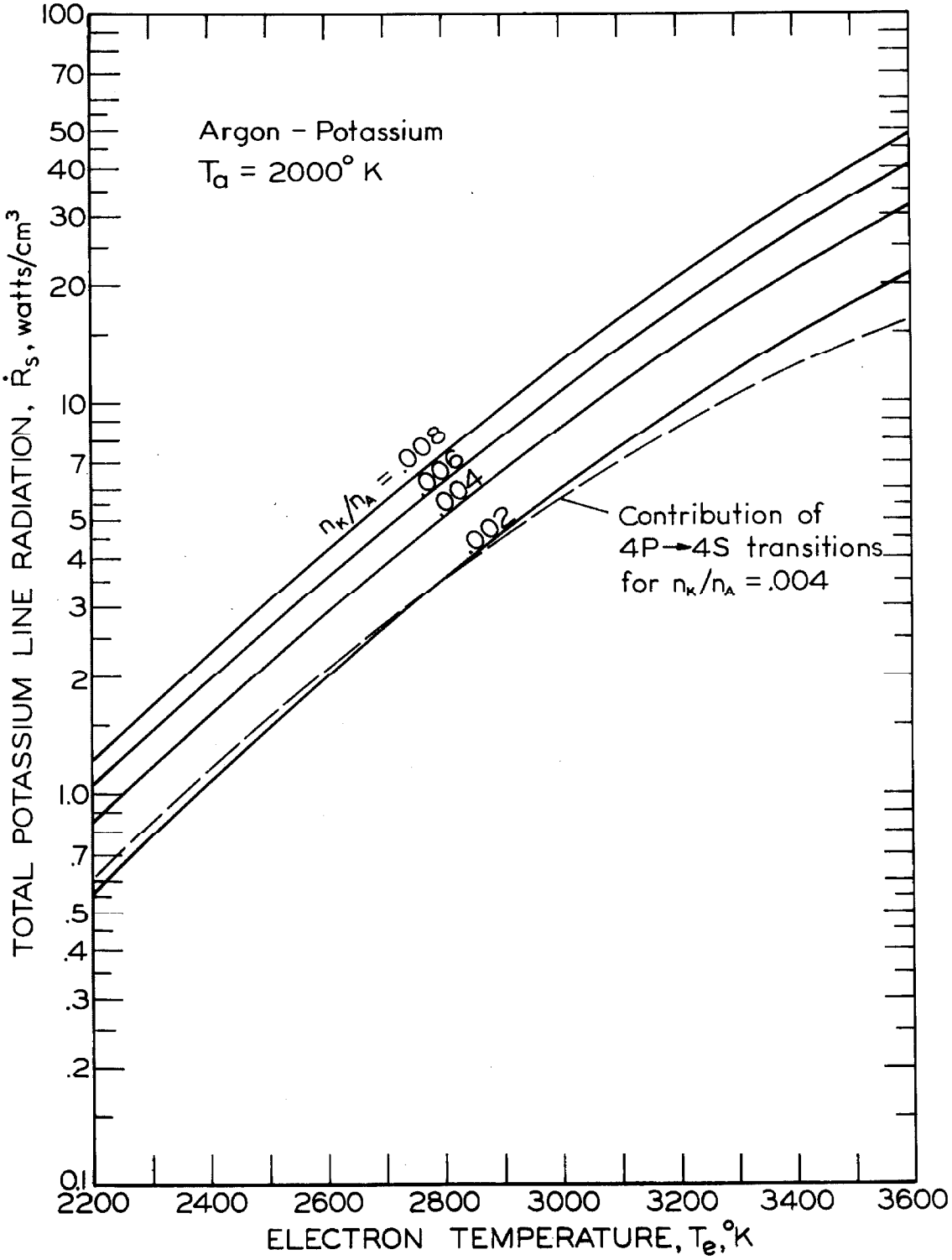

FIG. 35 STEADY STATE PLASMA RADIATION LOSSES

possible errors in the estimates of plasma geometry will not have significant effects on the radiation calculations, as compared to the possible errors in optical cross-section estimates, for example. This result also shows that radiation losses from the plasma can be very important in interpreting the results of these small-scale laboratory experiments; but for large enough systems, radiation losses can be reduced to the extent that they are negligible compared to elastic collision losses.

The principal uncertainty in the calculated results is undoubtedly that due to the rather crude estimates of Lorentz broadening half widths. The rather small uncertainties associated with the oscillator strengths are of no concern, and the uncertainties associated with the mean beam length calculations are probably also not critical. Fortunately, the calculated radiation will only depend approximately upon the square roots of these quantities. Thus, estimates of the above uncertainties give probable maximum uncertainties in the radiation loss calculations of $\pm$ 25 per cent. Note that this uncertainty does not affect any of the major conclusions that have been drawn in this work. For example, even when radiation losses are quite large, as at very low currents, then J^2 is approximately proportional to $\sigma\mathring{R}_s$, and thus the uncertainties in the calculated J values would only be about 13 per cent. This small uncertainty is clearly unimportant on the log σ versus log J plots, and for conditions where radiation losses are equal to or less than elastic collision losses, the uncertainty is even smaller.

As a final comment, after having completed these calcula-

tions, the author learned of the results of some radiation calculations for an argon-cesium plasma performed by Lutz[70]. These calculations were done for a plasma enclosed by infinite parallel planes with a method that does not lend itself readily to more complicated geometries. However, the mean beam length concept discussed here provides a simple means by which the calculated results for an infinite plane geometry can be applied to more useful geometrical configurations. The calculations of reference 70 assume dispersion broadening effects to be dominant, and so use of the mean beam length concept reduces the entire calculation to the very simple one defined by eqn. (B-13). For a transparent gas, the mean beam length for the infinite parallel plane case is just $L^o = 2d$, where d is the separation distance between planes[57, 58]. Olfe[59] shows that for the parallel plane case, under these broadening conditions, that $L/L^o = 8/9$. Thus, the radiation loss from a plasma with collision broadened line profiles enclosed between infinite parallel planes can be related to a similar plasma enclosed by boundaries of arbitrary geometrical configurations in terms of the mean beam length for the new geometry. For example, consider the finite cylindrical volumes discussed in this work. Then

$$\dot{R}_{s_{cyl}} = \frac{3}{4}\sqrt{\frac{L_{cyl}}{d}}\, d\left[\frac{A}{V}\right]_{cyl} \dot{R}_{s_{||plane}},$$

where L_{cyl} is the mean beam length of eqn. (B-4).

APPENDIX C

Assumptions and Approximations

This appendix gives a brief discussion of some of the assumptions and approximations that have been made in this work.

A. Maxwellian Distribution of Free Electron Energies[1-3]

The free electrons can be regarded as having an essentially Maxwellian distribution, for the conditions of these experiments, if their mutual interactions are sufficiently frequent to "Maxwellianize" the distribution by removing the effects of perturbations due to collisions with the various atomic species. That is, the net probability of mutual energy transfer between electrons must exceed the probability of energy loss to the atomic species by elastic and inelastic electron-atom encounters. This condition will be satisfied, provided that the following approximate inequalities hold.

1. Elastic collision energy transfer to atomic species m .

$$\nu_{e-e} >> \sum_m \frac{8}{3} \frac{m_e}{m_m} \nu_m ,$$

$$N_e \bar{c} \sqrt{2} Q_c >> \sum_m \frac{8}{3} \frac{m_e}{m_m} N_m \bar{c} Q_m$$

or

$$N_e >> \sum_m \frac{Q_m}{Q_c} \frac{m_e}{m_m} N_m .$$

Here, ν_{e-e} is the average electron-electron collision frequency, Q_c is the Coulomb cross section (see eqn. (10)), Q_m is the momentum transfer cross section for elastic electronic collisions with species m (see below eqn. (14)). For conditions of these experiments, the

inequality is satisfied for $N_e > 10^{12} - 10^{13}$ cm^{-3} .

2. Inelastic collision energy transfer to atomic species m . When electronic collisional processes dominate in determining the populations of the various energy levels (to be considered below), then excitation and ionization rates approximately balance de-excitation and recombination rates at the steady state. For this case, "depopulational or populational" effects on the tail of the distribution function are not important. During ionizational or recombinational relaxation, however, the tail of the distribution can be significantly altered from the Maxwellian form if electron densities are too low. For example, during the ionizational relaxation for potassium, the electron density must be high enough to satisfy the following approximate inequality, as follows from the discussion given in Section V.

Consider the effect on the distribution due to inelastic collisions resulting in excitations across an arbitrary gap U . Then we require

$$\nu_{e\text{-}e} U >> \frac{1}{N_e} \left.\frac{dN}{dt}\right|_U^u U ,$$

$$N_e \bar{c} \sqrt{2}\, Q_c\{U\} >> \frac{1}{N_e} \left.\frac{dN}{dt}\right|_U^u$$

or

$$N_e >> \left\{ \frac{\frac{1}{N_e} \left.\frac{dN}{dt}\right|_U^u}{\bar{c}\, Q_c\{U\}} \right\} ,$$

where $Q_c\{U\}$ is the Coulomb cross section evaluated at energy U.

Here, $\frac{dN}{dt}\Big|_{U}^{u}$ is the net rate of excitations across the arbitrary gap U. As mentioned in Section V, a quasi-steady condition is rapidly reached such that $\frac{dN}{dt}\Big|_{U}^{u} \cong \frac{dN}{dt}\Big|_{u\ min}$.

Consider the largest gap for potassium, 4p − 4s (1.61 ev), at the quasi-steady relaxational condition:

$$N_e \gg \frac{\frac{1}{N_e}\frac{dN}{dt}\Big|_{u\ min}}{\bar{c}\, Q_c\ \{1.61\ ev\}} \quad .$$

For these experiments, this inequality is satisfied for $N_e > 10^{12} - 10^{13}\ cm^{-3}$.

B. Electronic Collisional Equilibrium for Excited State Populations in Potassium[11]

The rate of de-excitation from the states just above an energy gap U is given by eqn. (19). For the lower lying gaps, most of the de-excitations come from the level ℓ, with number density N_ℓ and degeneracy g_ℓ located immediately above the gap. Values of $\frac{1}{N_\ell}\frac{dN}{dt}\Big|_{d}$ for the various low-lying states of potassium are given below as a function of electron density, and are valid for the electron temperature range of interest here. Also shown are the approximate reciprocal radiative lifetimes of these states[64].

Inspection of the Table C-I reveals that for all levels above the 5s level that for $N_e \gtrsim 10^{14}/cm^3$, the probability of collisional de-excitation is always at least 100 times the probability of radiative de-excitation. The 4p and 5s states actually have much longer effective lifetimes than those indicated in Table C-I, since reabsorption of emissions from these states is large. The radiative transfer

calculations described in Appendix B indicate that for $T_e \sim 2500^\circ K$, $N_c \sim 10^{14}/cm^3$, and $J \sim 1.5$ amp/cm^2, the ratio is about 50:1 in favor of electronic collisional de-excitation for the 4p state, and over 80:1 for the 5s state. For $T_e = 2200^\circ K$, $N_e = 2\times10^{13}/cm^3$, and $J = .4$ amp/cm^2, the ratio drops to about 15:1 and over 30:1 for the 4p and 5s states, respectively. Thus, for $N_e \gtrsim 10^{14}/cm^3$, the condition of electronic collisional equilibrium probably holds for all bound states in potassium in these dense plasmas.

TABLE C-I

Argon-Potassium, $n_K/n_A = .004$

States ℓ	Electronic Collisional De-Excitation Rate $\frac{1}{N_\ell}\frac{dN}{dt}\Big\vert_d$ (sec^{-1})	Reciprocal Mean Lifetime Neglecting Reabsorption $\frac{1}{\tau_r}$ (sec^{-1})
4p	$6\times10^{-8}\ N_e$	37×10^6
5s	$2\times10^{-6}\ N_e$	22×10^6
3d	$8\times10^{-6}\ N_e$	25×10^6
5p	$9\times10^{-6}\ N_e$	8×10^6
6s, 4d	$5\times10^{-6}\ N_e$	11×10^6, 4×10^6
4f	$2\times10^{-4}\ N_e$	10^6

C. Neglect of Atom-Atom Excitation Compared to Electron-Atom Excitation[19, 71]

The rates of either excitation or ionization from the ground state per unit volume can be written in terms of the linear slopes of the cross section versus energy curves near threshold as[19, 71],

$$\left.\frac{dN^*}{dt}\right|_{e-a} = N_e N_K \bar{c} C_{e-a} (E^* + 2kT_e) e^{-E^*/kT_e}$$

$$\left.\frac{dN^*}{dt}\right|_{a-a} = N_a N_K \bar{c} \sqrt{\frac{m_e}{2m_a}} C_{a-a} (E^* + 2kT_a) e^{-E^*/kT_a}$$

where Maxwellian distributions with average energies below threshold have been assumed for all species. Here, $\left.\frac{dN^*}{dt}\right|_{e-a}$ and $\left.\frac{dN^*}{dt}\right|_{a-a}$ are the excitation or ionization rates for electron-atom and atom-atom processes, respectively. E^* is either the excitation or ionization energy, and C_{e-a} and C_{a-a} are the respective cross-sectional slopes above threshold. If $T_e = T_a$, then electron-atom processes dominate if

$$\frac{N_e}{N_a} \gg \frac{C_{a-a}}{C_{e-a}} \sqrt{\frac{m_e}{2m_a}} .$$

For potassium in argon,

$$\frac{N_e}{N_a} \gg \frac{1}{330} \frac{C_{a-K}}{C_{e-K}} .$$

Existing data (e. g. references 19, 71, 72) for noble gases indicate $C_{a-a} \ll C_{e-a}$. In the absence of available data for the atom-atom cross sections for potassium, we assume

$$C_{e-K} \sim (.01 \text{ to } .001)\, C_{a-K}.$$

Then the above inequality becomes $N_e/N_a \gg 10^{-5}$. If N_a denotes the number density of argon, then we must have $N_e > 10^{13}/cm^3$ in order to neglect atom-atom processes. This result is not very satisfactory, since no data for atom-atom cross sections for potassium appear to be available to allow a more definite comparison.

Some information may be obtained by detailed balance considerations of available recombination data for cesium. Several

authors (see bibliography of reference 40) have found electron-electron-ion recombination dominant over electron-atom-ion recombination in cesium for conditions similar to those encountered here with potassium. These results indicate atom-atom processes to be negligible at electron densities above about $10^{13}/cm^3$.

D. Neglect of Dissociative Recombination

Harris[45] has measured the dependence of recombination rates in cesium on cesium seed pressure and concluded that dissociative recombination is important for $T_a < 1500^oC$, but that above this the electron-electron-ion process is dominant. Harris also approximately calculated the concentrations of the molecular ion, Cs_2^+, and shows that its concentration is quite negligible in this regard for $T_a > 1500^oC$. Similar approximate estimates using a calculation procedure similar to that used by Harris show that for the gas temperatures of the recombination experiments discussed here ($T_a \gtrsim 2000^oK$), that dissociative recombination is probably also negligible for the potassium measurements performed here.

E. Neglect of Diffusion Losses

The characteristic rate at which K^+ ions diffuse to the walls and recombine is given by (see Chapter 3 of reference 33)

$$\nu_d = D_a/\Lambda^2 ,$$

where D_a is the ambipolar diffusion coefficient for potassium, and Λ is the characteristic diffusion length for a cylinder:

$$\frac{1}{\Lambda^2} = \left(\frac{\pi}{L}\right)^2 + \left(\frac{2.4}{R}\right)^2 ,$$

where R is the cylinder radius and L is its length. For these plasmas

$\Lambda \cong .26$ cm.

Calculated values of ν_d based upon mobility values for K^+ in K and K^+ in A, the former estimated from the mobility value of Cs^+ in Cs[43, 44], indicate that diffusion loss rates are about 50 times smaller than measured volume recombination rates (see also Section V-B).

F. Low Current Densities*

Under conditions where atom-atom and electron-atom excitation and de-excitation mechanisms are of comparable magnitude, a knowledge of the magnitudes of these effects and the effects of radiative depopulation would be necessary to specify the populations of the excited states and the density of free electrons. The use of a simplified energy level structure, similar to that employed in reference 1, would probably be sufficient to describe gross plasma behavior in this region if all rate coefficients were known.

It is clear from the energy balance and the conductivity data that the two effects mentioned above could account for the observed data in this very low current range. The fact that the electrical conductivity measured for very low currents does appear to correspond to the translational temperature of the gas, as noted in Figure 16 and also from the measurements of Harris[72], would indicate either (1) that atom-atom excitation and ionization dominate, or (2) that electron-atom excitation and ionization essentially define the free electron density and that the electron temperature equals the gas temperature. The latter hypothesis seems uncertain since the calculated radiative

---

* See Section V-A.

losses, neglecting radiative depopulation,would require an electron temperature unreasonably lower than that of the gas. If radiative depopulation were enough to account for this difficulty, then it is doubtful that the free electron density would correspond to the equilibrium value at the electron temperature. This apparent dilemma does not appear to be easily resolved, and it may be probable that both atom-atom interaction and radiative depopulation may be important.

G. Nonuniformities

If we assume that the electric field is essentially constant throughout the test region in the steady state, we can calculate in an approximate way* what the effects of the nonuniform gas temperature profile (Figure 33) might be upon the electron temperature and electron density profiles by use of equation (3). The resulting calculations indicate the electron temperature to be within 10 per cent of its bulk value over most of the cross-sectional area. Note, however, that the resulting nonuniform electron density profile shows a larger variation. Thus about .5 mm from the walls, density deviations are somewhat larger (35 per cent). As noted in Section V-A, this has no large effect upon the conductivity - current density characteristics. It is possible, however, that these variations in electron density could explain some of the scatter of the recombination and ionization relaxation measurements.

* Calculation neglects the fact that $\mathring{R}_s$ as calculated is the volume averaged value, not the local value. For current densities above 2 amp/cm^2, this error should not be large.

APPENDIX D

Conductivity Maximization Calculation

We consider the slightly ionized case, $T_e \lesssim 3000^{\circ}K$, and look for a maximum in the electrical conductivity when either E or J is held constant, and the seed concentration is varied.

$$\sigma = \frac{e^2 N_e}{m_e \bar{c} \Sigma N_j Q_j} \sim \frac{N_e}{\sqrt{\epsilon_e}(1+\beta)} \quad \text{where } \beta \cong \frac{N_K}{N_A}\frac{Q_K}{Q_A} , \qquad (D\text{-}1)$$

where, for simplicity, we assume constant cross sections Q_K and Q_A for potassium and argon, respectively.

Further, for $T_e \lesssim 3000^{\circ}K$,

$$N_e^2 \cong \frac{(2\pi m_e k T_e)^{3/2}}{h^3} N_K e^{-V_o/kT_e} \sim \beta(\epsilon_e)^{3/2} e^{-\frac{3}{2}\frac{V_o}{\epsilon_e}} . \qquad (D\text{-}2)$$

Combining (D-1) and (D-2) gives

$$\sigma \sim \frac{\sqrt{\beta}}{(1+\beta)} \epsilon_e^{1/4} e^{-\frac{3}{4}\frac{V_o}{\epsilon_e}} . \qquad (D\text{-}3)$$

For constant J, and neglecting radiation losses completely,

$$J^2 = \frac{8}{3}\frac{m_e}{m_a}(\epsilon_e - \epsilon_a)\frac{e^2 N_e^2}{m_e} ,$$

or

$$J^2 \sim (\epsilon_e - \epsilon_a)\epsilon_e^{3/2}\beta e^{-\frac{3}{2}\frac{V_o}{\epsilon_e}} . \qquad (D\text{-}4)$$

For constant E, $J^2/\sigma = \sigma E^2$, which gives

$$E^2 \sim (\epsilon_e - \epsilon_a)\epsilon_e(1+\beta)^2 . \qquad (D\text{-}4a)$$

Now we maximize σ with respect to β:

$$\frac{d\sigma}{d\beta} = \left(\frac{\partial\sigma}{\partial\epsilon_e}\right)_\beta \frac{d\epsilon_e}{d\beta} + \left(\frac{\partial\sigma}{\partial\beta}\right)_{\epsilon_e} = 0 . \qquad (D\text{-}5)$$

The above formulas yield the following results. For constant J or for constant E ,

$$\beta_{opt} = \left\{ \frac{\frac{\epsilon}{\epsilon-1} - 1}{\frac{\epsilon}{\epsilon-1} + 2 + 3\frac{V_o}{\epsilon_e}} \right\} . \qquad \text{(D-6)}$$

where $\epsilon \equiv \epsilon_e/\epsilon_a \geq 1$.

Note that for $\epsilon \to 1$ that $\beta \to 1$, which is the optimum value calculated by Pinchak[37] for the equilibrium case where $\epsilon_e = \epsilon_a$.

As an example of the use of (D-6), consider the following case: for $\epsilon_e/\epsilon_a = 1.5$ ($T_e = 3000^{\circ}K$), $Q_K = 400\times10^{-16}$ cm^2, $Q_A = 10^{-16}$ cm^2, $\beta_{opt} \cong .06$, and $(n_K/n_A)_{opt} \cong .0002$.

Note that the ratios of current densities for equal electron temperature, but different β values, are given by $J_1/J_2 = \sqrt{\beta_1/\beta_2}$. Thus, the current density corresponding to a given electron temperature decreases markedly as seed concentration decreases, as shown in Figures 2 and 3.

LIST OF SYMBOLS

N	Number density, cm^{-3}
$\mathring{\Omega}$	Rate of elastic energy loss per unit volume from free electrons, $watts/cm^3$
V_i	Excitation energy of state i , as measured relative to the ground state
$\mathring{R}$	Radiative loss per unit volume, $watts/cm^3$
$\mathring{R}_{b-b}$	Radiative loss per unit volume, $watts/cm^3$, due to bound-bound transitions
$\mathring{R}_{f-b}$	Radiative loss per unit volume, $watts/cm^3$, due to free-bound transitions
$\mathring{R}_{f-f}$	Radiative loss per unit volume, $watts/cm^3$, due to free-free transitions
$\mathring{R}_s$	Radiative loss per unit volume at steady state, $watts/cm^3$, see eqn. (3)
ϵ_e	Mean translational energy of electrons, $\frac{3}{2} kT_e$
ϵ_a	Mean translational energy of atomic species, $\frac{3}{2} kT_a$
σ	Electrical conductivity, mhos/cm
E	Electric field strength, volts/cm
V_o	Ionization potential of potassium = 4.34 ev
J	Current density, amp/cm^2
A_{mn}	Einstein coefficient for spontaneous emission of radiation for transition from state m to state n , sec^{-1}
n	Arbitrary state index
T	Temperature, ^oK
K	Potassium
K^+	Potassium ion

h	Planck's constant
ν	Frequency
e^-	Electron
X	Arbitrary atomic species
g	degeneracy
E_n	Binding energy of state n
m	Atomic or electronic mass
k	Boltzmann constant
f_o	Electron velocity distribution function
c	Electron speed; speed of light
$\bar{c}$	Mean electron speed; $\bar{c} = \sqrt{(8kT_e)/(\pi m_e)}$
e	Electron charge
Q_c	Coulomb cross section
Q_m	Momentum transfer cross section for elastic electronic collisions with either neutral or ionized species m
Q_n	Momentum transfer cross section for elastic electronic collisions with neutral species n
Σ_n	Sum over neutral species
Σ_m	Sum over both neutral species and ionized species
σ_c	Close encounter conductivity
σ_s	Distant encounter conductivity
$\bar{\nu}_m$	Energy-averaged collision frequency for elastic electronic collisions with species m , eqn. (14)
U	Energy gap between two adjacent atomic energy levels, see eqn. (18)
E_k, g_k	Binding energy and degeneracy of energy level located immediately below energy gap U

E_i	Binding energy of arbitrary level located below gap U
N_i	Number density of arbitrary level located below gap U
E_ℓ, g_ℓ	Binding energy and degeneracy of energy level located immediately above energy gap U
α	Recombination rate coefficient; $\alpha = \frac{-1}{N_e^2} \frac{dN_e}{dt}$
α_r	Radiative recombination rate coefficient, $\alpha_r = \frac{-1}{N_e^2} \frac{dN_e}{dt}$
A	Argon; duct cross-sectional area
Cs	Cesium
N_1, g_1	Number density and degeneracy of ground state
γ	Defined below eqn. (19)
ϵ^*	Characteristic energy; $\epsilon^* \sim 0\{\epsilon_e\}$
ϵ	ϵ_e/ϵ_a
n_K/n_A	Initial concentration of potassium in argon
n_K/n_{He}	Initial concentration of potassium in helium
I	Current, amps; light intensity, arbitrary units
E^*	Average energy release to free electrons for recombination in upper states, $E^* \cong$ binding energy of level immediately above critical gap (not E^* defined in Appendix C)
τ_r	Relaxation time for ionization; mean radiative lifetime
τ_c	Characteristic time, $(N_{eo}V_o)/(\sigma_o E^2)$
μsec	10^{-6} sec
Z	Ionic charge in units of electronic charge (Z = 1 for this work)
g	Gaunt factor (eqn. (B-1)), here $g \sim 1$; g principal quantum number (eqn. (B-7))
L	Mean beam length for arbitrary plasma
L^o	Transparent gas mean beam length

d	Diameter, see eqn. (B-4)
ℓ	Length, see eqn. (B-4)
μ	Reduced mass, $\mu = (m_1 m_2)/(m_1+m_2)$, below eqn. (B-5)
b_c	Collision broadening (half) half-widths, cm^{-1}
b_s	Stark broadening (half) half-widths, cm^{-1}
b_d	Doppler broadening (half) half-widths, cm^{-1}
ω	Reciprocal wavelength, cm^{-1}
S	Integrated absorption, see eqn. (B-10)
R_L	Line radiancy, $watts/cm^2$

Subscripts and Superscripts

e	Electron
a	Atom
o	Initial
i	Any neutral or ionized atomic species; state index i
f	Final
c	Continuum; close encounters; collision
n	Neutral; arbitrary state index n
eq, equil	Equilibrium
A	Argon
K	Potassium
He	Helium
u	Up
d	Doppler; down
s	Stark; steady state
+	Ionized (superscript)

REFERENCES

1. BenDaniel, D. J. and Tamor, S., "Non-Equilibrium Ionization in Magnetohydrodynamic Generators," General Electric Tech. Information Series 62-RL-(2922E) (January 1962).

2. Griem, H., Plasma Spectroscopy, McGraw-Hill Book Co., New York (1964), Chapter 6.

3. Cahn, J. H., "Electronic Interaction in Electrical Discharges in Gases," Phys. Rev. 75, 293 (1949).

4. Bates, D. R., Kingston, A. E., and McWhirter, R. W. P., "Recombination Between Electrons and Atomic Ions. I. Optically Thin Plasmas," Proc. Roy. Soc. (London) A 267, No. 1330, 297-312 (May 22, 1962); and "II. Optically Thick Plasmas," Proc. Roy. Soc. (London) A270, 155-167 (1965).

5. Griem, H., "Validity of Local Thermal Equilibrium in Plasma Spectroscopy," Phys. Rev. 131, 1170-1176 (1963).

6. Robben, F., Kunkel, W. B., and Talbot, L., "Spectroscopic Study of Electron Recombination with Monatomic Ions in a Helium Plasma," Phys. Rev. 132, 2363-2371 (1963).

7. Hinnov, Einar and Hirschberg, J. G., "Electron-Ion Recombination in Dense Plasmas," Phys. Rev. 125, no. 3, 795-801 (1962).

8. Gryzinski, M., "Classical Theory of Electronic and Ionic Inelastic Collisions," Phys. Rev. 115, no. 2, 374-383 (1959); "Two Particle Collisions, I. General Relations for Collisions and II. Coulomb Collisions," Phys. Rev. 138, no. 2A, A305-A355 (1965). See Also "Classical Theory of Atomic Collisions, I. Theory of Inelastic Collisions," Phys. Rev. 138, no. 2A, A336-A358 (1965).

9. Bates, D. R. and Kingston, A. E., "Recombination and Energy Balance in a Decaying Plasma, Part I," Proc. Roy. Soc. A279, 10-31 (1964), and "Part II," Proc. Roy. Soc. A 279, 32-38 (1964).

10. Byron, S., Stabler, R. C., and Bortz, P., "Electron-Ion Recombination by Collisional and Radiative Processes," Phys. Rev. Letters 8, no. 9, 376-379 (1962).

11. Byron, S., Bortz, P. I., and Russell, G., "Electron-Ion Reaction Rate Theory: Determination of the Properties of Non-Equilibrium Monatomic Plasmas in MHD Generators and Accelerators and in ShockTubes," Proc. Fourth Symposium on Eng. Aspects of Magnetohydrodynamics, Univ. of California,

Berkeley (April 10-11, 1963).

12. Motley, R. W., and Kuckes, A. F., Proceedings of the Fifth International Conference on Ionic Phenomena, Munich 1961, North Holland Publishing Co., Amsterdam (1961).

13. Chapman, S. and Cowling, T. G., The Mathematical Theory of Non-Uniform Gases, Cambridge University Press, London (1961), Chapter 7.

14. Allis, W. P., "Motions of Ions and Electrons," Handbuch der Physik, Springer-Verlag, Berlin (1956), Vol. XXI, 383-444.

15. Lin, S. C., Resler, E. L., and Kantrowitz, A., "Electrical Conductivity of Highly Ionized Argon Produced by Shock Waves," J. Appl. Phys. 26, 95-109 (1955).

16. Chapman, S. and Cowling, T. G., The Mathematical Theory of Non-Uniform Gases, Cambridge University Press, London (1961), pp. 196, 245, 321, 348.

17. Spitzer, L. and Härm, R., "Transport Phenomena in a Completely Ionized Gas," Phys. Rev. 89, 977 (1953).

18. Cowling, T. G., "The Electrical Conductivity of an Ionized Gas in a Magnetic Field, with Applications to the Solar Atmosphere and the Ionosphere," Proc. Roy. Soc. (London) A183, 453 (1945).

19. Petschek, H. and Byron, S., "Approach to Equilibrium Ionization Behind Strong Shock Waves in Argon," Ann. Phys. 1, 270-315 (1957).

20. Frost, L. S., "Conductivity of Seeded Atmospheric Pressure Plasmas," J. Appl. Phys. 32, 2029-2036 (1961).

21. Margenau, H. "Formulas for Estimating Widths of Spectral Lines Emitted from Plasmas and Their Limits of Validity," Proceedings of the 4th International Conference on Ionization Phenomena in Gases, North-Holland Publishing Co., Amsterdam (1960), Vol. 2, p. 799.

22. Griem, H., Plasma Spectroscopy, McGraw-Hill Book Co., New York (1964), Chapter 4, and Tables, pp. 338-542.

23. Glennon, B. M. and Wiese, W. L., "Bibliography on Atomic Transition Probabilities," Nat. Bur. Std. (U. S.) Monograph 50 (August 1962).

24. Bates, D. R., and Damgaard, A., "The Calculation of the Absolute Strengths of Spectral Lines," Phil. Trans. Roy. Soc.

(London) A242, 101-122 (1949).

25. Penner, S. S., Quantitative Spectroscopy and Gas Emissivities, Addison-Wesley Publishing Co., Reading, Mass. (1959), Chapter 4.

26. Massey, H. S. W. and Burhop, E. H. S., Electronic and Ionic Impact Phenomena, Oxford University Press, London (1956), p. 12.

27. Kerrebrock, J. L., "Conduction in Gases with Elevated Electron Temperatures," Engineering Aspects of Magnetohydrodynamics, Columbia University Press, New York (1962), pp. 327-346; also Kerrebrock, J. L., "Non-Equilibrium Effects on Conductivity and Electrode Heat Transfer in Ionized Gases," Guggenheim Jet Propulsion Center, California Institute of Technology, TN 4 (November 1960).

28. Robben, F., "Nonequilibrium Ionization in a Magnetohydrodynamic Generator," Phys. Fluids 5, 1308 (1962).

29. Westendorp, W., Bishop, C., Hurwitz, H., Goldman, L, and BenDaniel, D., "Nonthermal Ionization in Transient Helium-Cesium Discharges," Phys. Fluids 4, 786 (1961).

30. BenDaniel, D. and Bishop, C., "Nonequilibrium Ionization in a High-Pressure Cesium-Helium Transient Discharge," Phys. Fluids 6, 300-306 (1963).

31. Ramsauer, C. and Kollath, R., "Winkelverteilung bei der Streuung Langsamer Electronen an Gasmolekülen," Ann. Phys. 12, 529-561 (1932).

32. Brode, R. B., "Absorption Coefficient for Slow Electrons in Alkali Metal Vapors," Phys. Rev. 34, 673-678 (1929).

33. Brown, S. C., Basic Data of Plasma Physics, MIT Press, Cambridge, Mass., and John Wiley and Sons, New York (1959), p. 31.

34. Gould, L. and Brown, S. C., "Microwave Determination of the Probability of Collisions of Electrons in Helium," Phys. Rev. 95, 897-903 (1954).

35. Ramsauer, C. and Kollath, R., "Uber der Wirkungsquersnit der Edelgasmoleküle geneguber Electronen unterhalb 1 Volt," Annalen der Physik 3, 536 (1929).

36. Normand, C. E., "The Absorption Coefficient for Slow Electrons in Gases," Phys. Rev. 35, 1217-1225 (1930).

37. Pinchak, A. C., "Experimental Investigation of Gas Phase and Surface Phenomena in a Seeded Plasma," Ph. D. Thesis, California Institute of Technology (June 1963).

38. Sheindlin, A., Batenin, V., and Asinovsky, E., "Experimental Investigation of Non-Equilibrium Ionization in a Mixture of Potassium and Argon," International Symposium on MHD Power Generation, Paris, 6-11 July, 1964; Session 2b, Paper 27a.

39. Taylor, J. B. and Langmuir, I., "The Evaporation of Atoms, Ions, and Electrons from Cesium Films on Tungsten," Phys. Rev. 44, no. 6, 423-458 (1933).

40. Dugan, J. V., Jr., "Three-Body Collisional Recombination of Cesium Seed Ions and Electrons in High-Density Plasmas with Argon Carrier Gas," NASA TN D-2004 (Oct. 1964).

41. Robben, F., "Electronic Rate Processes in Nonequilibrium Plasmas," AIAA Aerospace Sciences Meeting, 20-22 January, 1964, New York City; Preprint No. 64-56.

42. Allen, C. W., Astrophysical Quantities, The Athlone Press, London (1963), p. 90.

43. Chanin, L. M. and Steen, R. D., "Mobilities of Cesium Ions in Cesium," Phys. Rev. 132, 2554-2557 (1963).

44. Davies, R. H., Mason, E. A., and Munn, R. J., "High Temperature Transport Properties of Alkali Metal Vapors," Phys. Fluids 8, no. 3, 444-452 (1965).

45. Harris, L. P., "Ionization and Recombination in Cesium-Seeded Plasnas near Thermal Equilibrium," General Electric Co. Rep. 64-RL-3698G (June 1964).

46. Kerrebrock, J. and Hoffman, M., "Nonequilibrium Ionization Due to Electron Heating: I. Theory; II. Experiments," AIAA Journal 2, 1072-1087 (1964).

47. Kerrebrock, J., "Magnetohydrodynamic Generators with Nonequilibrium Ionization," AIAA Journal 3, no. 4, 591-601 (1965).

48. Zukoski, E., Cool, T., and Gibson, E., "Nonequilibrium Electrical Conductivity in a Seeded Plasma," AFOSR 64-0848, Daniel and Florence Guggenheim Jet Propulsion Center, California Institute of Technology (April 1964); also, Zukoski, E., Cool, T., and Gibson, E., "Experiments Concerning Nonequilibrium Conductivity in a Seeded Plasma," AIAA Journal 2, no. 8, 1410-1417 (1964).

49. Brederlow, G., Eustis, R., and Riedmüller, W., "Measurement of the Electron and Stagnation Temperatures in a Linear Argon-Potassium MHD Generator," International Symposium on MHD Power Generation, Paris, 6-11 July, 1964; Session 2b, Paper 21.

50. Cool, T.A. and Zukoski, E.E., "Recombination Rates and Non-Equilibrium Electrical Conductivity in a Seeded Plasma," Sixth Symposium on Engineering Aspects of Magnetohydrodynamics, 21-22 April, 1965; preprints, pp. 121-134.

51. Brederlow, G., Hodgson, R., and Riedmüller, W., "Non-equilibrium Electrical Conductivity and Electron Temperature Measurements in Electric Fields and Crossed Electric and Magnetic Fields," Sixth Symposium on Eng. Aspects of Magnetohydrodynamics, 21-22 April, 1965; preprints, p.137.

52. Gaydon, A. and Wolfhard, H., Flames, Their Structure, Radiation, and Temperature, Chapman and Hall, Ltd., London (1960).

53. Kingston, A.E., "Excitation and Ionization of Hydrogen Atoms by Electron Impact," Phys. Rev. 135, no. 6A, A1529-A1536 (1964).

54. Zukoski, E.E. and Cool, T.A., "Nonequilibrium Electrical Conductivity Measurements in Argon and Helium Seeded Plasmas," AIAA Journal 3, no. 2, 370-371 (1965).

55. BenDaniel, D., "Ionizational Transients in Cesium," Phys. Fluids 6, no. 7, 1034-1035 (1963).

56. Spitzer, L., Jr., "The Temperature of Interstellar Matter, II," Astrophysical Journal 109, no. 3, 338 (1949).

57. Hottel, H.C., "Radiant-heat Transmission," Heat Transmission, ed. W.H. MacAdams. McGraw-Hill Book Co., New York (1954), pp. 86-89.

58. Jakob, M., Heat Transfer, Vol. II, John Wiley and Sons, New York (1959), pp. 99-115.

59. Olfe, D.B., "Mean Beam Length Calculations for Radiation from Nontransparent Gases," J. Quant. Spectr. Radiative Transfer 1, 169-176 (1961).

60. Hinnov, E., "A Method of Determining Optical Cross Sections," J. Optical Soc. of America 47, no. 2, 151-155 (1957).

61. Hinnov, E. and Kohn, H., "Optical Cross Sections from Intensity-Density Measurements," J. Opt. Soc. Am. 47, 156-162 (1957).

62. Mitchell, A. C. G. and Zemansky, M. W., Resonance Radiation and Excited Atoms, Cambridge University Press, London (1934), p. 179.

63. Chen, S. and Takeo, M., "Broadening and Shift of Spectral Lines Due to the Presence of Foreign Gases," Reviews of Modern Physics 29, no. 1, 20-73 (1957).

64. Heavens, O. S., "Radiative Transition Probabilities of the Lower Excited States of the Alkali Metals," J. Opt. Soc. Am. 51, no. 10, 1058-1061 (1961).

65. Stone, P. and Agnew, L., "Plasma-Broadened Cesium Lines," Phys. Rev. 127, 1157-1162 (1962); see also Stone, P., "Cesium Oscillator Strengths," Phys. Rev. 127, no. 4, 1151-1153 (1962).

66. Voigt, W., Münch. Ber., p. 603 (1912). (Cf. Chapter 3 of reference 62 above.)

67. Reiche, F., Verhandl. deut. physik. Ges. 15, 3 (1913). (Cf. Chapter 3 of reference 62 above.)

68. Lowan, A. N. and Blanch, G., "Tables of Planck's Radiation and Photon Functions," J. Opt. Soc. Am. 30, 70-79 (1940).

69. van der Held, E. M. F., Z. Physik 70, 508 (1931). (Cf. Chapter 3 of reference 62, and reference 25, above.)

70. Lutz, M., "Radiant Energy Loss from a Cesium-Argon Plasma to an Infinite Plane Enclosure," Avco Everett Research Lab. Res. Rept. 175 (September 1963).

71. Harwell, K. E. and Jahn, R. G., "Initial Ionization Rates in Shock-Heated Argon, Krypton, and Xenon," Phys. Fluids 7, no. 2, 214-222 (1964).

72. Kelly, A. J., "Atom-Atom Ionization Mechanisms and Cross Sections in Noble Gases and Noble Gas Mixtures," Ph. D. Thesis, California Institute of Technology (June 1965).

73. Harris, L. P., "Electrical Conductivity of Potassium-Seeded Argon Plasmas near Thermal Equilibrium," General Electric Research Lab. Rept. No. 63-RL-3334G (May 1963).